ERDC/GSL TR-10-19

Geotechnical and Structures Laboratory

US Army Corps
of Engineers®
Engineer Research and
Development Center

Field Testing and Load Rating of the World's First Thermoplastic Bridge

Bridge T-8518, Camp Mackall, Fort Bragg, North Carolina

Brett Commander and Henry Diaz-Alvarez

June 2010

ERDC/GSL TR-10-19
June 2010

Field Testing and Load Rating of the World's First Thermoplastic Bridge

Bridge T-8518, Camp Mackall, Fort Bragg, North Carolina

Brett Commander

Bridge Diagnostics, Inc.
1965 57th Court North, Suite 106
Boulder, CO 80301

Henry Diaz-Alvarez

Geotechnical and Structures Laboratory
U.S. Army Engineer Research and Development Center
3909 Halls Ferry Road
Vicksburg, MS 39180-6199

Final report

Prepared for U.S. Army Installation Management Command
Arlington, VA 22202

Under Installation Technology Transition Program

Abstract: Live-load tests were conducted on Bridge T-8518 located on Tuckers Road in Camp Mackall near Fort Bragg, North Carolina. This bridge was tested because it was constructed of a new structural material consisting primarily of recycled plastic lumber (RPL). The primary goal of the testing was to obtain the responses of the bridge to the live loads in order to determine its load capacity ratings for both civilian and military vehicles and, specifically, to determine if the RPL structure could safely carry an M1 tank.

A finite element model of the entire superstructure was developed and used to calculate the responses of the RPL bridge. The results from the calculations were reasonably accurate when compared with the measured field data but were very sensitive to small variations in load position due to the spacing of the bridge beams and the flexibility of the plank deck.

Once a realistic yet conservative model of the structure was obtained, load ratings were computed based on an allowable stress approach. Allowable stress limits that were provided by the manufacturer corresponded to stresses that could be applied to the RPL material for a long period of time with deformations 100% recoverable once the load was removed. These stress limits were a small fraction of the ultimate stress limits for RPL. However, an ultimate load capacity would be difficult to calculate because it would result in highly nonlinear and time-dependent responses with extremely large deformations.

The load rating results apply only to the bridge superstructure. Deformations of the RPL piles were measured during the load test, but no assessment could be made concerning the pile capacity. The pile capacity should be verified from the design engineer and the piling contractor to ensure that the piles have sufficient bearing strength to withstand the load limits of the superstructure.

Contents

Figures and Tables

Figures

Tables

Preface

The U.S. Army Engineer Research and Development Center's (ERDC) Construction Engineering Research Laboratory (CERL) requested the assistance of the ERDC Geotechnical and Structures Laboratory (GSL) in conducting a live-load testing and load rating determination of a thermoplastic bridge in Camp Mackall, North Carolina. The testing of Bridge T-8518, summarized in this report, was sponsored by the Assistant Chief of Staff for Installation Management under the U.S. Army's Installation Technology Transition Program. Points of contact were Richard Lampo, CERL, and Ali Achmar, Army Installation Management Command.

Load testing was performed under contract to ERDC by personnel of Bridge Diagnostics, Inc. (BDI), under the supervision of Brett Commander, BDI. Instrumentation support for the load testing was provided by personnel of BDI and the ERDC Information Technology Laboratory. Henry Diaz-Alvarez, Structural Engineering Branch (StEB), GSL, and Brett Commander, BDI, performed the finite element modeling of the load tests and load rating calculations, and prepared this report. The authors were assisted in the testing phase by Kevin Tillman, Rodney Gonzalez, and Orlando Carrasquillo, StEB.

During this investigation, Terry R. Stanton was Chief, StEB; Bartley P. Durst was Chief, Geosciences and Structures Division; Dr. William P. Grogan was Deputy Director, GSL; and Dr. David W. Pittman was Director, GSL.

COL Gary E. Johnston was Commander and Executive Director of ERDC. Dr. Jeffery P. Holland was Director.

Unit Conversion Factors

Multiply	By	To Obtain
degrees Fahrenheit	(F-32)/1.8	degrees Celsius
feet	0.3048	meters
foot-pounds force	1.355818	joules
inches	0.0254	meters
inch-pounds (force)	0.1129848	newton meters
kips (force)	4.448222	kilonewtons
miles per hour	0.44704	meters per second
ounces (U.S. fluid)	2.957353 E-05	cubic meters
pounds (force)	4.448222	newtons
pounds (force) per foot	14.59390	newtons per meter
pounds (force) per inch	175.1268	newtons per meter
pounds (mass) per cubic inch	2.757990 E+04	kilograms per cubic meter
square feet	0.09290304	square meters
square inches	6.4516 E-04	square meters
tons (force)	8,896.443	newtons
tons (2,000 pounds, mass)	907.1847	kilograms

1 Introduction and Summary of Results

A joint investigation that involved field load testing of a new bridge constructed of recycled plastic lumber (RPL) and calculating its load ratings was conducted by personnel of Bridge Diagnostics, Inc. (BDI), and the U.S. Army Engineer Research and Development Center (ERDC). The bridge, numbered T-8518, is located on Tuckers Road in Camp Mackall near Fort Bragg, North Carolina. Bridge T-8518 is a new three-span structure constructed entirely of RPL. RPL is a wood-like product made from recovered plastic or recovered plastic mixed with other materials and can be used as a substitute for concrete, wood, and metals. The product is clean, nontoxic, and nonporous and lasts longer than wood. In addition, all types of RPL, except for wood-filled RPL, are moisture and chemical resistant, impervious to insects, flexible (can be curved and shaped), maintenance free, and need no sealants or preservatives.

Instrumentation for the load tests included strain transducers, vertical displacement sensors, and foil strain gages placed at 94 locations on the bridge deck, deck support beams, and pile foundations. Results of these measurements were used to validate results from a detailed finite element model, which was used to calculate the bridge's responses to the loads from a 72-kip dump truck and to verify that an M1 tank could safely cross the bridge. Subsequently, the model was used to generate a military load classification (MLC) for the bridge deck, based on the assumption that the pile foundations could also support the loads.

Detailed descriptions of the bridge and the load tests are given in Chapter 2, and results of a preliminary analysis of the load test data are presented in Chapter 3. Chapter 4 describes the detailed finite element model developed for the bridge structure and comparisons of the calculated bridge responses with the measured field data. Procedures for calculating the bridge load ratings and results of these calculations are in described in Chapter 5. Chapter 6 presents conclusions and recommendations from this investigation.

2 Structural Testing Information

Bridge T-8518 is a three-span structure constructed entirely of RPL members. This includes the entire superstructure and the piles. It was constructed in a manner similar to a timber bridge with relatively short longitudinal stringers and a plank deck. The stringers were 18-in. by 18-in. I-beams with 3-in.-thick flanges and a 5-in.-thick web. The I-beams were manufactured as two T-sections that were glued and screwed together (Figure 1). The stringers were continuous over the three spans and placed adjacent to each other with space between the flanges. Each span was approximately 12 ft long with relatively simple bearing connections. The 3-in.-thick by 12-in.-wide deck planks were aligned transversely across the bridge and attached by deck screws to the top flange of the I-beams. The substructure consisted of abutments with three RPL piles and interior piers with four piles driven about 60 ft deep. The design pile capacity was an allowable load of 40 kips with an ultimate load of at least 120 kips.

Instrumentation installed by BDI personnel consisted of 57 strain transducers and seven vertical displacement sensors. The purpose of the instrumentation was to determine the load transfer characteristics of the superstructure. Strain transducers were attached with glue-mounted tabs (Figure 2) and were typically located at midspan and near the supports of the stringers. An interior bent was also instrumented as was one pile. Vertical displacements were measured at midspan of six adjacent stringers (Figure 3) at Span 1 and also at the bent immediately adjacent to an interior pile. The locations of the sensors on the structure are shown in Figure 4 through 8. All sensor measurements were recorded with the BDI Wireless Structural Testing System STS-WiFi.

Additional instrumentation, consisting of 30 foil strain gages arranged into 10-rosette configurations (Table 1), was installed by ERDC personnel and also recorded by the BDI STS-WiFi. The foil gages were mounted prior to construction of the bridge. However, only six rosettes functioned at the time of the load test. The locations of the functioning rosette gages are shown in Figure 9. All of the BDI and ERDC data were processed as a function of truck position and imported into a spreadsheet for ERDC to analyze.

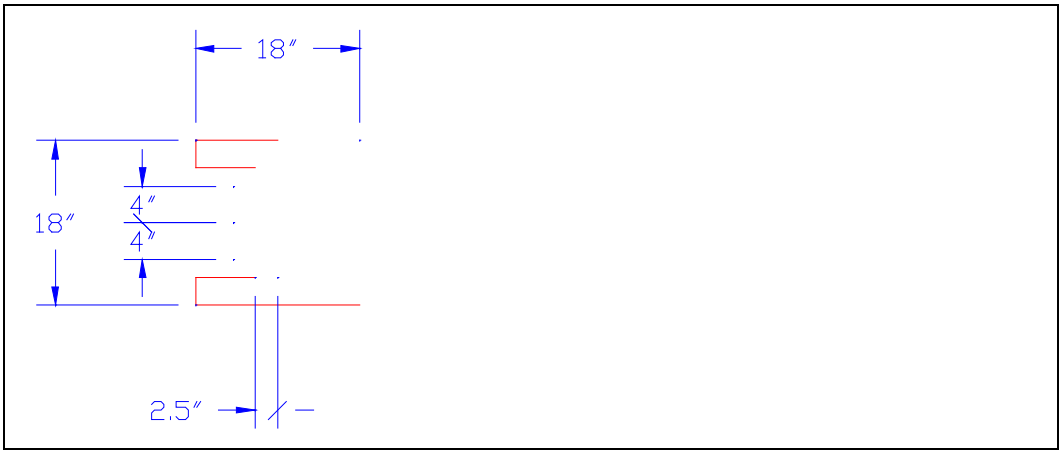

Figure 1. RPL cross section and material properties.

Figure 2. Strain transducers on RPL stringers.

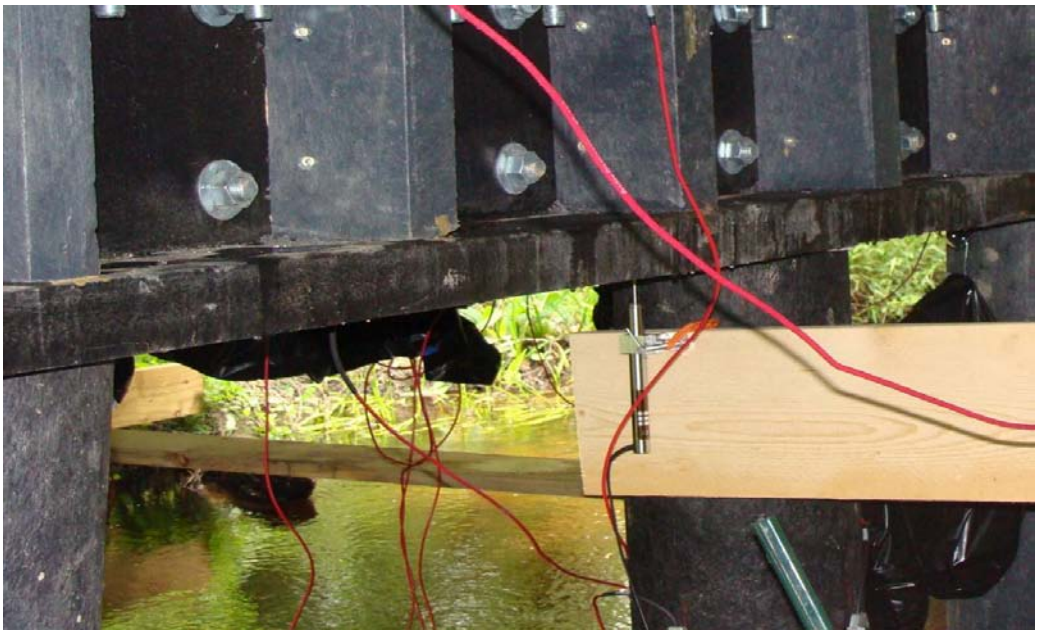

Figure 3. LVDT at interior bent adjacent to column.

Table 1. Strain gage rosette configuration.

ERDC Gage ID	BDI Gage ID	ERDC Gage ID	BDI Gage ID	ERDC Gage ID	BDI Gage ID
R2-45L	ARM-8(B)[1]	R2-90	ARM-7(B)	R2-45R	ARM-10(B)
R4-45L	ARM-6(B)	R4-90	ARM-4(B)	R4-45R	ARM-3(B)
R5-45L	ARM-11(B)	R5-90	ARM-9(B)	R5-45R	ARM-5(B)
R7-45L	ARM-7(A)	R7-90	ARM-10(A)	R7-45R	ARM-4(A)
R9-45L	ARM-6(A)	R9-90	ARM-3(A)	R9-45R	ARM-8(A)
R10-45L	ARM-9(A)	R10-90	ARM-5(A)	R10-45R	ARM-11(A)

[1] (A) indicates quarter-arm setup 1; (B) indicates quarter-arm setup 2.

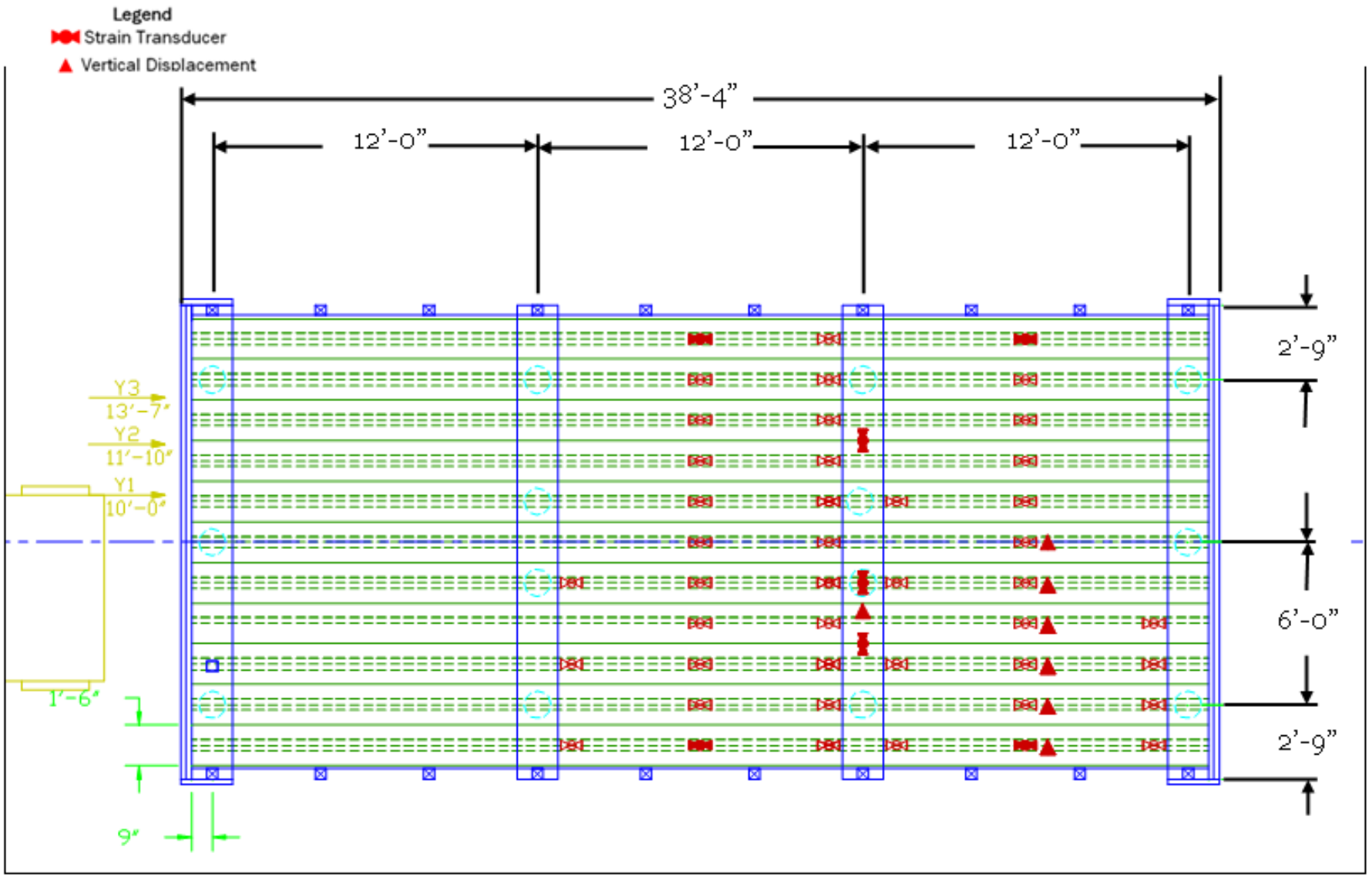
Legend
Strain Transducer
Vertical Displacement
38'-4"
12'-0"
12'-0"
12'-0"
2'-9"
6'-0"
2'-9"
Y3
13'-7"
Y2
11'-10"
Y1
10'-0"
1'-6"
9"

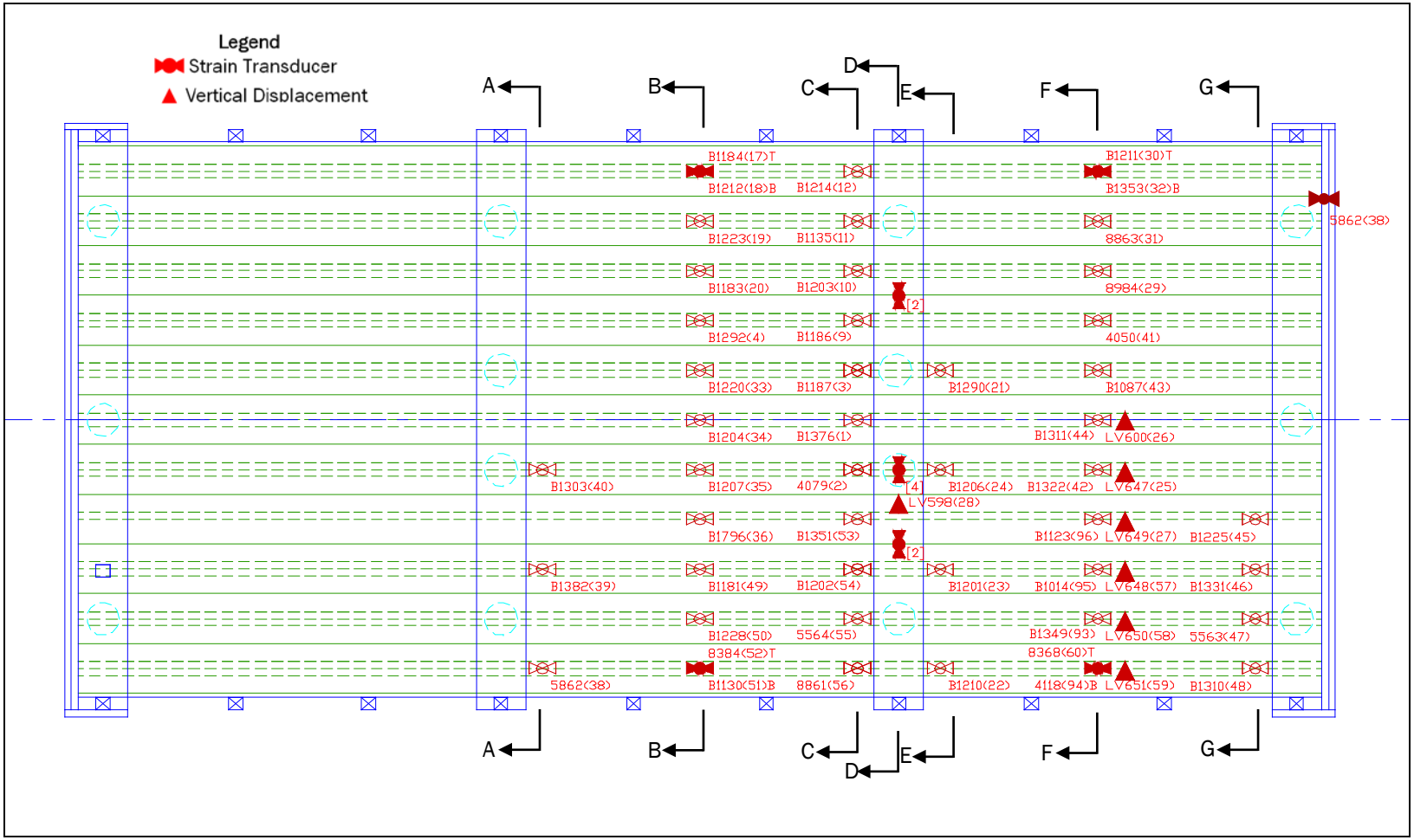

Figure 5. Structure plan with BDI sensor locations and sensor numbers.

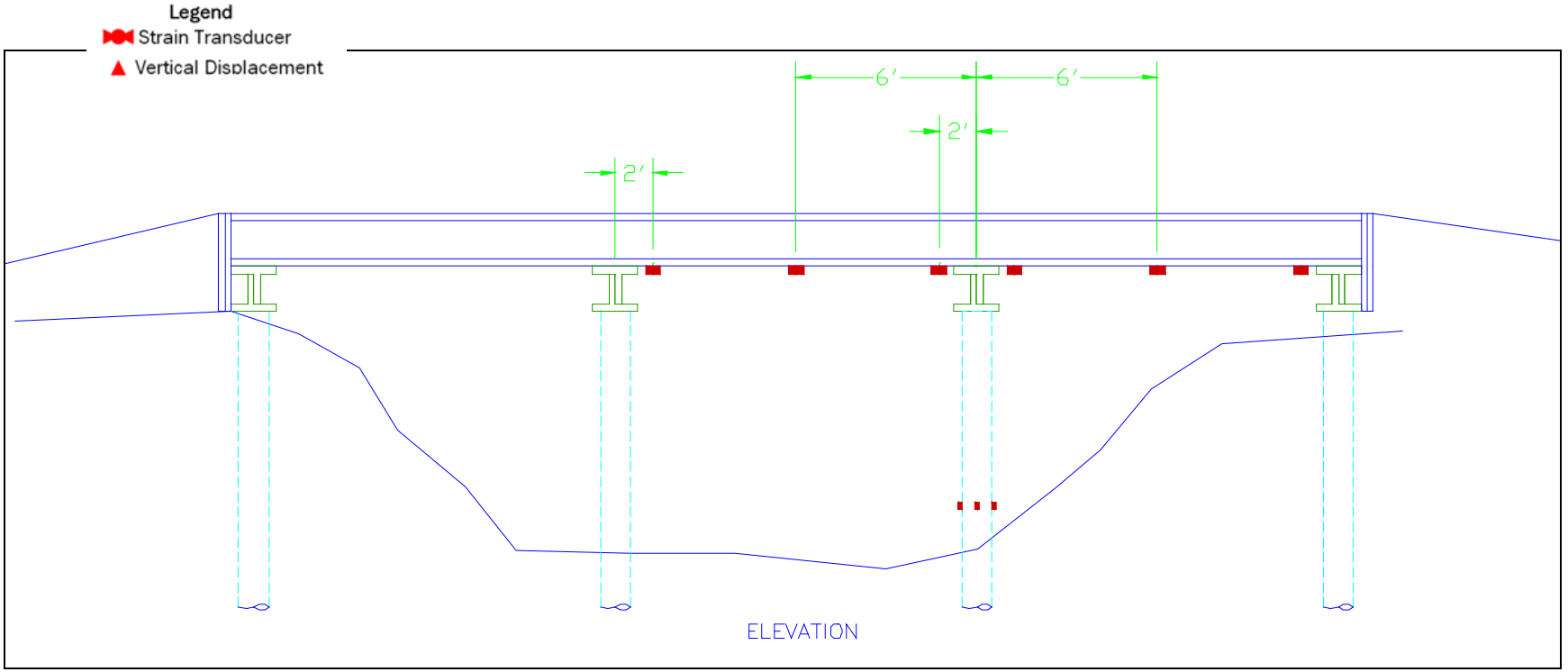

Figure 6. Elevation view of BDI sensors on superstructure.

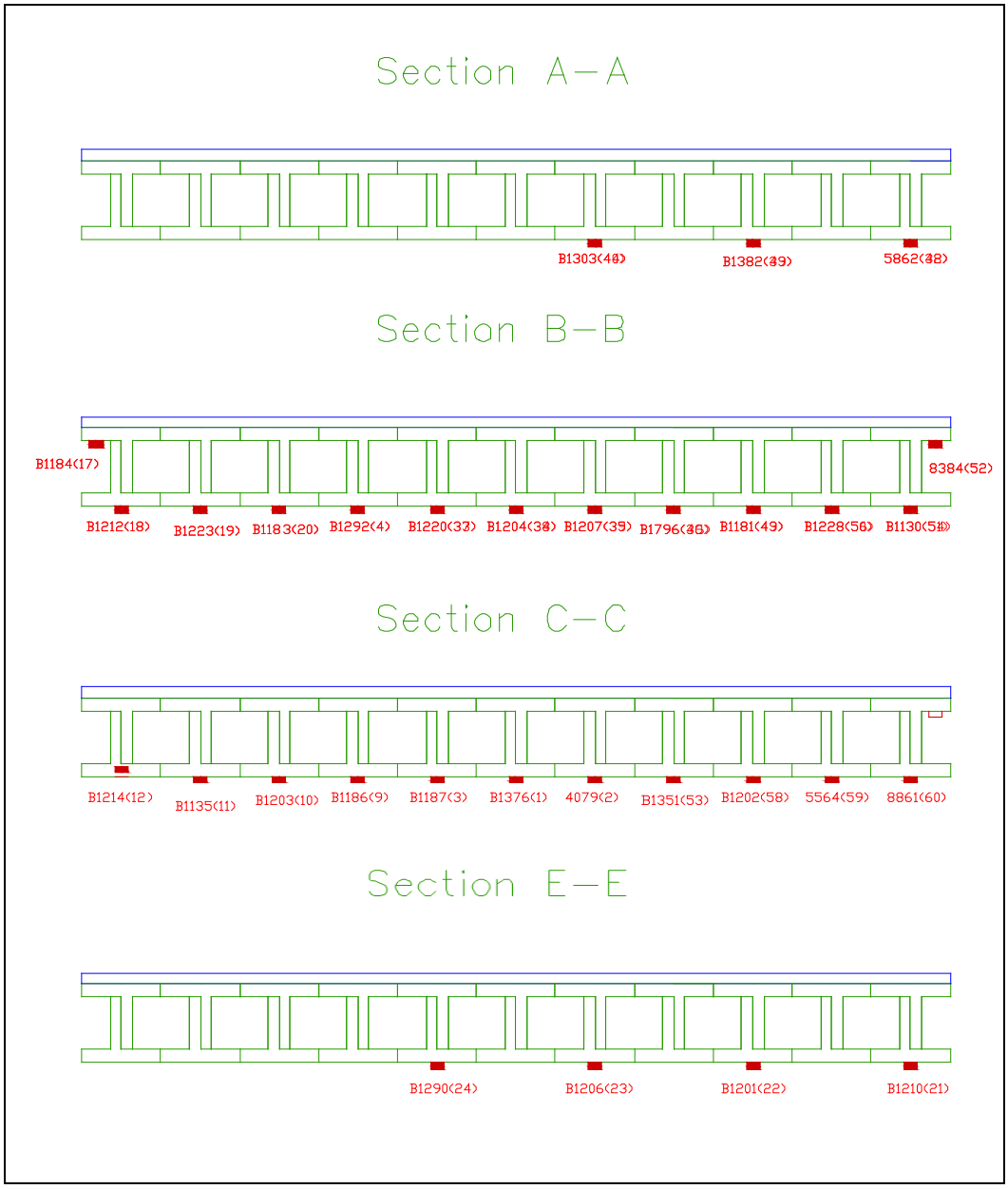

Figure 7. Sensor locations and numbers for cross sections A-A through E-E.

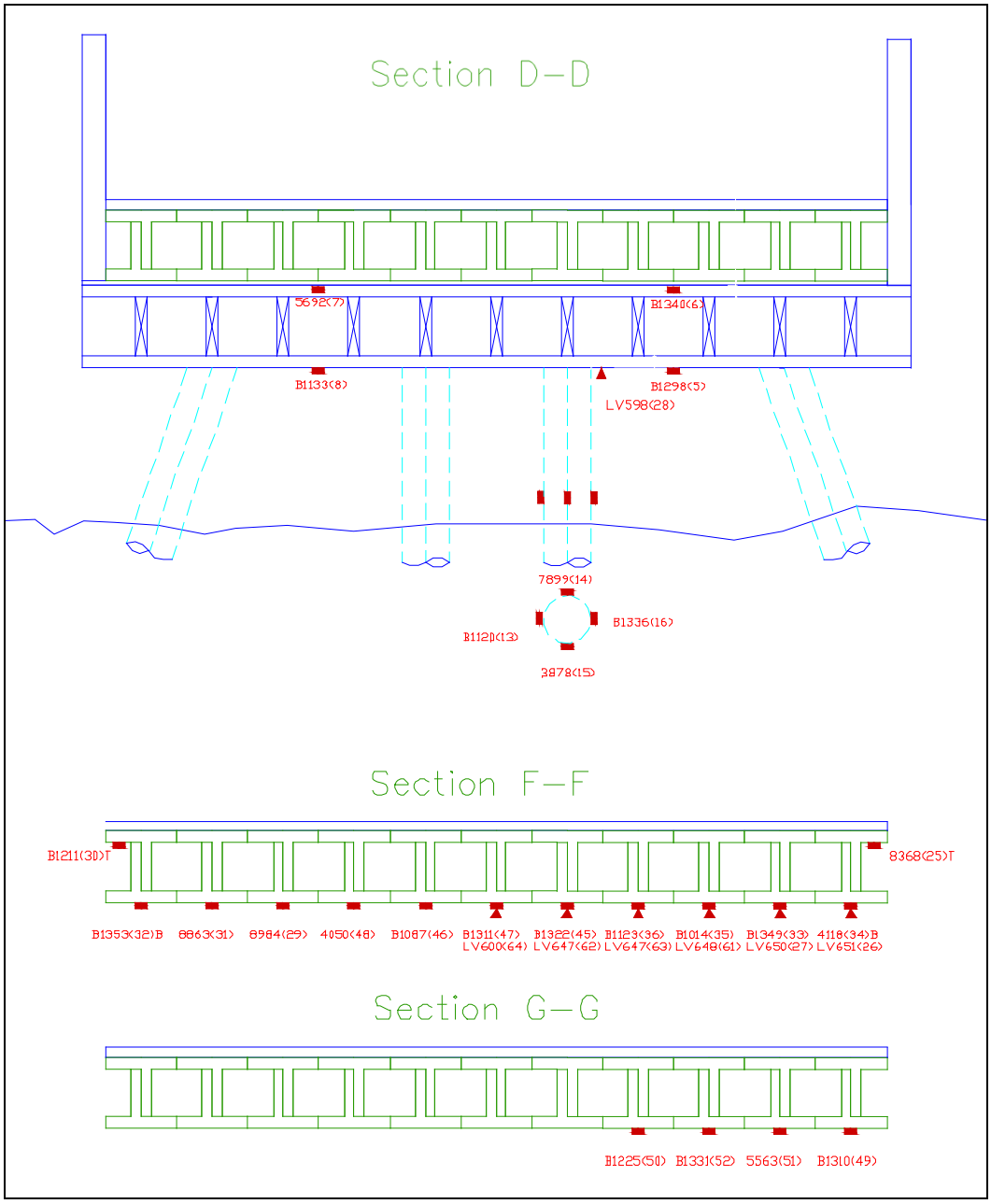

Figure 8. Sensor locations and numbers for cross sections D-D through G-G.

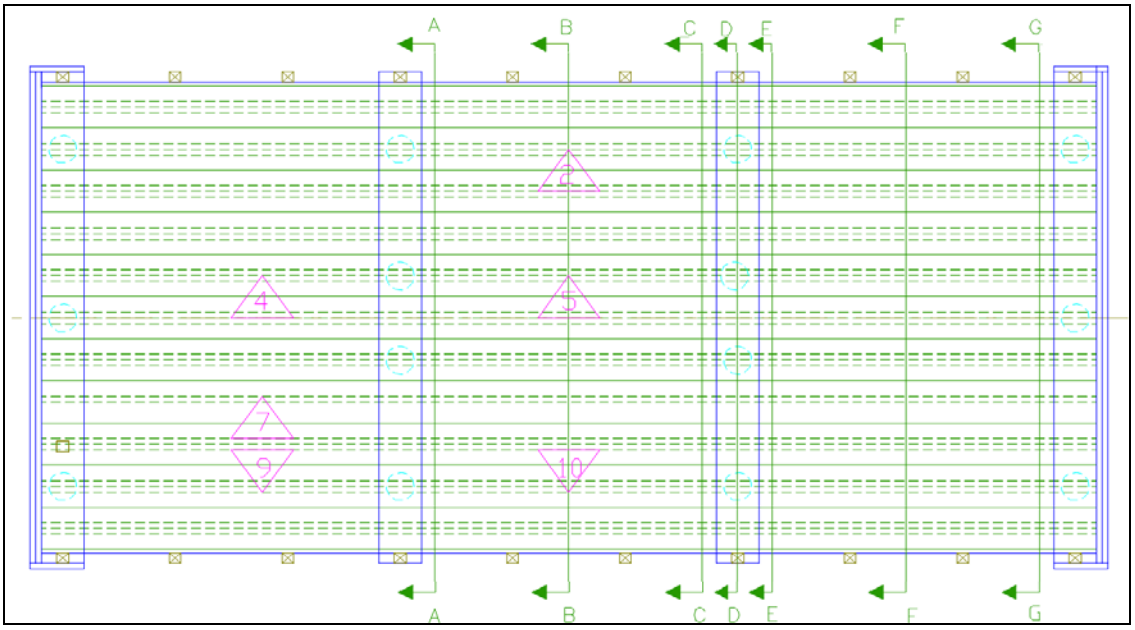

Figure 9. Functional rosette gage locations.

As the live-load tests were performed, strains and displacements were recorded as a specific vehicle was driven across the bridge along prescribed paths. All measurements were recorded at a rate of 40 Hz. Vehicle position was monitored along with the sensor measurements, so that all measured responses could be correlated with applied load. Most of the tests were conducted quasi-statically with the vehicles traveling 3 to 5 mph. Because of the visco-elastic nature of the RPL, two static tests were also performed to capture the responses of sustained loads. Initial tests were conducted with a 72.8-kip dump truck shown in Figure 10. The dump truck was driven across the bridge along three paths, and each path was repeated at least once to verify reproducibility in responses and test procedures. After it was determined that it would be safe, the controlled load tests were repeated with an M1 tank as shown in Figure 11. Due to the width of the tank relative to the bridge, only a single path was used for the load test.

Information specific to the truck load test is in Table 2, and the field notes are shown in Appendix B. The gross weights and wheel rollout distances (required for tracking positions across the structure) for truck and tank are provided in Tables 3 and 4, respectively. “Footprints” of the vehicles, including wheel weights, are shown in Figure 12 and Figure 13, respectively.

Appendix C is an outline of the general field testing procedures, developed by BDI, and the specifications for the BDI strain transducers and the wireless structural testing system, also developed by BDI, are in Appendix D.

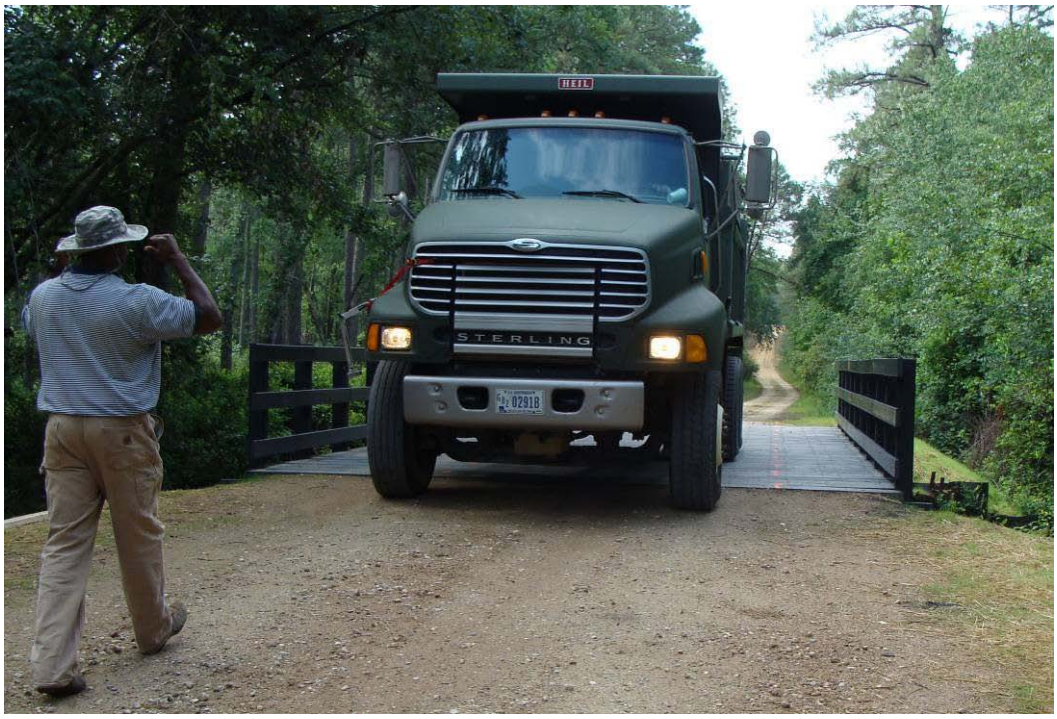

Figure 10. Dump truck crossing bridge during initial test.

Figure 11. M1 tank crossing bridge during final test.

Table 2. Structure description and testing notes.

Item	Description	
Structure Name	Plastic Bridge over Big Muddy Creek	
BDI Project Number	090428NC	
Testing Date	June 10, 2009	
Client's Structure ID #	T-8518	
Location/Route	Tuckers Road, Camp Mackall, North Carolina	
Structure Type	Recycled Plastic Lumber bridge	
Total Number of Spans	3	
Span Length(s)	All Spans: 12' (c-c of bearings)	
Skew	0°	
Structure/Roadway Width	17'-6" / 16'-6"	
Wearing Surface	RPL decking (3"x12")	
Other Structure Info	N/A	
Spans Instrumented	North end-span and center span	
Test Reference Location (X = 0, Y = 0)	Southeast corner of deck	
Test Vehicle Direction	North	
Test Beginning Point	-10' from Reference Location	
Lateral Load Position(s)	3 (symmetrically located)	
Number/Type of Sensors	57 strain transducers and 7 LVDTs – BDI Setup 18 foil gages in rosette configurations (10 rosettes)	
STS Sample Rate	Slow Speed: 40 Hz	
Number of Test Vehicles	2	
Structure Access Type	Ground, Waders	
Structure Access Provided by	BDI / ERDC	
Traffic Control Provided by	N/A	
Total Field Testing Time	16 hr	
Field Notes	See Appendix B	
Visual Condition	New structure	
Test File Information *File Name*	*Lateral Position*	*Comments*
Plastic3S_1.dat	Y1	Good but LVDTs did not return to 0.0
Plastic3S_2.dat	Y1	Better– drove truck further off bridge –LVDTs 0
Plastic3S_3.dat	Y2	Good
Plastic3S_4.dat	Y2	Good
Plastic3S_5.dat	Y3	Good
Plastic3S_6.dat	Y3	
Plastic3S_7.dat	Y2	Stopped truck – front axle middle Span 3
PlasticQA_1.dat	Y3	¼-arms on Girder 9 (R7,R9&R10) – Good
PlasticQA_2.dat	Y3	Good
PlasticQA_3.dat	Y2	Good
PlasticQA_4.dat	Y2	Good

Item	Description	
PlasticQB_1.dat	Y1	¼-arms on Girder 3&6 R(8,7,10,6,4,3,11,9,5)
PlasticQB_2.dat	Y1	Good
PlasticQB_3.dat	Y2	Good
PlasticQB_4.dat	Y2	Good
PlasticQB_5.dat	Y3	Good
PlasticQB_6.dat	Y3	Good

Table 3. Dump truck load information.

Vehicle Type - Tandem rear axle dump truck (see Figure 12)	
Gross Vehicle Weight (GVW)	72,800 lb
Wheel Rollout 5 Revs	54'-2" (10.83' / rev)
No. of Crawl Speed Passes	15
No. of High Speed Passes/Speed	1/25 mph
No. of Static Tests	1

Table 4. M1 tank load information.

Vehicle Type – M1 tank (see Figure 13)	
Gross Vehicle Weight (GVW)	144,288 lb
Wheel Rollout 10 Revs	71'-2" (7.12' / rev)
No. of Crawl Speed Passes	5
No. of static tests	1

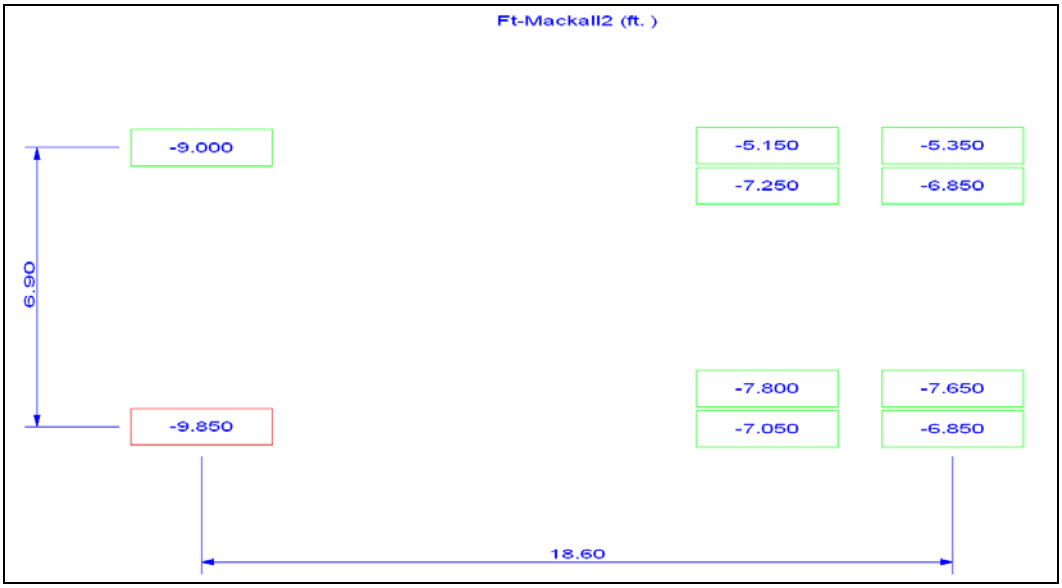

Figure 12.Tandem rear axle dump truck footprint with wheel weights (in kips).

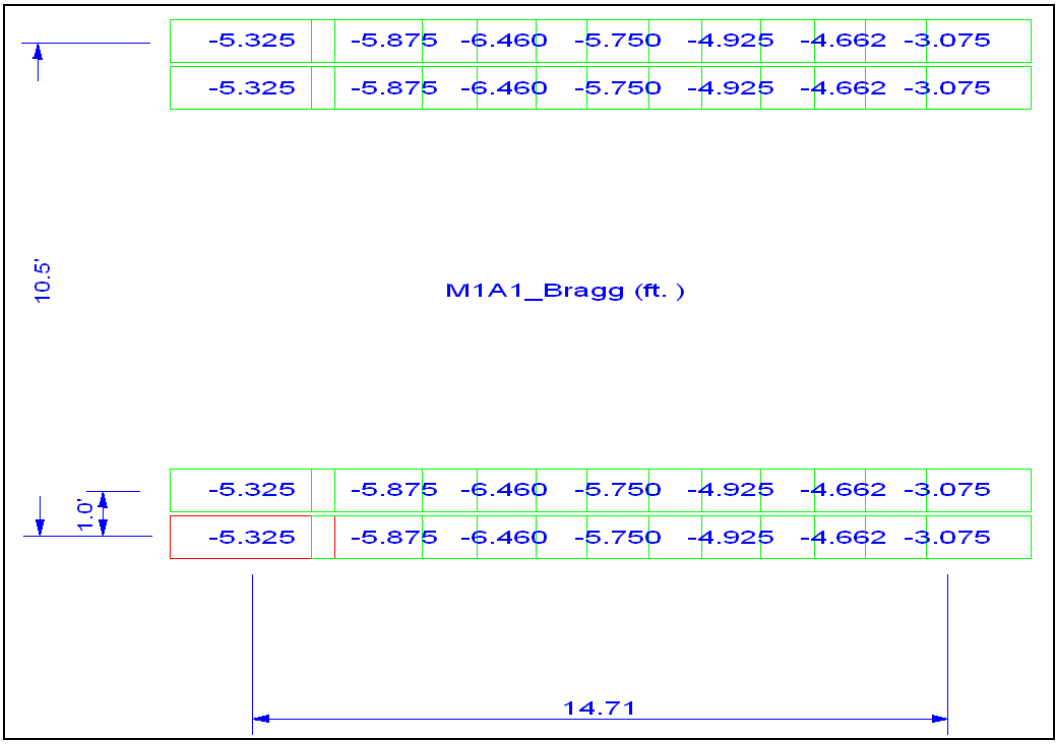

Figure 13. M1 tank footprint with weight distribution (in kips).

3 Preliminary Investigation of Test Results

Background

All of the field data were first examined graphically to provide a *qualitative* assessment of the data and the structure's live-load response. Some of the indicators of data quality included reproducibility between identical truck crossings, elastic behavior (strains returning to zero after truck crossing), and any unusually shaped responses that might indicate nonlinear behavior or possible gage malfunctions.

In addition to providing a data "quality check," the information obtained during the preliminary investigation was used to determine appropriate modeling procedures and helped establish the direction that the analysis should take. Several representative response histories are provided in Appendix A. For all plots, "load position" on the x-axis is referencing the location of the front axle as the test vehicle travels across the bridge.

Preliminary data review observations

- *Reproducibility and linearity:* Responses from duplicate truck crossings were examined for both the dump truck crossing and the M1 tank crossing to determine if all responses returned to zero after each load cycle. Figure 14 and 15 show strain and displacement histories, respectively, from the dump truck crossing. Both responses were highly reproducible, indicating that the structural responses were elastic and the load test procedures were well duplicated. Strain and displacement histories from the M1 crossing also had a high degree of reproducibility, as shown in Figure 16 and Figure 17. More variability occurred in the data for the tank crossing due to the difficulty in steering and following an exact path, as compared with the data for the dump truck.

- *End restraint:* As with most bridge structures, some degree of end restraint was observed at the abutment beam bearing locations. Figure 18 shows the bottom flange stress history from a location near the abutment beam bearing. Three interesting (although relatively unimportant) observations can be made. First was the presence of negative stress spikes. These appeared at the instant each axle reached

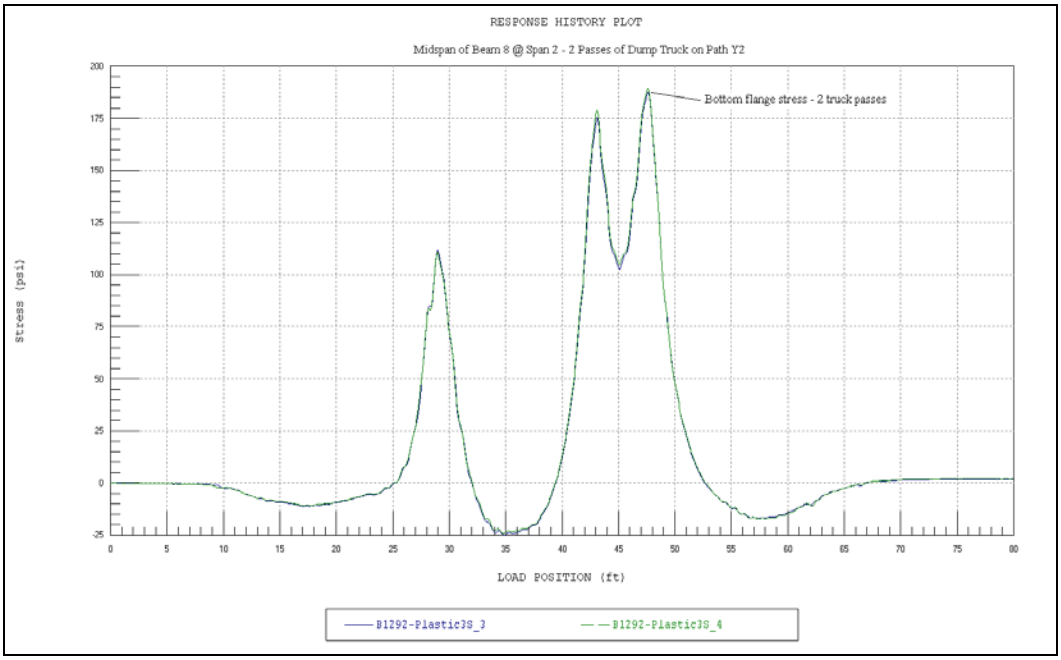

Figure 14. Reproducibility of dump truck test results – strain histories.

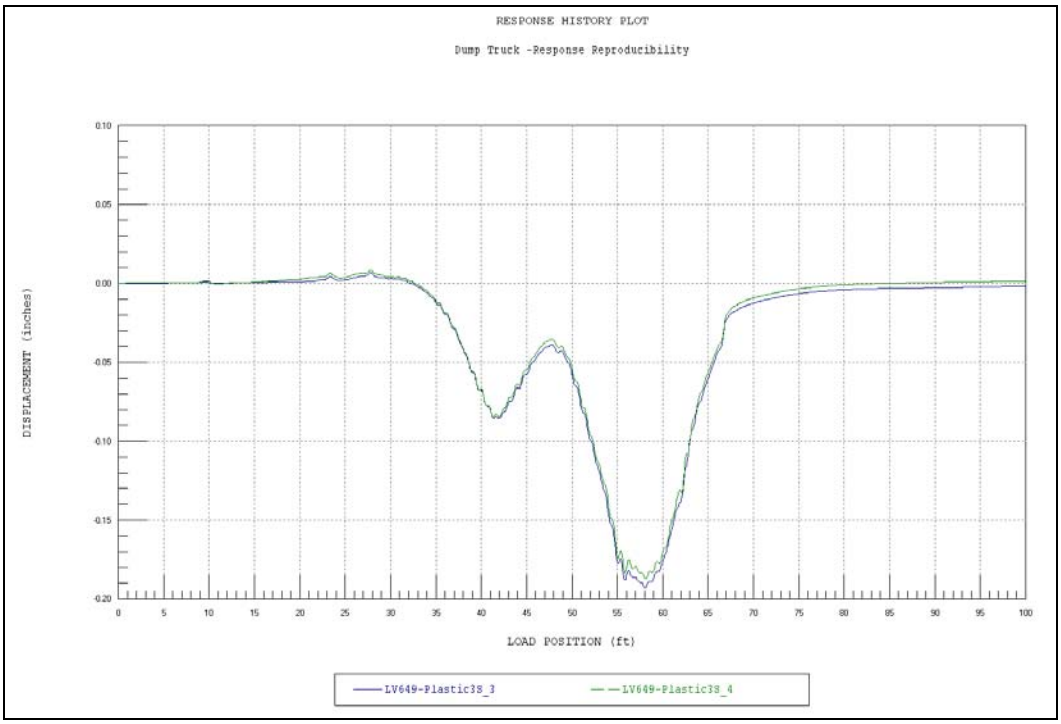

Figure 15. Reproducibility of dump truck test results – displacement histories.

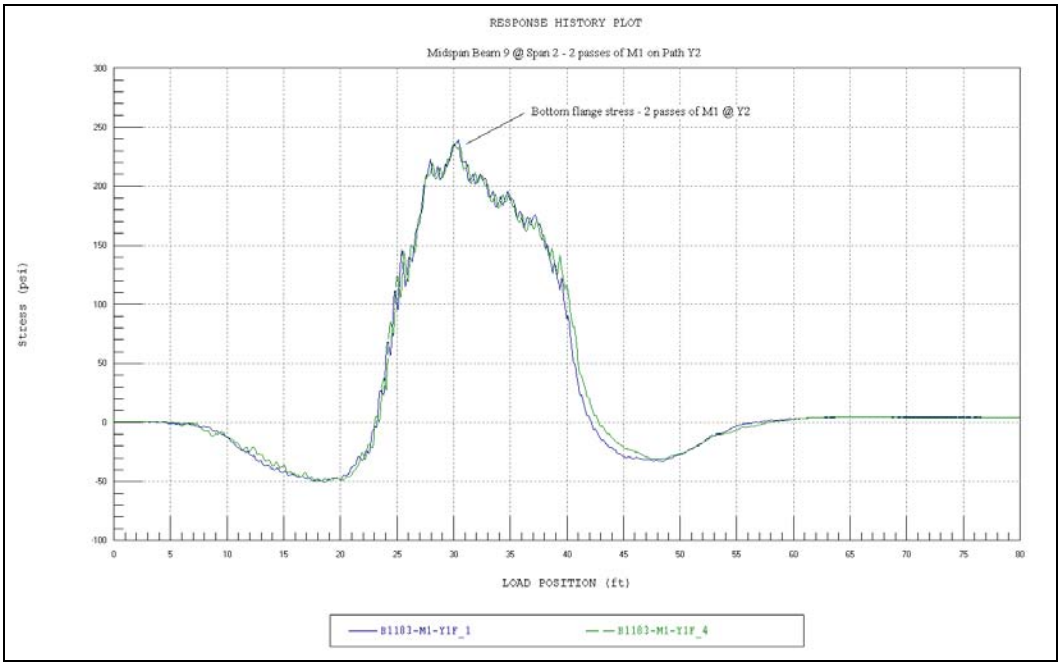

Figure 16. Reproducibility of M1 tank test results – strain histories.

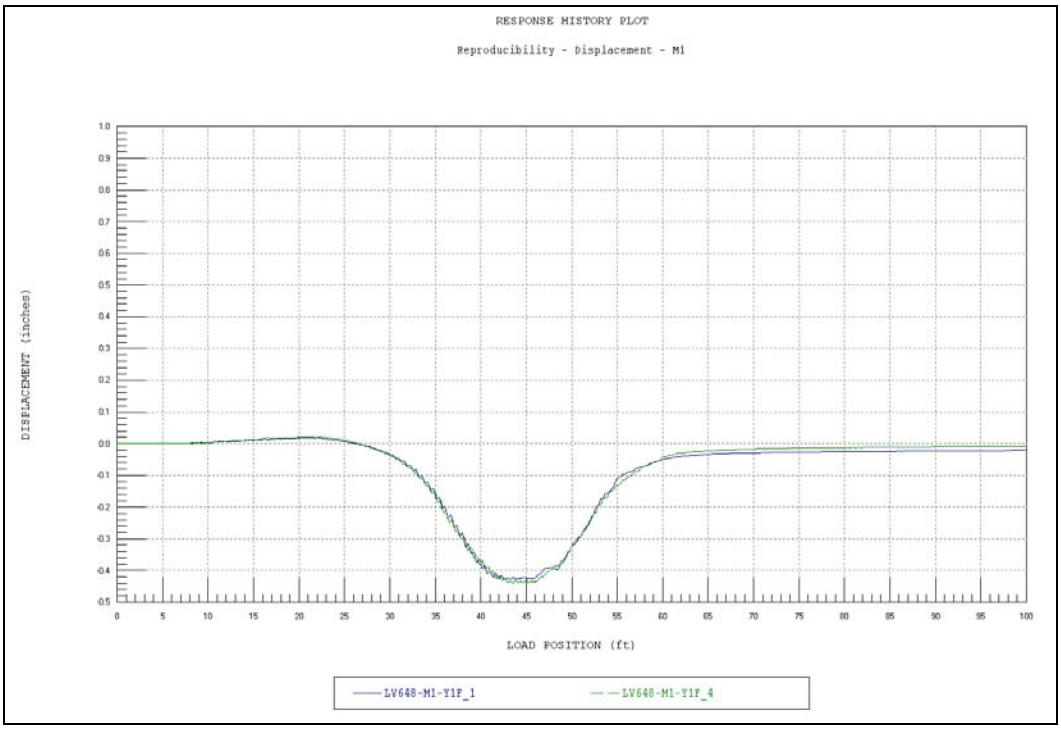

Figure 17. Reproducibility of M1 tank test results – displacement histories.

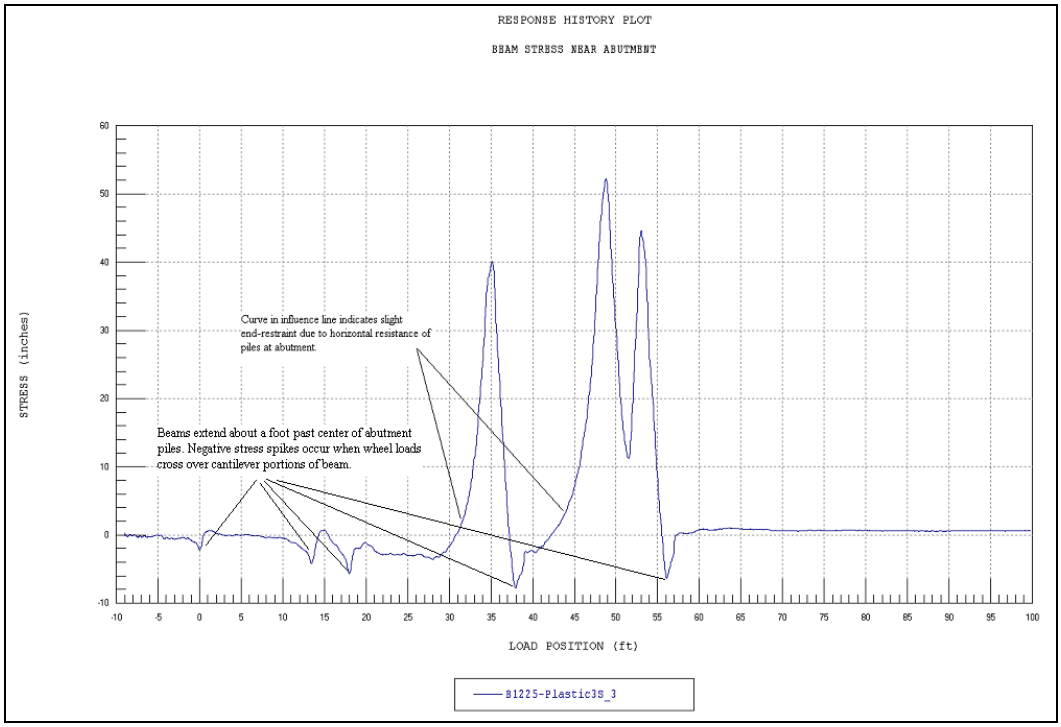

Figure 18. Response effects due to beam end restraint.

the very end of the beams. The negative stress was the result of the beams extending slightly past the center of the abutment piles such that a small cantilever effect was obtained. The fact that this cantilever effect was detectable indicates that very little rotational restraint was present at the beam bearings. The second observation was the tendency for the stress history to drift in the negative direction (compression), even though the primary flexural response was positive when the axles crossed Span 3. The negative trend in stress was an indication that the ends were restrained against axial motion. The downward flexure/displacement in the beams caused the bottom flanges to displace outward. The resistance to this displacement caused a small degree of axial compression in the beam. The third observation was the slight curve in the stress influence lines and was related to the second observation in that it was a function of the horizontal resistance applied to the bottom flange of the beams. The theoretical influence near a simple support would be straight lines associated with each axle response. The curved influence indicates some degree of end restraint, such that a negative moment at the bearing condition is present. While the support cannot resist significant moment, the horizontal reaction was applied eccentrically to the beam's neutral axis and created a small amount of negative moment. This effect is important to the model

calibration procedures only because it can reduce the measured midspan moment by several percent. The end restraint should be ignored for load rating purposes.

- *Pile and beam displacement:* Displacements were measured at mid-span of six beams and at an interior bent immediately adjacent to a vertical pile. In most bridge structures, the bents and abutments are assumed to be very rigid compared with the superstructure. However, since the piles were made from the same recycled plastic material as the superstructure, the displacement in the piles was a significant portion of the overall superstructure displacement. Figure 19 and Figure 20 show the displacement histories at a beam midspan location and the pile at Bent 2 due to the truck and tank crossing, respectively. For the dump truck crossing, the pile displacement was approximately 45% of the beam displacement. During the tank crossing, the pile accounted for approximately the same percentage of displacement, but the magnitudes were approximately double those from the dump truck crossing.

- *Visco-elastic response:* The responses from the tank were large enough that visco-elastic behavior was notable. Responses did return to zero, but a duration of 1 min or more was required for complete recovery. This behavior was observed from the data from the initial tests. Therefore, one of the tank tests was conducted with the tank parked on the middle of the bridge for a period of 5 min before it was driven fully off. Figure 21 shows the displacement history during the static test. The visco-elastic behavior is first noted during the static loading as the displacements continue to increase over a period of a few minutes, and then again during the recovery process after the load was removed. The observed response essentially confirms the intended theoretical behavior, so it is not a concern but is interesting to observe in a structural system.

- *Lateral distribution:* As a means of observing lateral distribution of wheel loads, bottom flange stresses associated with maximum midspan moments were plotted for all beams at a midspan cross section. Figure 22 through Figure 24 show the stress distribution for all three truck crossings. Stress distribution produced by the M1 tank is shown in Figure 25. The general observation is that the deck is relatively flexible. However, due to the close spacing of the RPL beams, the lateral wheel load distribution is reasonably good. The apparent wheel load

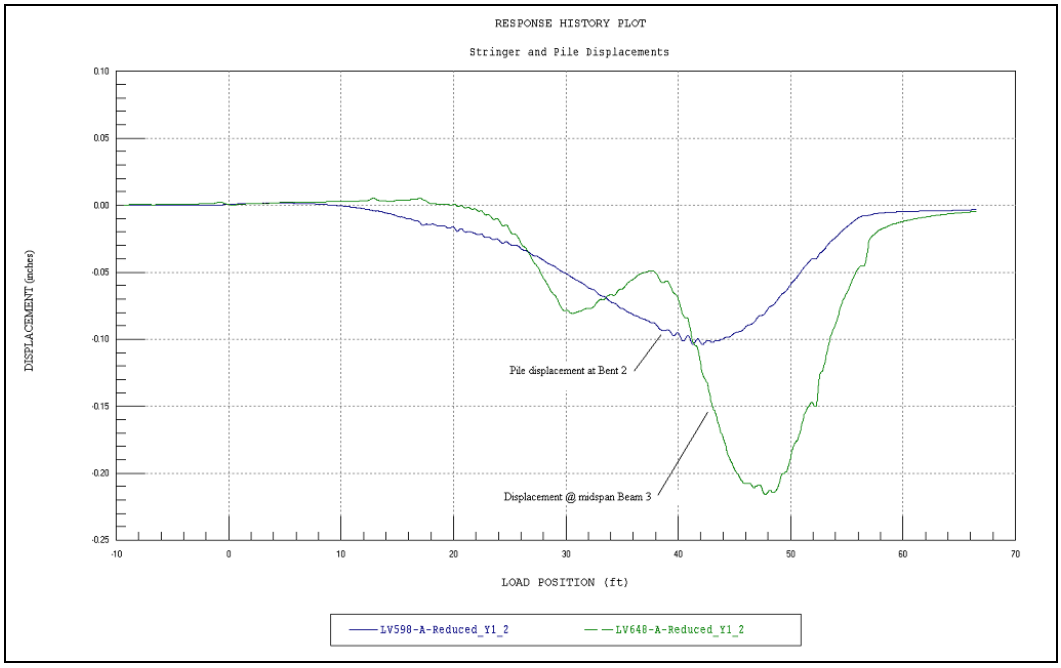

Figure 19. Beam and pile displacements due to 72-kip dump truck.

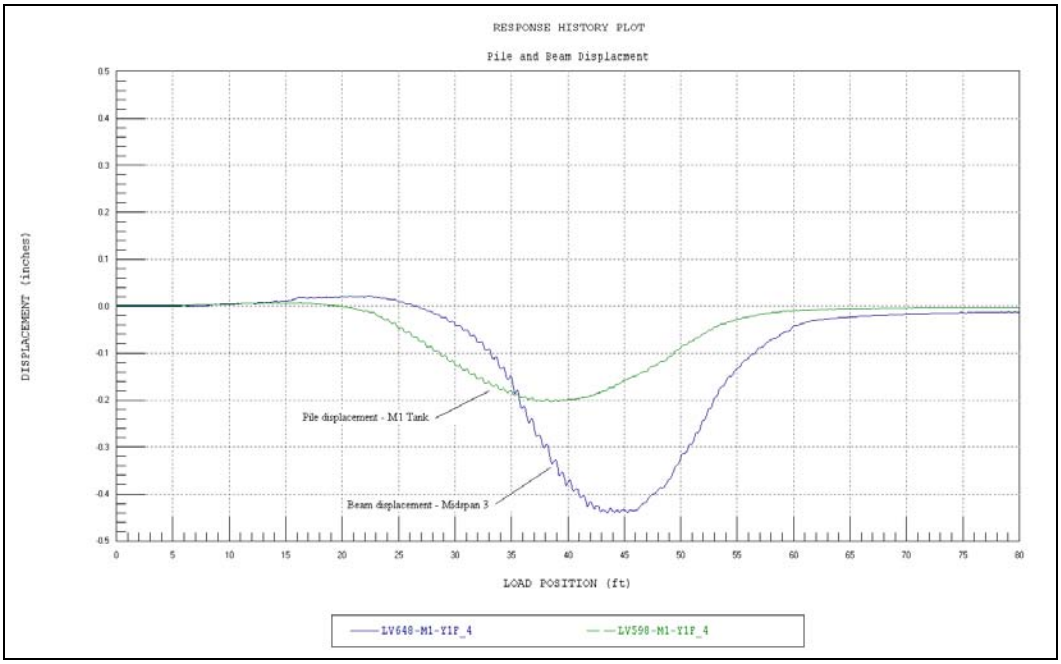

Figure 20. Beam and pile displacements due to 144-kip M1 tank.

distribution factor for a single beam is approximately 41% for the dump truck and 34% for the M1 tank. Symmetry in the lateral load distribution is reasonably good, as well.

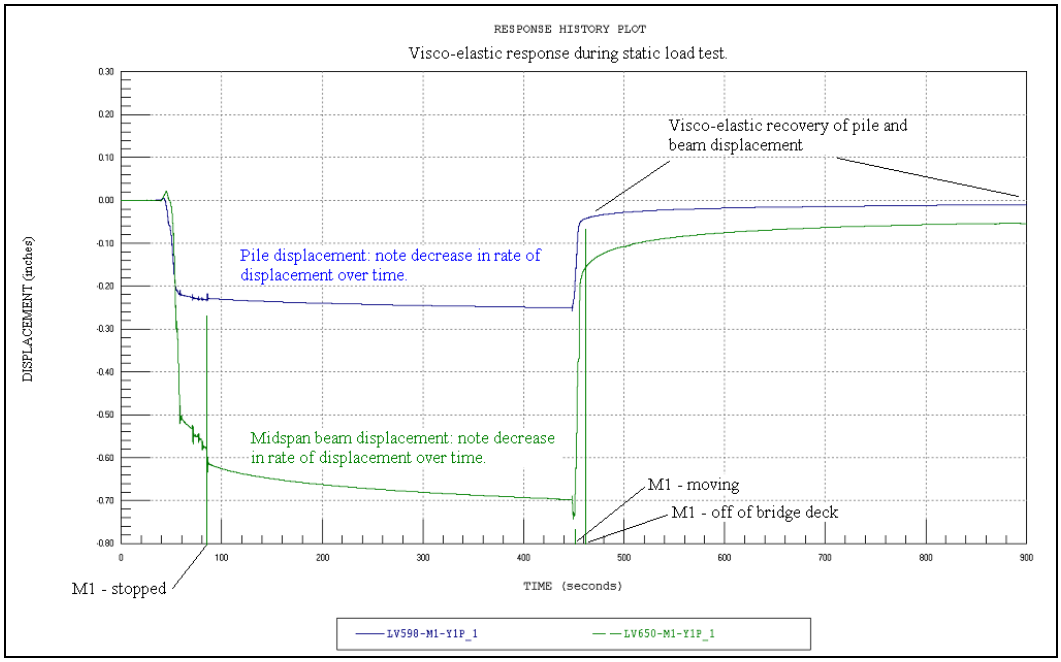

Figure 21. Visco-elastic displacement observed during static test – M1 tank.

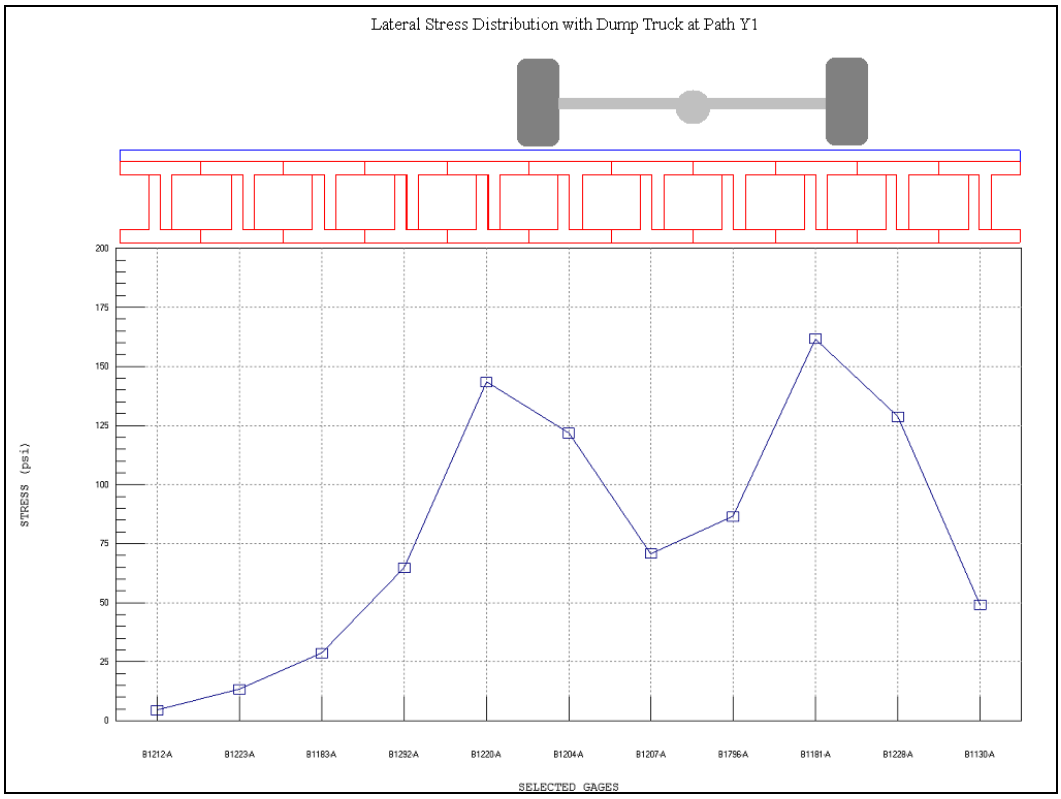

Figure 22. Lateral strain distribution at midspan – dump truck @ Y1.

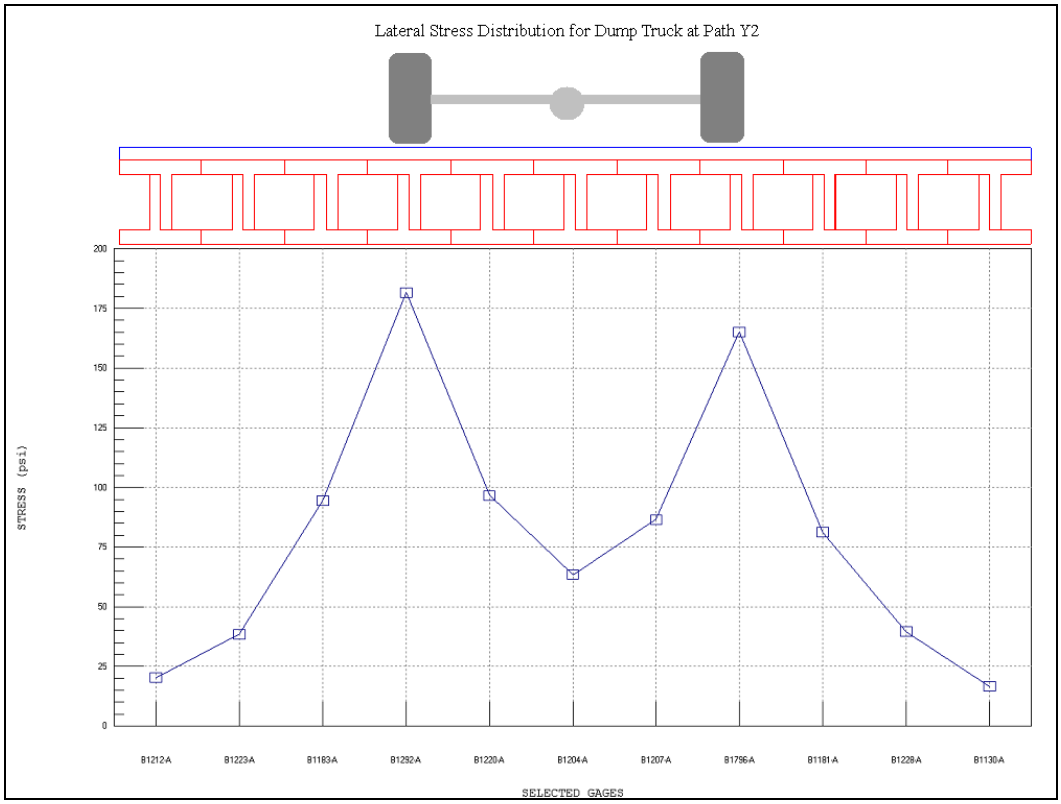

Figure 23. Lateral strain distribution at midspan – dump truck @ Y2.

- *Peak stress measurements:* Maximum strain and displacement measurements were extracted from each crossing and converted to stress using an elastic modulus of 350 ksi. Table 5 presents the peak values from the dump truck crossings, and Table 6, the M1 tank stress peak values. The maximum stress values for the dump truck and tank were 223 and 297 psi, respectively. Peak displacements for the vehicles were 0.216 and 0.525 in., respectively. It is important to note that these peak responses were due to live load only, and little to no dynamic component was generated during the load test procedures.

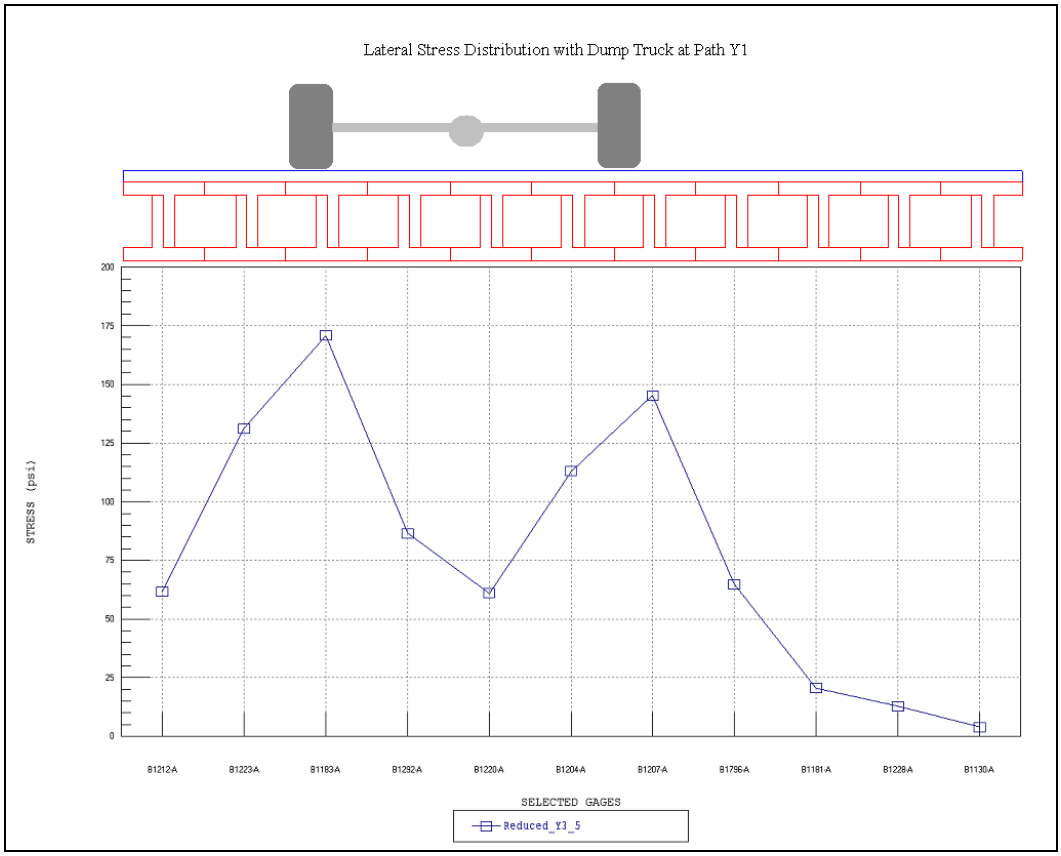

Figure 24. Lateral strain distribution at midspan – dump truck @ Y3.

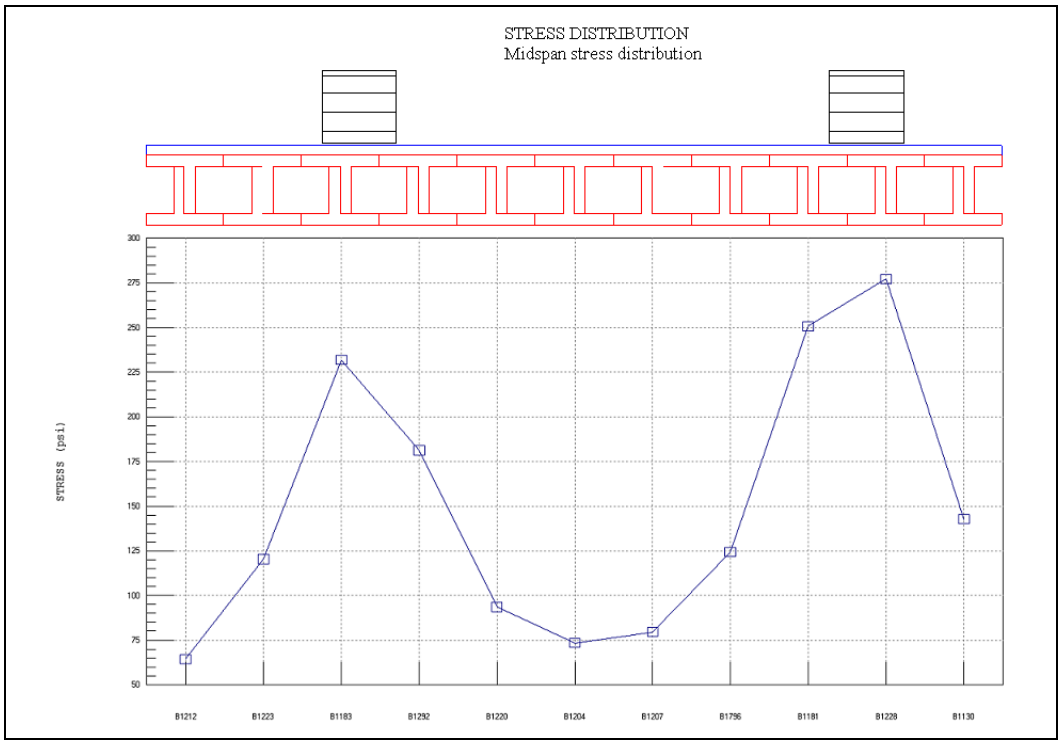

Figure 25. Lateral strain distribution at midspan – M1 tank.

Table 5. Peak stress and displacement during dump truck crossings.

Location	Gage ID	Peak Stress for Each Truck Path, psi					
		Path Y1		Path Y2		Path Y3	
		Min	Max	Min	Max	Min	Max
Pile Cap East Bottom	B1298-A	-2.0	54.6	-2.5	160.3	-1.9	79.5
Pile Cap East Top	B1340-A	-25.2	3.9	-59.2	4.1	-26.7	1.1
Pile Cap West Bottom	B1133-A	-0.5	48.3	-0.9	80.5	-1.2	27.0
Pile Cap West Top	5692-A	-6.5	1.6	-16.0	6.1	-10.8	2.0
Pile East	B1336-A	-92.8	1.7	-77.0	1.7	-49.7	2.3
Pile North	7899-A	-98.4	1.9	-89.6	1.8	-70.7	2.3
Pile South	3878-A	-71.1	1.9	-67.6	2.0	-65.8	2.2
Pile West	B1120-A	-69.3	1.9	-76.0	2.0	-89.3	2.3
Span 2 @ Midspan - Beam 1 - Btm	B1130-A	-14.1	52.2	-5.8	18.5	-1.0	4.1
Span 2 @ Midspan - Beam 1 - Top	8384-A	-27.6	5.6	-7.7	2.9	-2.1	6.0
Span 2 @ Midspan - Beam 10	B1223-A	-6.9	14.7	-13.0	45.2	-20.1	134.1
Span 2 @ Midspan - Beam 11 - Btm	B1212-A	-2.6	5.5	-9.1	23.3	-23.0	73.5
Span 2 @ Midspan - Beam 11 - Top	B1184-A	-2.1	3.7	-7.3	2.6	-30.5	5.0
Span 2 @ Midspan - Beam 2	B1228-A	-16.5	136.9	-12.0	43.8	-5.9	13.7
Span 2 @ Midspan - Beam 3	B1181-A	-21.8	168.7	-17.7	83.0	-11.7	24.1
Span 2 @ Midspan - Beam 4	B1796-A	-22.5	86.5	-20.9	171.5	-16.3	66.2
Span 2 @ Midspan - Beam 5	B1207-A	-22.1	77.0	-20.3	89.6	-18.2	148.4
Span 2 @ Midspan - Beam 5	B1322-A	-14.6	80.2	-14.2	98.7	-20.8	150.8
Span 2 @ Midspan - Beam 6	B1204-A	-21.3	127.7	-23.6	72.5	-18.9	114.8

Table 5. (Continued)

Location	Gage ID	Peak Stress for Each Truck Path, psi					
		Path Y1		Path Y2		Path Y3	
		Min	Max	Min	Max	Min	Max
Span 2 @ Midspan - Beam 6	B1311-A	-15.9	134.4	-13.6	81.2	-12.8	119.4
Span 2 @ Midspan - Beam 7	B1220-A	-19.5	151.9	-21.2	100.1	-22.5	72.1
Span 2 @ Midspan - Beam 8	B1292-A	-17.6	64.8	-24.9	187.9	-24.8	92.1
Span 2 @ Midspan - Beam 8	4050-A	-14.9	85.1	-23.0	223.3	-20.0	113.4
Span 2 @ Midspan - Beam 9	B1183-A	-13.1	31.9	-19.8	97.3	-23.8	174.0
Span 2 @ Pier 1 - Beam 1	5862-A	-20.5	43.4	-9.0	20.9	-1.1	4.1
Span 2 @ Pier 1 - Beam 3	B1382-A	-37.8	74.9	-28.5	35.4	-10.6	12.0
Span 2 @ Pier 1 - Beam 5	B1303-A	-32.9	33.7	-38.9	43.8	-54.3	75.3
Span 2 @ Pier 2 - Beam 1	8861-A	-19.3	35.4	-7.5	13.2	-2.1	2.0
Span 2 @ Pier 2 - Beam 10	B1135-A	-6.5	9.7	-13.3	23.1	-25.7	63.4
Span 2 @ Pier 2 - Beam 11	B1214-A	-1.2	2.6	-3.0	8.6	-10.0	20.3
Span 2 @ Pier 2 - Beam 2	5564-A	-27.5	63.4	-12.4	21.6	-6.5	8.4
Span 2 @ Pier 2 - Beam 3	B1202-A	-34.3	80.9	-24.5	32.2	-10.4	12.2
Span 2 @ Pier 2 - Beam 4	B1351-A	-24.3	38.2	-32.1	78.1	-19.5	23.5
Span 2 @ Pier 2 - Beam 5	4079-A	-27.9	33.6	-30.2	42.0	-35.0	76.3
Span 2 @ Pier 2 - Beam 6	B1376-A	-32.4	50.8	-25.9	30.0	-27.2	48.3
Span 2 @ Pier 2 - Beam 7	B1187-A	-34.0	77.4	-31.1	46.6	-24.3	31.0
Span 2 @ Pier 2 - Beam 8	B1186-A	-18.2	20.3	-26.4	73.2	-18.8	33.8
Span 2 @ Pier 2 - Beam 9	B1203-A	-9.1	11.2	-19.7	23.8	-26.6	51.1
Span 3 @ Abutment - Beam 1	B1310-A	-6.8	30.3	-4.3	14.9	-0.7	8.3

Table 5. (Continued)

Location	Gage ID	Peak Stress for Each Truck Path, psi					
		Path Y1		Path Y2		Path Y3	
		Min	Max	Min	Max	Min	Max
Span 3 @ Abutment - Beam 2	5563-A	-4.3	28.5	-3.9	12.0	-3.0	5.5
Span 3 @ Abutment - Beam 3	B1331-A	-11.2	130.6	-8.8	58.1	-8.3	17.1
Span 3 @ Abutment - Beam 4	B1225-A	-6.3	28.3	-7.8	52.2	-7.2	13.6
Span 3 @ Midspan - Beam 1 - Btm	4118-B	-11.2	55.7	-6.8	21.1	-1.8	7.3
Span 3 @ Midspan - Beam 1 - Top	8368-A	-42.0	4.3	-12.5	3.3	-1.0	5.9
Span 3 @ Midspan - Beam 10	8863-A	-6.7	16.9	-10.8	55.3	-15.1	163.1
Span 3 @ Midspan - Beam 11 - Btm	B1353-A	-5.4	7.7	-9.5	27.9	-14.2	100.4
Span 3 @ Midspan - Beam 11 - Top	B1211-A	-0.7	1.0	-4.2	0.5	-14.5	1.4
Span 3 @ Midspan - Beam 2	B1349-B	-14.1	109.5	-10.7	38.5	-5.8	16.5
Span 3 @ Midspan - Beam 3	B1014-B	-24.1	155.7	-16.4	69.3	-9.3	31.5
Span 3 @ Midspan - Beam 4	B1123-B	-15.6	80.9	-19.8	138.3	-14.0	68.3
Span 3 @ Midspan - Beam 9	8984-A	-8.9	41.0	-15.6	105.3	-24.4	187.2
Span 3 @ Pier 2 - Beam 1	B1210-A	-18.2	39.9	-8.2	18.1	-1.7	1.2
Span 3 @ Pier 2 - Beam 3	B1201-A	-46.9	104.6	-30.1	48.3	-11.2	16.7
Span 3 @ Pier 2 - Beam 5	B1206-A	-27.4	38.5	-32.1	49.4	-44.1	78.1
Span 3 @ Pier 2 - Beam 7	B1290-A	-42.0	74.2	-28.6	46.2	-18.6	36.1
Peak stress		-98.4	191.4	-89.6	223.3	-89.3	187.2

Table 5. (Concluded)

Location	Gage ID	Peak Displacement for Each Truck Path, in.					
		Path Y1		Path Y2		Path Y3	
		Min	Max	Min	Max	Min	Max
Displ Interior Pile @ Pier 2	LV598-A	-0.104	0.002	-0.095	0.002	-0.072	0.002
Displ Span 3 @ Midspan - Beam 1	LV651-A	-0.144	0.005	-0.052	0.005	-0.005	0.005
Displ Span 3 @ Midspan - Beam 2	LV650-A	-0.196	0.005	-0.082	0.006	-0.023	0.006
Displ Span 3 @ Midspan - Beam 3	LV648-A	-0.216	0.005	-0.133	0.007	-0.048	0.008
Displ Span 3 @ Midspan - Beam 4	LV647-A	-0.146	0.007	-0.158	0.007	-0.174	0.011
Displ Span 3 @ Midspan - Beam 5	LV649-A	-0.165	0.005	-0.193	0.007	-0.104	0.012
Displ Span 3 @ Midspan - Beam 6	LV600-A	-0.183	0.005	-0.133	0.005	-0.161	0.005
Peak displacements		-0.216	0.007	-0.193	0.007	-0.174	0.012

Table 6. Peak stress and displacement during M1 tank crossing.

Location	Gage ID	Stress, psi	
		Min	Max
Pile Cap East Bottom	B1298	-5.5	256.7
Pile Cap East Top	B1340	-70.6	8.3
Pile Cap West Bottom	B1133	-14.4	14.1
Pile Cap West Top	5692	-21.5	5.7
Pile East	B1336	-156.5	10.5
Pile North	7899	-167.1	9.5
Pile South	3878	-116.4	5.8
Pile West	B1120	-117.3	5.3
Span 2 @ Midspan - Beam 1 - Btm	B1130	-46.6	151.6
Span 2 @ Midspan - Beam 1 - Top	8384	-87.1	26.4
Span 2 @ Midspan - Beam 10	B1223	-45.2	123.3
Span 2 @ Midspan - Beam 11 - Btm	B1212	-45.4	71.3
Span 2 @ Midspan - Beam 11 - Top	B1184	-32.1	13.8
Span 2 @ Midspan - Beam 2	B1228	-53.0	296.6
Span 2 @ Midspan - Beam 3	B1181	-53.1	267.2
Span 2 @ Midspan - Beam 4	B1796	-44.0	129.4
Span 2 @ Midspan - Beam 5	B1207	-32.1	83.9
Span 2 @ Midspan - Beam 5	B1322	-28.1	68.6
Span 2 @ Midspan - Beam 6	B1204	-30.9	77.5
Span 2 @ Midspan - Beam 6	B1311	-26.5	64.7
Span 2 @ Midspan - Beam 7	B1220	-31.9	96.4
Span 2 @ Midspan - Beam 7	B1087	-30.6	110.7
Span 2 @ Midspan - Beam 8	B1292	-43.8	187.1
Span 2 @ Midspan - Beam 8	4050	-38.1	221.9
Span 2 @ Midspan - Beam 9	B1183	-51.0	235.8
Span 2 @ Pier 1 - Beam 1	5862	-55.7	113.6
Span 2 @ Pier 1 - Beam 3	B1382	-53.4	81.9
Span 2 @ Pier 1 - Beam 5	B1303	-29.7	53.1
Span 2 @ Pier 2 - Beam 1	8861	-68.5	91.5
Span 2 @ Pier 2 - Beam 10	B1135	-34.0	34.0
Span 2 @ Pier 2 - Beam 11	B1214	-14.3	22.0
Span 2 @ Pier 2 - Beam 2	5564	-57.6	124.5
Span 2 @ Pier 2 - Beam 3	B1202	-58.1	91.7
Span 2 @ Pier 2 - Beam 4	B1351	-29.9	45.7
Span 2 @ Pier 2 - Beam 5	4079	-30.7	45.4
Span 2 @ Pier 2 - Beam 6	B1376	-25.2	38.1
Span 2 @ Pier 2 - Beam 7	B1187	-27.9	44.1
Span 2 @ Pier 2 - Beam 8	B1186	-28.1	46.3

Location	Gage ID	Stress, psi	
		Min	Max
Span 2 @ Pier 2 - Beam 9	B1203	-36.1	49.0
Span 3 @ Abutment - Beam 1	B1310	-19.9	81.8
Span 3 @ Abutment - Beam 2	5563	-7.3	56.4
Span 3 @ Abutment - Beam 3	B1331	-18.0	174.7
Span 3 @ Abutment - Beam 4	B1225	-8.0	27.8
Span 3 @ Midspan - Beam 1 - Btm	4118	-37.5	118.6
Span 3 @ Midspan - Beam 1 - Top	8368	-116.6	27.3
Span 3 @ Midspan - Beam 10	8863	-36.6	146.4
Span 3 @ Midspan - Beam 11 - Btm	B1353	-36.1	85.1
Span 3 @ Midspan - Beam 11 - Top	B1211	-14.9	4.5
Span 3 @ Midspan - Beam 2	B1349	-35.9	168.1
Span 3 @ Midspan - Beam 3	B1014	-49.3	239.7
Span 3 @ Midspan - Beam 4	B1123	-31.7	107.4
Span 3 @ Midspan - Beam 9	8984	-42.3	268.8
Span 3 @ Pier 2 - Beam 1	B1210	-75.8	96.5
Span 3 @ Pier 2 - Beam 3	B1201	-84.0	107.5
Span 3 @ Pier 2 - Beam 5	B1206	-39.5	45.9
Span 3 @ Pier 2 - Beam 7	B1290	-35.4	42.6
Peak stress values		-167.10	296.60

Location	Gage ID	Displacement, in.	
Displ Interior Pile @ Pier 2	LV598	-0.203	0.007
Displ Span 3 @ Midspan - Beam 1	LV651	-0.449	0.021
Displ Span 3 @ Midspan - Beam 2	LV650	-0.525	0.022
Displ Span 3 @ Midspan - Beam 3	LV648	-0.440	0.022
Displ Span 3 @ Midspan - Beam 4	LV647	-0.180	0.016
Displ Span 3 @ Midspan - Beam 5	LV649	-0.271	0.019
Displ Span 3 @ Midspan - Beam 6	LV600	-0.159	0.016
Peak displacements		-0.525	0.022

4 Modeling, Analysis, and Data Correlation

Discussion

All of the information discussed in Chapter 3 was determined by simply viewing the field data and was used by an engineer to get a good understanding of the structural responses. This information was then used to help generate a representative finite element model (shown in Figure 26. Details regarding the structure model and analysis procedures are provided in Table 7.

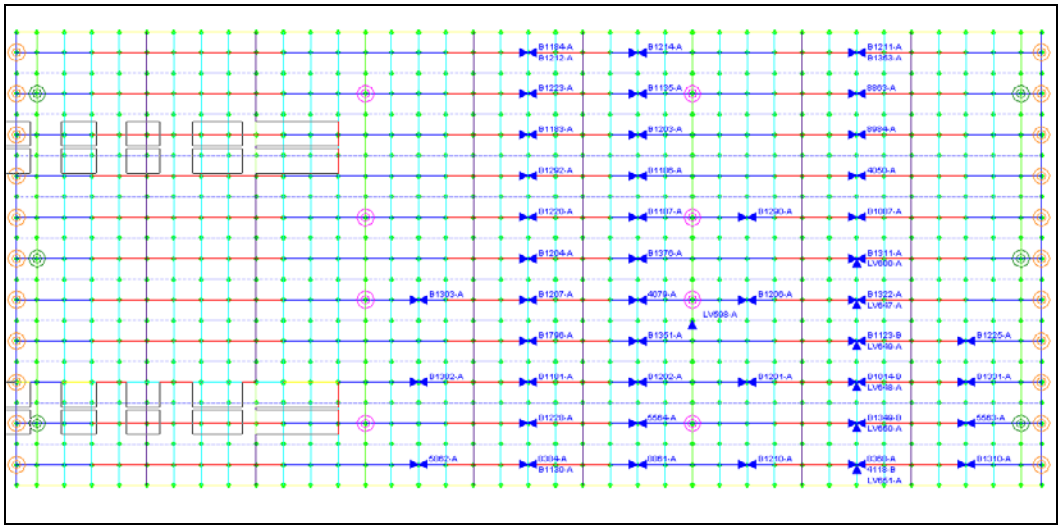

Figure 26. Finite element model of superstructure.

Once the model was developed, the load testing procedures were essentially "reproduced" using the BDI WinSAC structural analysis and correlation software. Two-dimensional "footprints" of each loading vehicle were applied to the top surface of the model along the same paths that the actual test vehicles crossed the bridge. A direct comparison of strain values on the structure was then made between the analytical predictions and the experimentally measured results. The initial model was then "calibrated" by modifying various properties and boundary conditions until the results matched those measured in the field. A complete outline of this process is provided in Appendix E.

Table 7. Analysis and model details.

Analysis Type	Linear-elastic finite element - stiffness method
Model Geometry	Planer grillage composed of frame elements, nodes, and springs
Nodal Locations	Nodes placed at all bearing locations Nodes at each deck element intersection (12-in. intervals)
Model Components	Frame elements for all beams, deck boards, and bents Spring elements at each pile location
Live Load	2-D footprint of test dump truck consisting of 10 vertical point loads and the M1 tank. The truck path was simulated by series of load cases with the truck moving at 1-ft increments.
Dead Load	Self-weight of structure
Total Number of Strain Comparisons	55 measurement locations x 162 load positions = 8910 strain comparisons
Model Statistics	897 Nodes 2224 Elements 11 Cross section/Material types 162 Load cases 55 Gage locations
Adjustable Parameters for Model Calibration	1. RPL modulus for all elements 2. Effective moment of inertia of beams, +M and –M 3. Effective moment of inertia of bents 4. Vertical stiffness of pile springs 5. Horizontal resistance of pile springs

The goal of the finite element analysis is to obtain a model that can simulate the structural responses obtained during the load test and then provide a basis for load rating standard design and rating loads. An iterative process of response comparisons and model calibrations was performed until an acceptable match was obtained. The process of model calibration included identification of various aspects of the structural behavior, such as the effective lateral stiffness, continuity of the beams over the piers, effective end restraint, and general consistency of behavior at various points. The primary limitation in the analysis was that it was linear-elastic. Fortunately, bridge structures are generally linear-elastic up to the operating limit, which is well beyond the design loads. In some cases, structural bearings can generate nonlinear end restraint, in which case a best-fit linear approximation is obtained. An additional limitation of the analysis related to this structure is that the linear-elastic analysis cannot generate the time-dependent visco-elastic responses observed with loads applied for a substantial duration. Fortunately, most vehicle crossings are short duration, and the viscous response magnitude is relatively small compared with the linear response at the allowable stress level.

In this case, the majority of the model calibration effort was spent in simulating the flexibility of the piles, the flexibility of the deck, and the actual truck paths. Because of the close beam spacing and flexible deck, the measured responses were very sensitive to small changes in lateral truck position. Variations in the truck path, as small as 4 in. left or right, had a significant effect on each beam's stress history. Because of this, it was easier to match the dump truck data, as it was easier for the dump truck to travel in a straight line than it was for the tank. Even then, small variations occurred along each path, so less effort was put into matching each perfectly, and more effort was put into matching maximum stresses at each instrumented cross section.

Model calibration results

Various stiffness parameters were modified to obtain the best possible match between the measured and computed responses. In this case, the model was calibrated based on strain and displacement measurements. The goal of the calibration was to be able to accurately match the response value at every gage location for every load condition as closely as possible—with the ability to match the minor load responses being just as important as matching the maximum values. This ensured that the model had the same load transfer characteristics as the real structure. Realizing that some inaccuracy would always be present due to variations in truck path, a secondary goal was to match the peak stress at each instrumented cross section. The optimization process relied on an engineer's ability to determine what stiffness values might be different than what was initially assumed. The engineer was also required to define reasonable upper and lower limits for each variable. This process entailed visual examination of the response comparison histories and determining what structural parameters would influence the response behavior so as to obtain a better correlation. An optimization algorithm built into the analysis program automated the iterations so as to obtain the stiffness values that provide the best solution. Many manual iterations were required to determine the correct set of properties to adjust, and it was a function of the engineer's experience and the complexity of the structure.

The following outline describes what stiffness parameters were adjusted, along with discussions on the effect on the structural performance. Following the optimization procedures, the model produced a 0.9745 correlation coefficient, which can be considered a good match for this structure. The parameter and model accuracy values used in the initial

model and obtained for the final model are provided in Table 8. Appendix G contains a description of each error value.

Table 8. Model accuracy and parameter values.

Modeling Parameter		Initial Model Value	Final Model Value
RPL modulus - E	(ksi)	350	350
Beam stiffness - I	(in.^{4})	6876	10280
Deck stiffness - I	(in.^{4})	27	27
Deck @ diaphragm locations – I	(in.^{4})	27	672
Pile bearing stiffness – Fz	(k/in.)	10000	121
Pile horizontal stiffness @ pier Fx & Fy	(k/in.)	0	10
Pile horizontal stiffness @ abut Fx & Fy	(k/in.)	0	20
Vertical end-plate bearing – Fx	(k/in.)	0	63
Error Parameters – 36-ton Dump Truck		**Initial Model Value**	**Final Model Value**
Absolute error		49062	18814
Percent error		43.6	5.1
Scale error		6.3	2.8
Correlation coefficient		0.7727	0.9745
Error Parameters – M1 tank			**Final Model Value**
Absolute error			10752
Percent error			9.1
Scale error			8.3
Correlation coefficient			0.9542

RPL material stiffness

The modulus of the plastic material provided by the design specifications was 350 ksi. Results from early optimization cycles ranged from 350 to 400 ksi. There appeared to be some variation in stiffness for the deck and the beams. It could not entirely be determined if the variations were related to material properties or to construction/geometry effects. To simplify the problem, it was assumed that the modulus for all components was 350 ksi and that any variation in stiffness was a geometric effect (i.e., composite action between the deck and beams). One of the challenges here was that the modulus was approximately 1/10th of concrete and 1/100th of steel.

Deck stiffness

The modulus value of 350 ksi provided the best overall lateral distribution for the deck. In general, there was no justification for additional geometric stiffness. One exception was that the location of the internal blocking members and the transverse decking member attached to the bottom did provide additional load transfer through the deck. This was generated primarily by the axial-force couple obtained from the top deck elements and the bottom transverse element. This stiffening effect is therefore dependent on the tightness of the deck screws and may not be a permanent condition.

Beam stiffness

Based on the deck properties it was assumed that a modulus of 350 ksi was appropriate; however, the beams tended to be stiffer than initially modeled. The additional stiffness was therefore assumed to be due to geometric properties. Slight composite behavior between the deck and the beams appeared to be present. Providing the composite behavior in the model did in fact improve the correlation with the load test data. The level of composite behavior was relatively minor since it was generated by planks and not a continuous slab. It was also apparent the composite behavior was highly variable. While it was important to identify the effect of the deck attachment, the composite behavior should not be accounted for during load rating procedures. It is likely that the deck screws will loosen with time and normal usage of the deck.

Pile stiffness

This bridge was somewhat unusual in that the vertical stiffness of the piles had a significant effect on the live-load responses. Normally, the foundation responses are negligible compared with the superstructure responses. In this case, the piles had displacements on the same order of magnitude as those obtained from the beam flexure. The piles were modeled with elastic spring elements that had stiffness terms in the vertical and horizontal directions. The resulting vertical spring stiffness was slightly greater than AE/L of the piles where A is the cross-sectional area, E is the modulus of elasticity, and L is the length of the pile. It would appear that the majority of the pile resistance was therefore obtained from the toe resistance, with minor contribution from skin friction. The piles

also provided significant horizontal resistance. The interior piers were simulated based on $12EI/L^3$, with I being the moment of inertia and L being the length of pile above grade. Additional horizontal resistance was present at the abutments due to the soil pressing against vertical end plates.

Tank wheel loads

Due to the flexibility of the deck and the close beam spacing, the actual width of each wheel load had to be simulated. Normally, each wheel load is applied as a single point load. While this worked reasonably well with the dump truck, it was necessary to apply each tank wheel load as two side-by-side wheel loads, similar to dual tires. It was assumed that the tank tracks provided little load distribution longitudinally but provided a relatively wide foot print. By modeling each wheel load as two point loads separated by 12 in., the model correlation was greatly improved.

Following the optimization procedures, the model produced acceptable accuracy. The parameter and model accuracy values used in the initial model and obtained for the final model are provided in Table 8.

It was noted that the results of the M1 tank analysis were not as accurate as the dump truck responses. The primary reason is that the actual truck path traveled by the M1 was more variable and more difficult to model. It is also likely that the responses from the M1 are less linear because of the low material modulus and the relatively high stress. A resulting correlation of 0.95 is still reasonable, and the fact that the model results for the M1 crossing were conservative was verified.

5 Load Rating Procedures and Results

The goal of producing an accurate model was to predict the structure's actual live-load behavior when subjected to design or rating loads. This approach is essentially identical to standard load rating procedures, except that a “field-verified” model was used to determine live-load responses instead of a beam-line analysis with load distribution factors. Appendix F provides a detailed outline of the load rating procedures.

Once the finite element model was calibrated to field conditions, engineering judgment was used to address any optimized parameter that may change over time or that may be unreliable with heavy loads or future deterioration. In the case of this bridge, the majority of the optimized parameters remained the same for rating purposes. Some changes were made to add a level of conservatism to the ratings. The effective beam stiffness (I) was reduced to the noncomposite value since it was conceivable that the deck screws would loosen over time and with repeated load cycles. The additional lateral load transfer provided by the bottom decking member located at the rail post locations was also eliminated, as this condition was also dependent on the tightness of the deck screws.

Because the bridge was constructed of RPL components, there are no applicable American Association of State Highway and Transportation Officials (AASHTO) specifications for the material. Basic material properties were provided by the bridge designer and the RPL manufacturer. The response behavior of the material was defined as elastoplastic meaning it had primarily elastic behavior combined with time-dependent fluid properties. Allowable stress and ultimate stress values were given for axial, flexure, and shear responses. The allowable stress values corresponded to stress limits that the members could withstand for a long period of time (25 years) and still return to their original state after the load was removed. The ultimate stress values were generally three to four times greater than the allowable stresses. Because of the extremely low modulus compared with most structural materials, displacements associated with ultimate stresses would be extremely large, and the responses would be well out of the linear range. Therefore, the most appropriate load rating method was determined to be allowable stress. The allowable stresses provided were assumed to be consistent with inventory load rating limits

because it was at a stress level that could be applied repeatedly and remain in service for a long duration.

For allowable stress design (ASD), the entire factor of safety is built into the stress limit. This means that the dead- and live-load responses are given the same level of importance and reliability, and a load factor of 1.0 is applied to both load effects. While this is generally not the case, it suggests a factor of safety against collapse of at least 3. Material properties provided by the bridge designer are listed in Table 9. The shear and moment member capacities computed for the beams and bents are provided in Table 10and Table 11, respectively.

Table 9. RPL material properties.

Response Type	Value
Elastic modulus, ksi	350
Allowable compression parallel to grain, psi	1000
Allowable flexural stress, psi	600
Allowable shear strength parallel to grain, psi	350
Unit weight, pci	0.032

Table 10. Allowable moment capacities.

Member	F_b (ksi)	Y_b (in.)	I_x (in.^{4})	S_{xb} (in.^{3})	ϕM_n (kip-in.)
Beam +M	0.60	9	6876	764	458
Beam -M	0.60	9	6876	764	458

Table 11. Allowable shear capacities.

Member	F_{vh} (ksi)	T (in.)	I_x (in.^{4})	Q (in.^{3})	ϕV_n (kip)
Beam	0.35	5	6876	495	24.3

Load ratings were performed on the calibrated model according to AASHTO Load and Resistance Factor Rating (LRFR) methods using the allowable stress/serviceability limit state. An impact factor of 33% was applied to all live-load responses.

Because of the narrow width of the bridge, loading was limited to single-lane loading. Several load paths were applied to obtain maximum responses for each component, but there were no combined truck paths.

Furthermore, since there was no room for pedestrians or additional equipment on the bridge when a truck was crossing, the AASHTO LRFD factor for single-lane loading of 1.2 was not applicable. A condition factor of "good" was selected because the bridge was new. A listing of the load and resistance factors is provided in Tables F1 and F2.

The configuration and layout for frequently used AASHTO and military vehicles used for load rating are given in Appendix F. The dead load of the structure was applied automatically within the program based on the material unit weight and the member cross-sectional dimensions. The applied load paths for each loading vehicle are listed in Table 12.

The load rating factors for the four AASHTO vehicles and the MLC tracked and wheeled vehicles for moment and shear are in Table 13 and 14, respectively. The values were very similar for most load configurations. For the vehicles examined for this report, the controlling rating factor was always flexure of the RPL beams. The critical load rating factors and corresponding load limits from Tables 13 and 14 are in Table 15. Table 16 contains an example computation of an inventory load rating factor for a midspan beam element with HS-20 loading, and Table 17 is an example computation of an inventory load rating factor for a midspan beam element with MLC (tracked) loading.

It should be noted that the above load ratings are applicable only to the superstructure. It is assumed that the pile bearing capacities are sufficient to handle the maximum superstructure loads.

Table 12. Load path locations.

Rating Vehicle	Paths	Location
AASHTO and Military Rating Vehicles	1	Driver tire 2 ft from edge of roadway
	2	Driver tire 3 ft from edge of roadway
	3	Driver tire 4 ft from edge of roadway

Table 13. Vehicle rating factors and responses – positive moment in RPL beams.

Truck	Location	Maximum Response		Inventory Limits	
		DL (K-in.)	LL (K-in.)	RF	Tons
HS-20	Midspan beam	22.02	207.01	1.62	58.3
Type 3	Midspan beam	22.02	143.68	2.34	58.5
Type 3S2	Midspan beam	22.02	129.40	2.59	93.2
Type 3-3	Midspan beam	22.02	118.28	2.84	113.6
MLC (tracked)[1]	Midspan beam	22.02	330.03	1.02	73.4
MLC (wheeled)[2]	Midspan beam	22.02	288.58	1.10	88.0

[1] MLC (tracked) based on M1 tank.

[2] MLC (wheeled) based on hypothetical MLC 80 with maximum single axle.

Table 14. Vehicle rating factors and responses – shear in RPL beams.

Truck	Location	Maximum Response		Inventory Limits	
		DL, kips	LL, kips	RF	Tons
HS-20	Beam @ pier	0.86	11.10	1.62	58.3
Type 3	Beam @ pier	1.91	7.10	2.62	65.5
Type 3S2	Beam @ pier	1.91	6.49	2.65	95.4
Type 3-3	Beam @ pier	1.91	5.85	2.95	118.0
MLC (tracked)[1]	Beam @ pier	1.91	16.25	1.06	76.3
MLC (wheeled)[2]	Beam @ pier	1.91	12.16	1.42	113.6

[1] MLC (tracked) based on M1 tank.

[2] MLC (wheeled) based on hypothetical MLC 80 with maximum single axle.

Table 15. Critical load rating factors and weights.

Rating Vehicle	Location	LRFR - Inventory	
		RF	Tons
HS-20	RPL Beams: + Moment	1.62	58.3
Type 3	RPL Beams: + Moment	2.34	58.5
Type 3S2	RPL Beams: + Moment	2.59	93.2
Type 3-3	RPL Beams: Shear	2.84	113.6
MLC (tracked)[1]	RPL Beams: + Moment	1.02	73.4
MLC (wheeled)[2]	RPL Beams: + Moment	1.10	88.0

[1] MLC Tracked computed from 72-ton M1 tank.

[2] MLC Wheeled computed from hypothetical case with maximum single axle.

Table 16. Rating factor calculation for HS-20.

Moment capacity available for dead load and live load at midspan.	M_{Cap}	458.0	kip-in.
Dead-load effect due to self-weight of structure	DW	22.02	kip-in.
Live-load effect (HS-20)	LL	207.01	kip-in.
Resistance factor for RPL in flexure	Φ_b	1.0	
Condition factor (good)	φ_c	1.0	
System factor (multiple girders/slab)	φ_s	1.0	
ASD dead-load factor	γ_{DC}	1.0	
ASD live-load factor	γ_{LL}	1.0	Inventory
Dynamic influence (impact) factor	IM	1.30	

Using Equation F1:

RF_{Inv} = [(1.0)(1.0)(458.0) – (1.0*22.02)] / (1.0*207.01*1.30) = **1.62**

Table 17. Rating factor calculation for M1 tank (tracked).

Moment capacity available for dead load and live load at midspan	M_{Cap}	458	kip-in.
Dead-load effect due to self-weight of structure	DW	22.02	kip-in.
Live-load effect (MLC70)	LL	330.03	kip-in.
Resistance factor for RPL in flexure	Φ_b	1.0	
Condition factor (good)	φ_C	1.0	
System factor (multiple girders)	φ_S	1.0	
LRFR dead-load factor for structural components and attachments	γ_{DC}	1.0	
Live-load factor	γ_{LL}	1.0	Inventory
Dynamic influence (impact) factor	IM	1.30	

Using Equation F1:

RF_{Inv} = [(1.0)(1.0)(458.0) – (1.0*22.02)] / (1.0*330.03*1.30) = **1.02**

6 Conclusions and Recommendations

Load tests were performed with a 72-kip dump truck and a 144-kip M1 tank crossing an RPL bridge. Results from both sets of tests indicated that the structure generally performed in a normal linear-elastic manner. Relatively small visco-elastic responses were observed with the heavier M1 tank. A long-duration static test with the tank showed that it took several minutes for deflections to stop moving while the bridge was loaded, and a similar amount of time for the measurements to return to zero after the load was removed. This behavior appeared to be consistent with the material properties of RPL and the intended design.

One difference between the load test results on the RPL bridge and other bridge structures was that strain and displacement magnitudes were relatively high. While this was expected due to the low modulus of the material, the notable observation was the amount of displacement induced in the substructure. Normally, bridge foundations have negligible deformation compared with the superstructure responses. In this case, the pile deflections were approximately 50% of the beam deflections. This is not seen as a problem with the bridge, particularly since it is single lane, the spans are short, and the bridge has no pedestrian traffic. However, it will be interesting to determine if there are any unintended long-term consequences due to the large deflections.

Load ratings for this bridge were computed using an allowable stress method. Because of the material properties, this was the only applicable method. The allowable stresses provided were within the linear response range and were associated with a stress limit where all deformations could be recovered after a 25-year load application. A load rating based on ultimate load would have been difficult because the responses would have been extremely nonlinear with large deflections. The load rating results indicated that the bridge performed as well as or better than designed. The inventory load rating factor for the HS-20 vehicle was 1.62, indicating it can handle HS-32. The load rating factor for the 144-kip M1 tank was 1.02, which provides a military load classification of MLC 73.

It is important to note that the load test, analysis, and load rating results are primarily an evaluation of the superstructure (beams and bent). While

deflections of the piles were measured and maximum reaction loads were determined for each pile, the load test does not provide insight concerning the capacity of the piles. The design notes for the piles indicated an allowable load of 40 kips and an ultimate load of at least 120 kips per pile. The specified allowable load per pile provides a lower load rating than obtained for the superstructure. The ultimate load capacity is sufficient to obtain the necessary load rating using LRFD methods. Notes from the pile-driving contractor indicated that the piles were driven to 75 kips. It is assumed that this load limit corresponds to an allowable load and that the ultimate load would be at least three times this value. If this is the case, the pile capacities are well beyond the superstructure load limit. The allowable pile capacity necessary to be approximately equal to the allowable superstructure capacity would be 50 kips per pile.

The load rating factors and conclusions presented in this report are provided as recommendations based on the structure's response behavior and condition at the time of load testing. The structure was brand new and considered to be in good condition. Any structural degradation or damage must be considered in future load ratings.

References

American Association of State Highway and Transportation Officials (AASHTO). 2003. *Manual for the condition evaluation and load and resistance factor rating (LRFR) of highway bridges*. Washington, DC.

_____. 2004. *AASHTO LRFD bridge design specifications (includes 2005 and 2006 interims)*. 3d ed. Washington, DC.

Commander, B. 1989. An improved method of bridge evaluation: comparison of field test results with computer analysis. MS thesis, Univ. of Colorado, Boulder.

Department of the Army. 2002. *Military nonstandard fixed bridging*. Field Manual 3-34.343. Washington, DC.

Gerstle, K. H., and M. H. Ackroyd. 1990. *Behavior and design of flexibly-connected building frames*. (AISC) *Engineering Journal* 27(1):22–29.

Goble, G., J. Schulz, and B. Commander. 1992. Load prediction and structural response. Final report FHWA DTFH61-88-C-00053. University of Colorado, Boulder.

Lichtenstein, A. G. 1995. *Bridge rating through nondestructive load testing*. Technical Report NCHRP Project 12-28(13)A. Washington, DC: National Cooperative Highway Research Program, Transportation Research Board.

Schulz, J. L. 1989. Development of a digital strain measurement system for highway bridge testing. MS thesis, University of Colorado, Boulder.

_____. 1993. In search of better load ratings. *Civil Engineering (ASCE)* 63(9):62–65.

Appendix A: Measured and Computed Stress and Displacement

While statistical terms provide a means of evaluating the relative accuracy of various modeling procedures or helping to determine the improvement of a model during a calibration process, the best conceptual measure of a model's accuracy is by visual examination of the response histories. The graphs presented as Figures A1–42 contain measured and computed strain histories from each truck path. In each graph of strain versus longitudinal front axle position, the continuous lines represent the measured strain at the specified gage location as a function of truck position as it traveled across the bridge. Computed strains are shown as markers at discrete truck intervals.

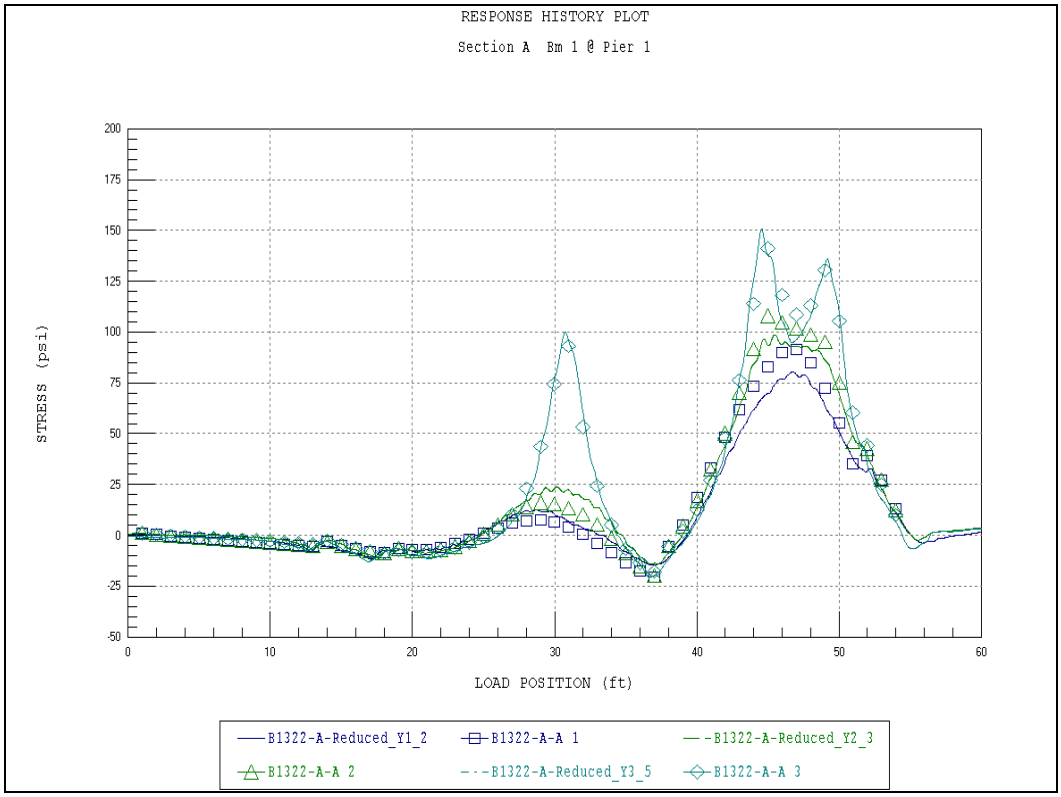

Figure A1. Strain comparison – Sec A – Beam 1.

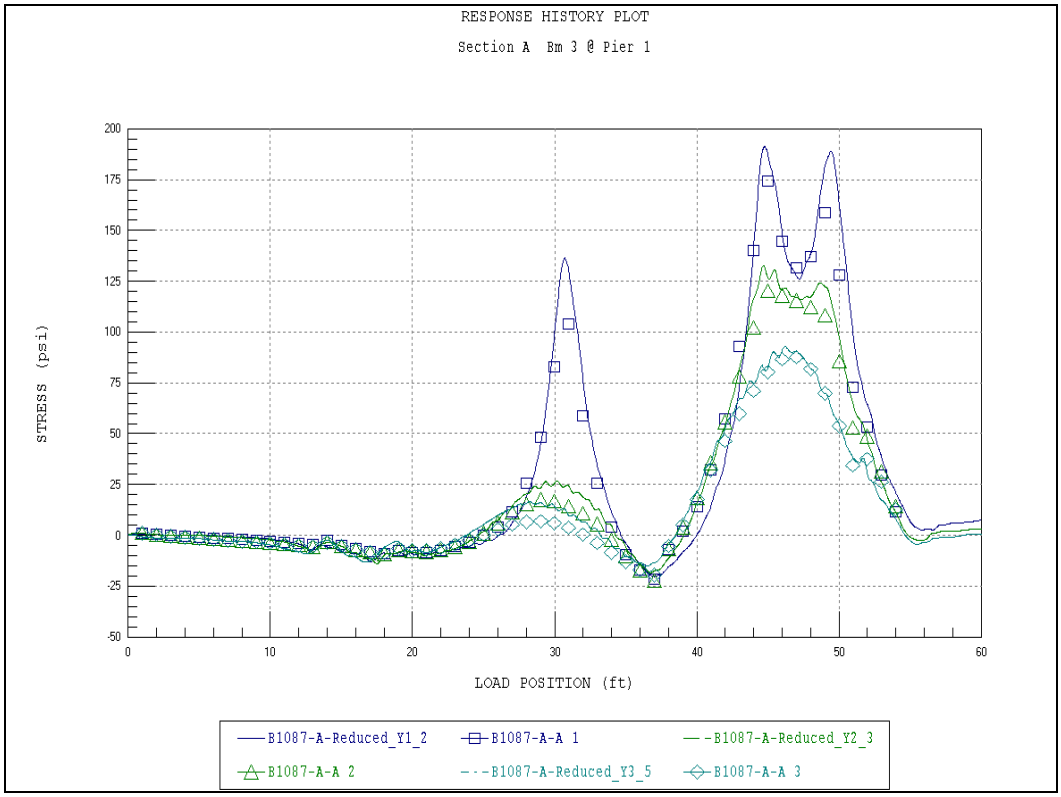

Figure A2. Strain comparison – Sec A – Beam 3.

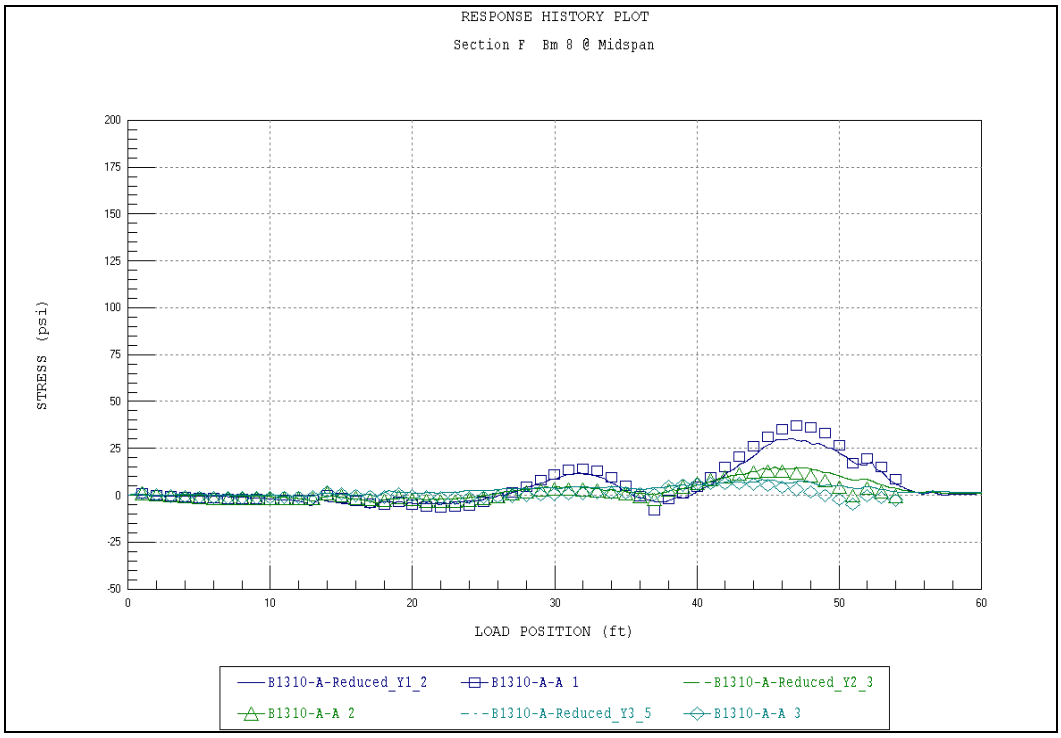

Figure A3. Strain comparison – Sec F – Beam 8.

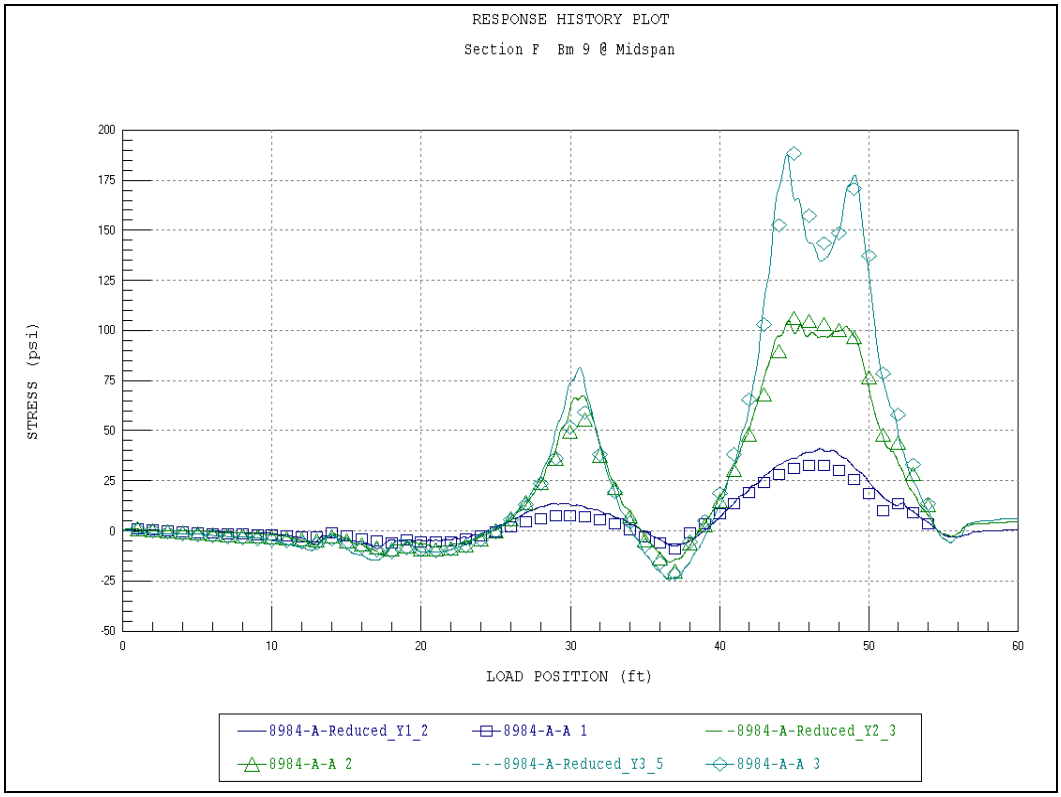

Figure A4. Strain comparison – Sec F – Beam 9.

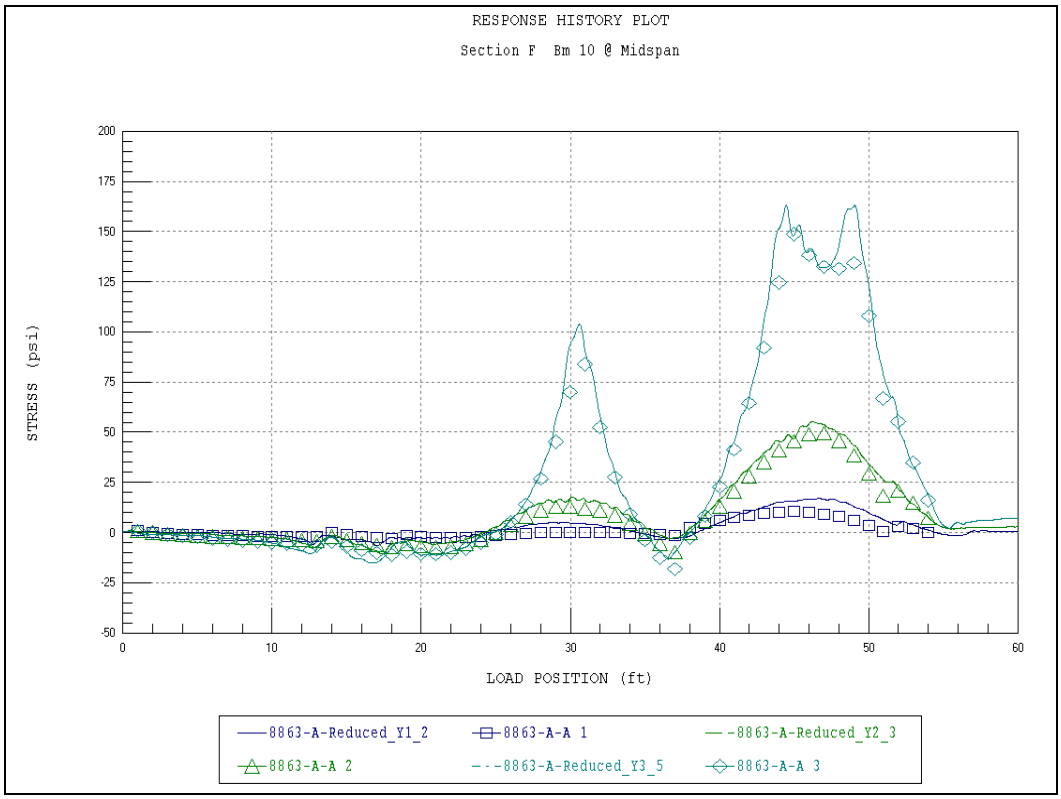

Figure A5. Strain comparison – Sec F – Beam 10.

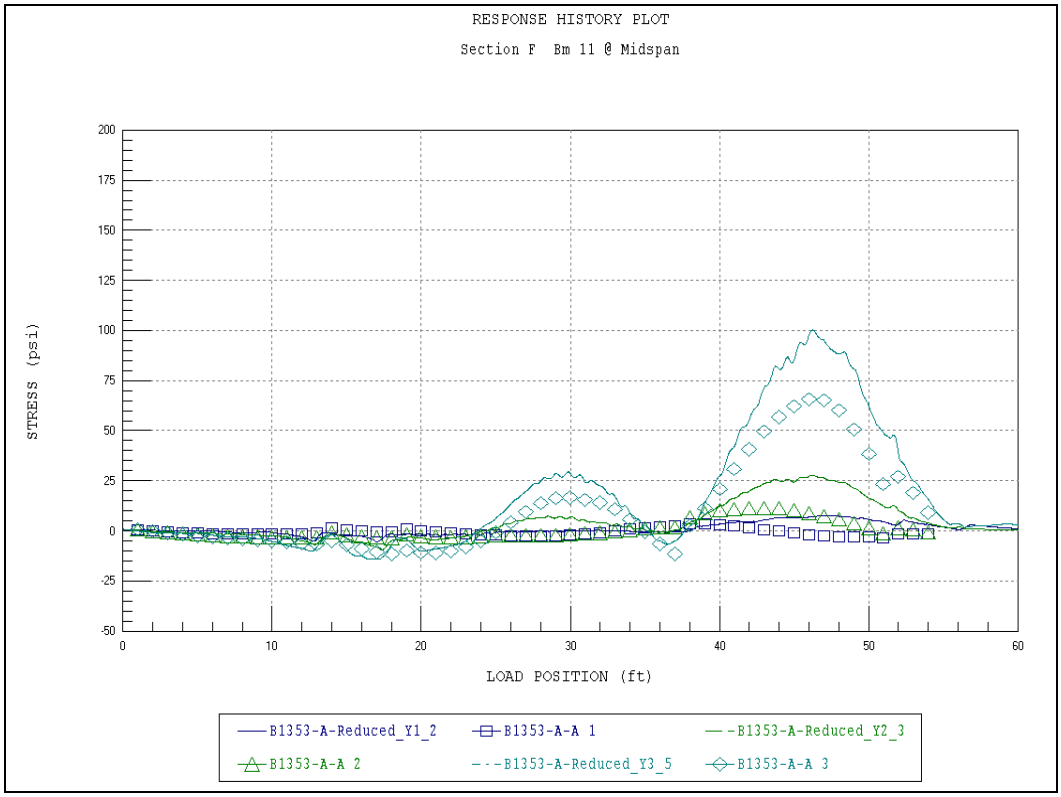

Figure A6. Strain comparison – Sec F – Beam 11.

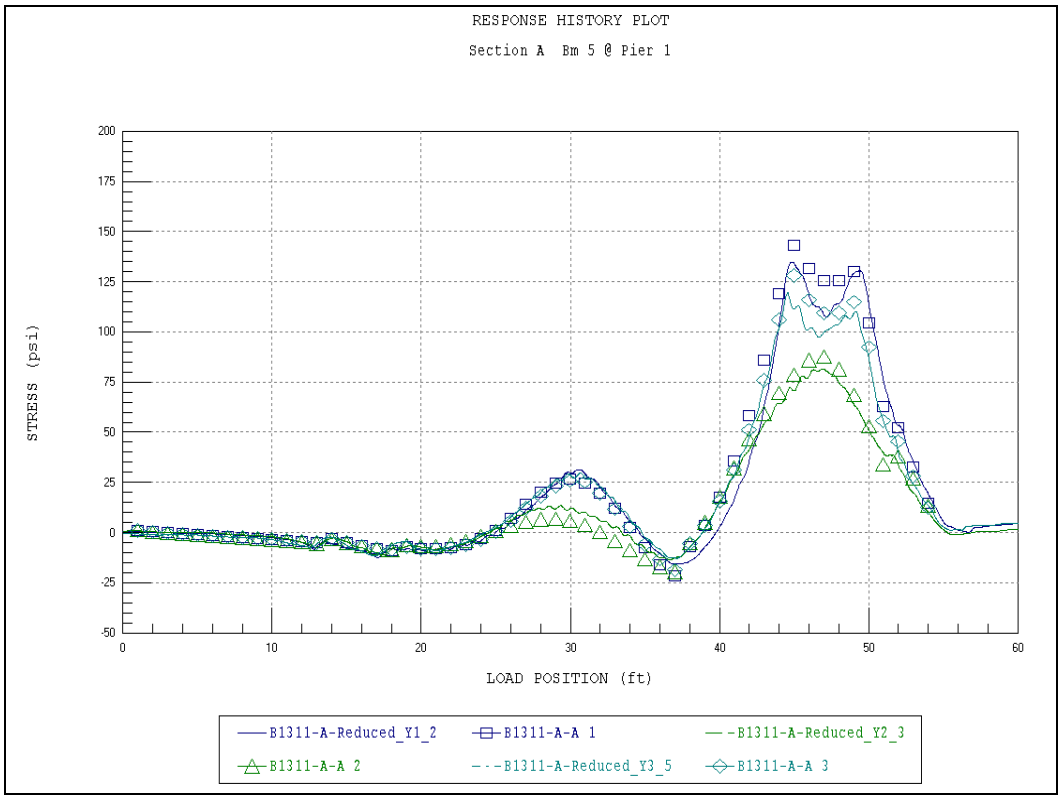

Figure A7. Strain comparison – Sec A – Beam 5.

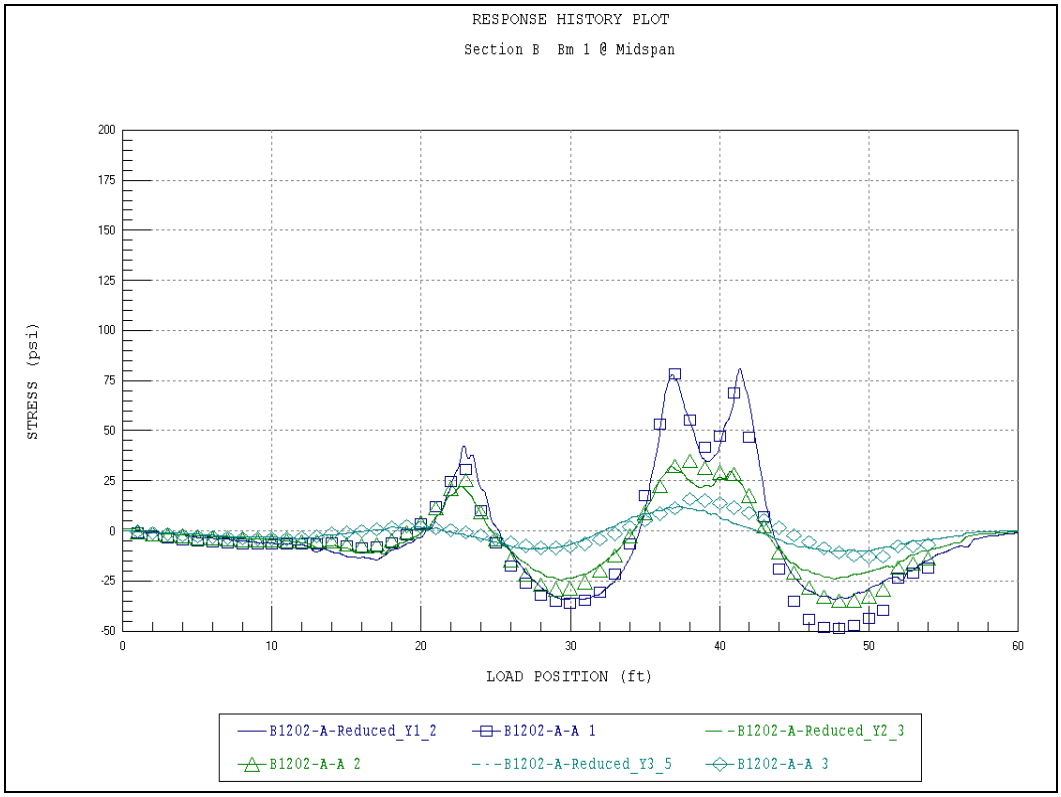

Figure A8. Strain comparison – Sec B – Beam 1.

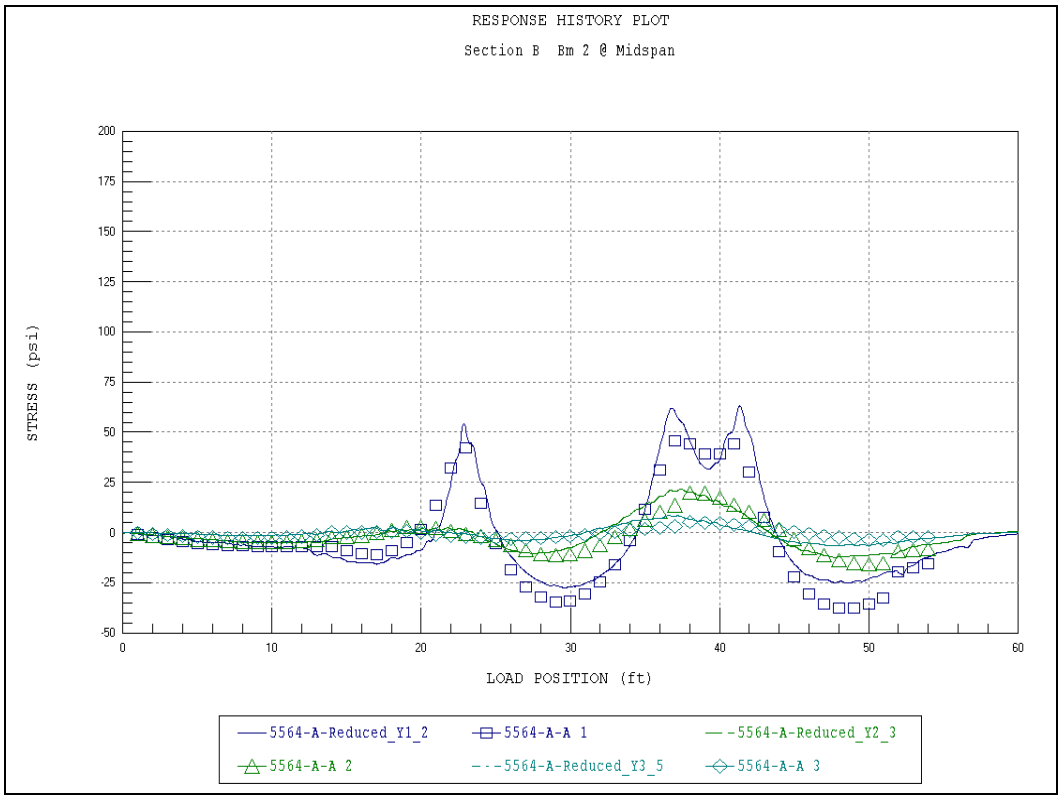

Figure A9. Strain comparison – Sec B – Beam 2.

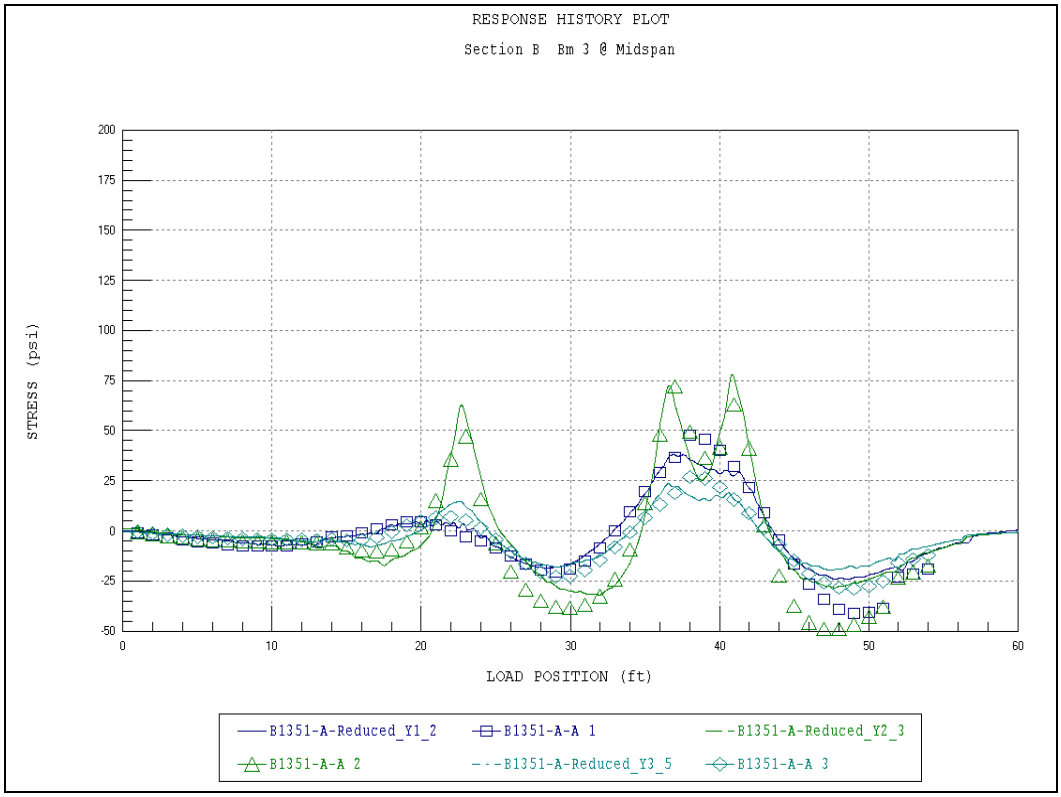

Figure A10. Strain comparison – Sec B – Beam 3.

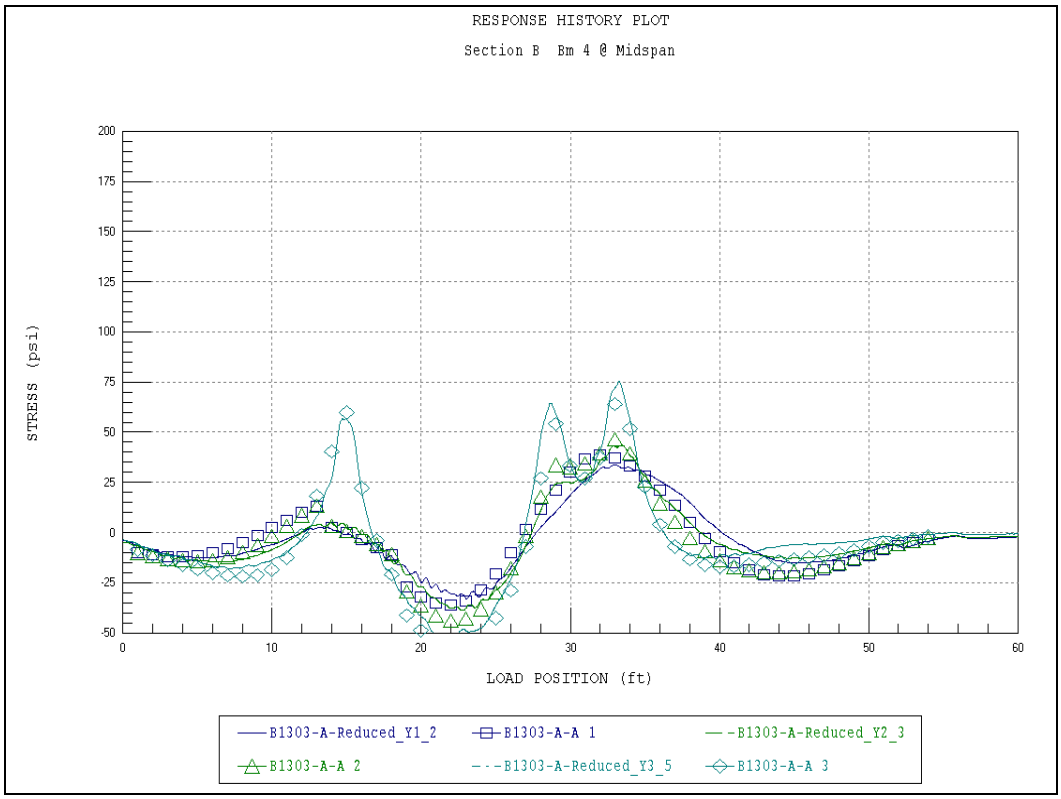

Figure A11. Strain comparison – Sec B – Beam 4.

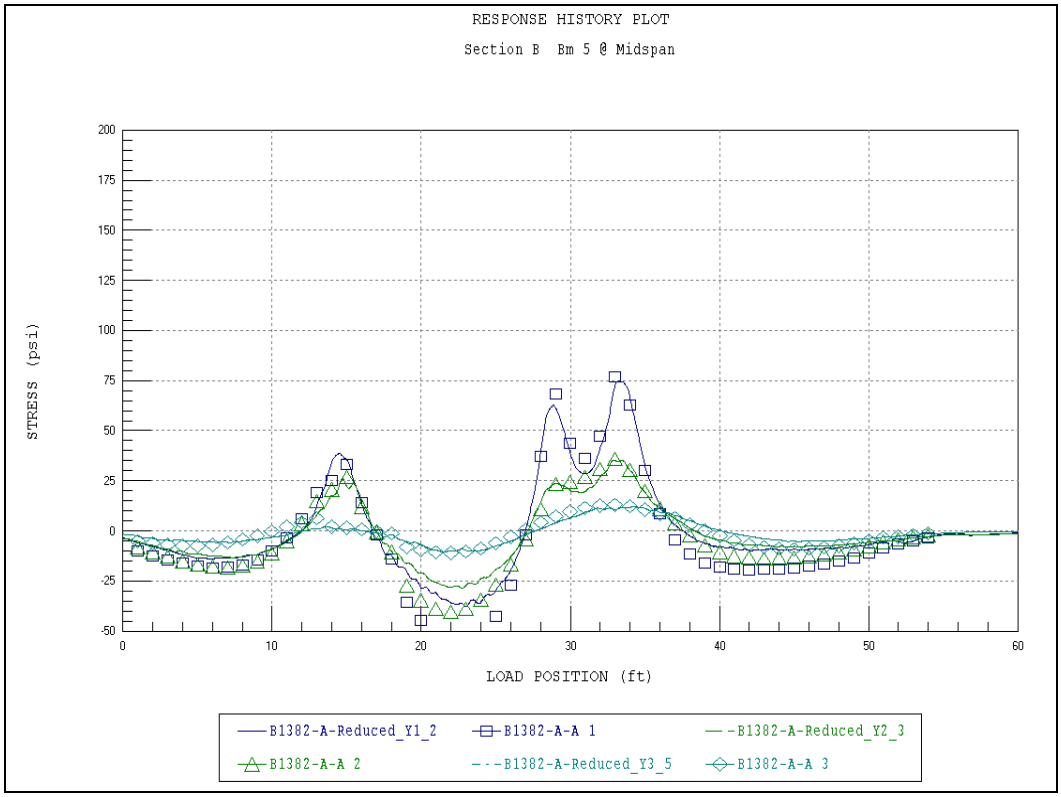

Figure A12. Strain comparison – Sec B – Beam 5.

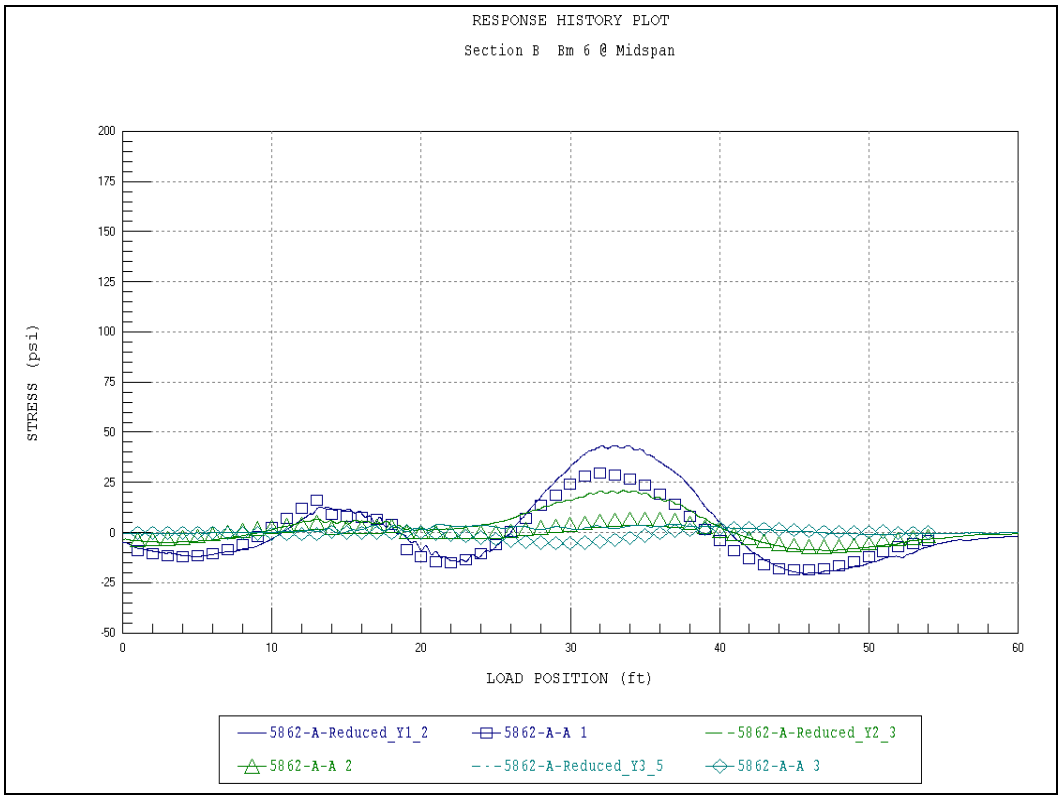

Figure A13. Strain comparison – Sec B – Beam 6.

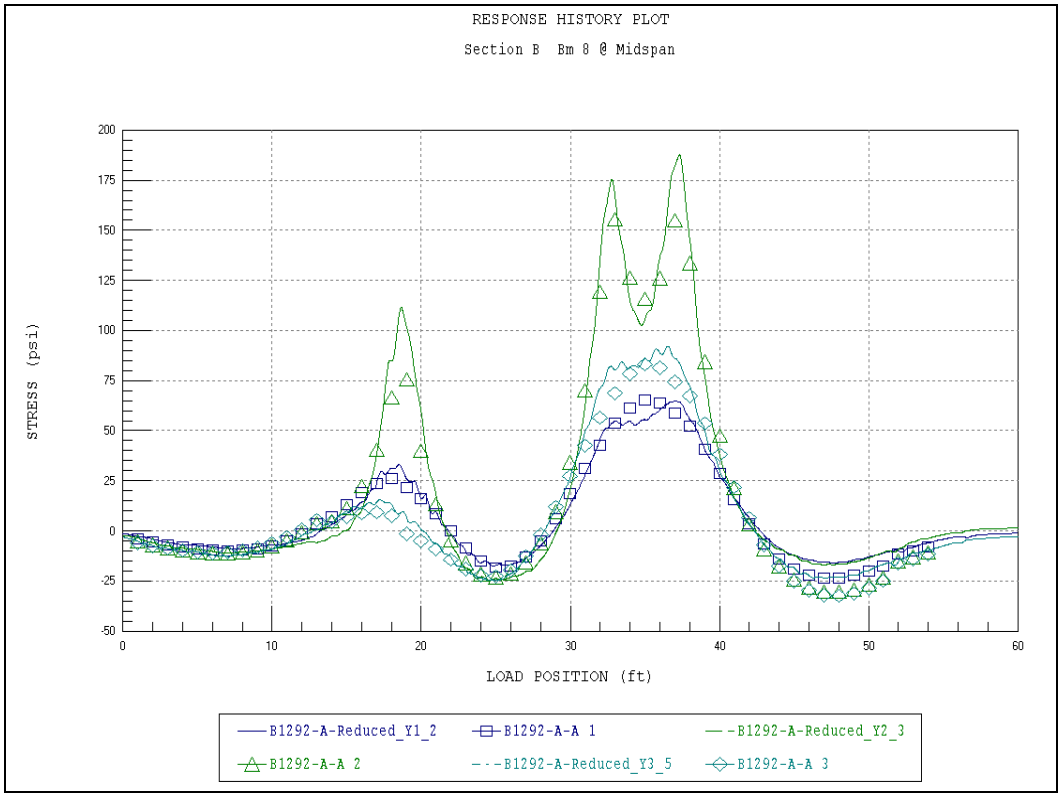

Figure A14. Strain comparison – Sec B – Beam 8.

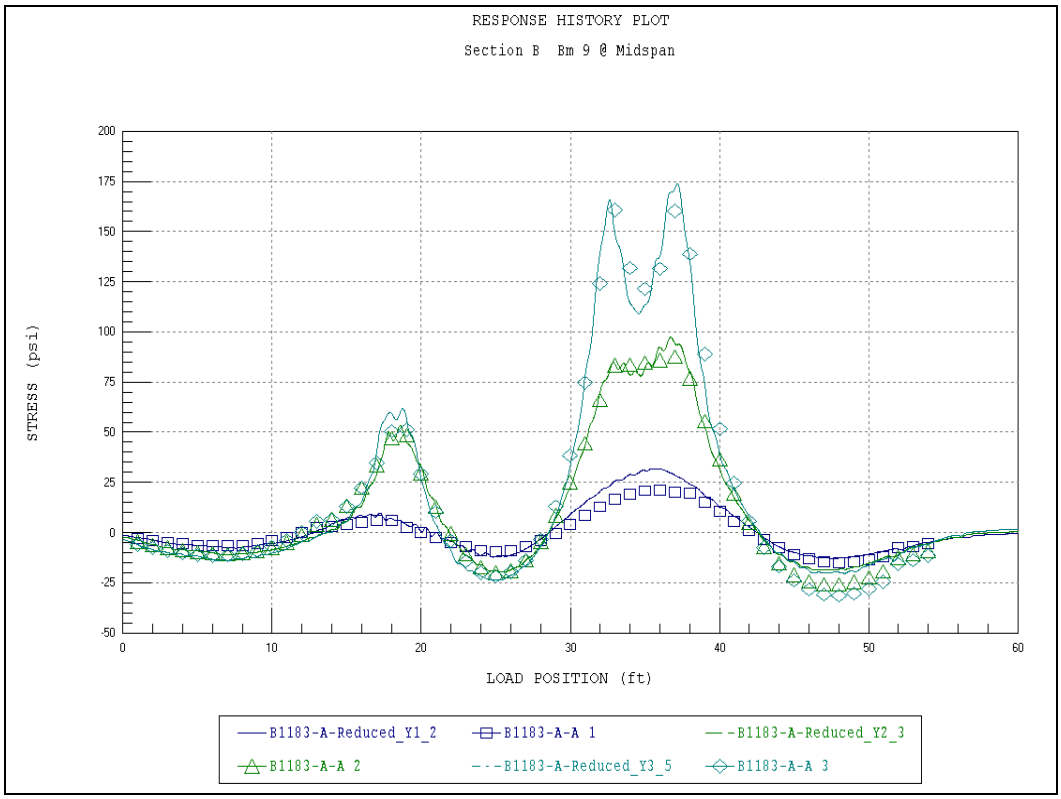

Figure A15. Strain comparison – Sec B – Beam 9.

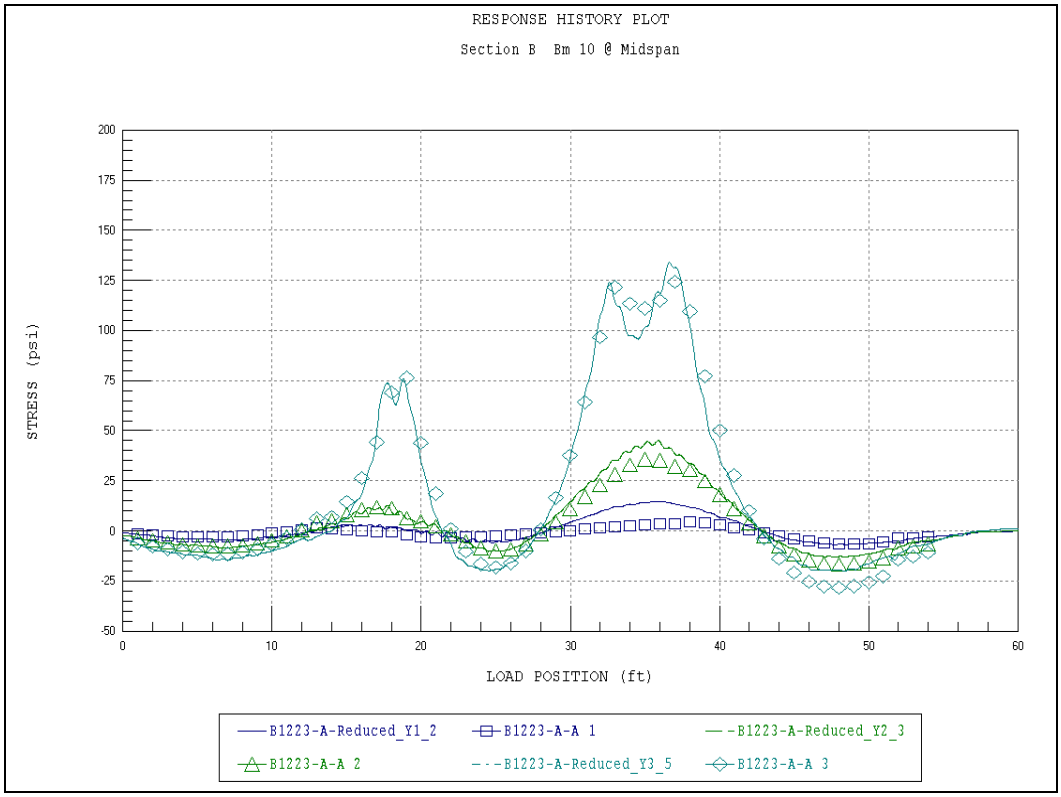

Figure A16. Strain comparison – Sec B – Beam 10.

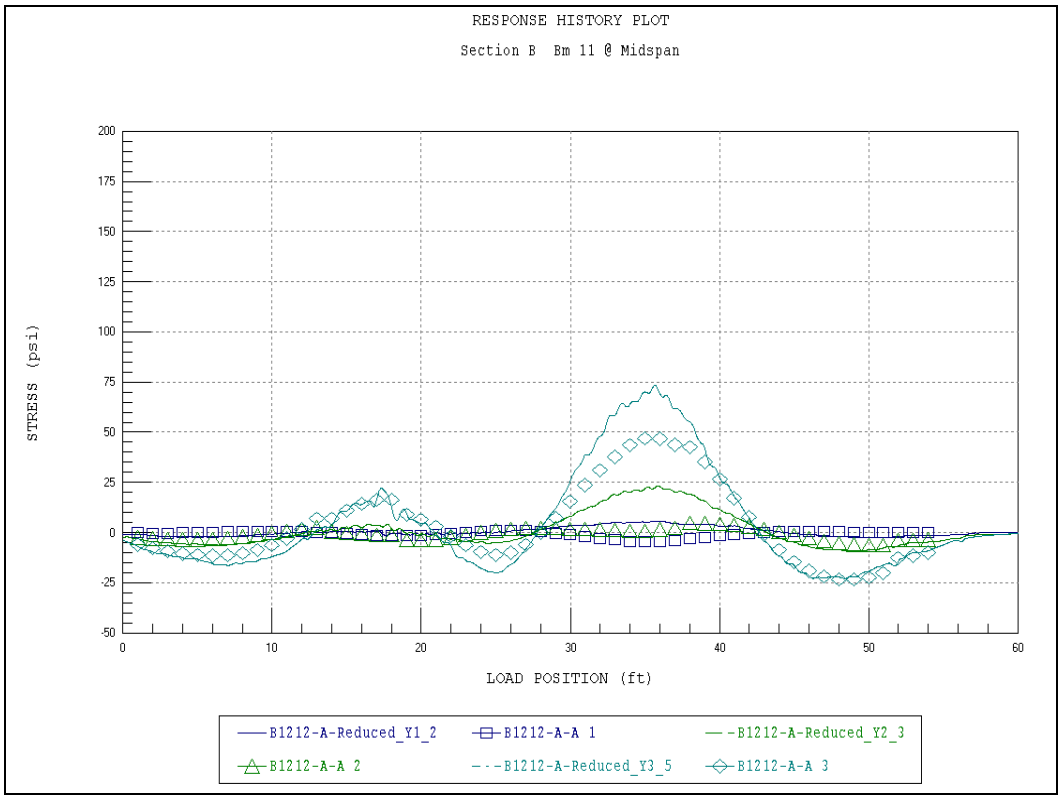

Figure A17. Strain comparison – Sec B – Beam 11.

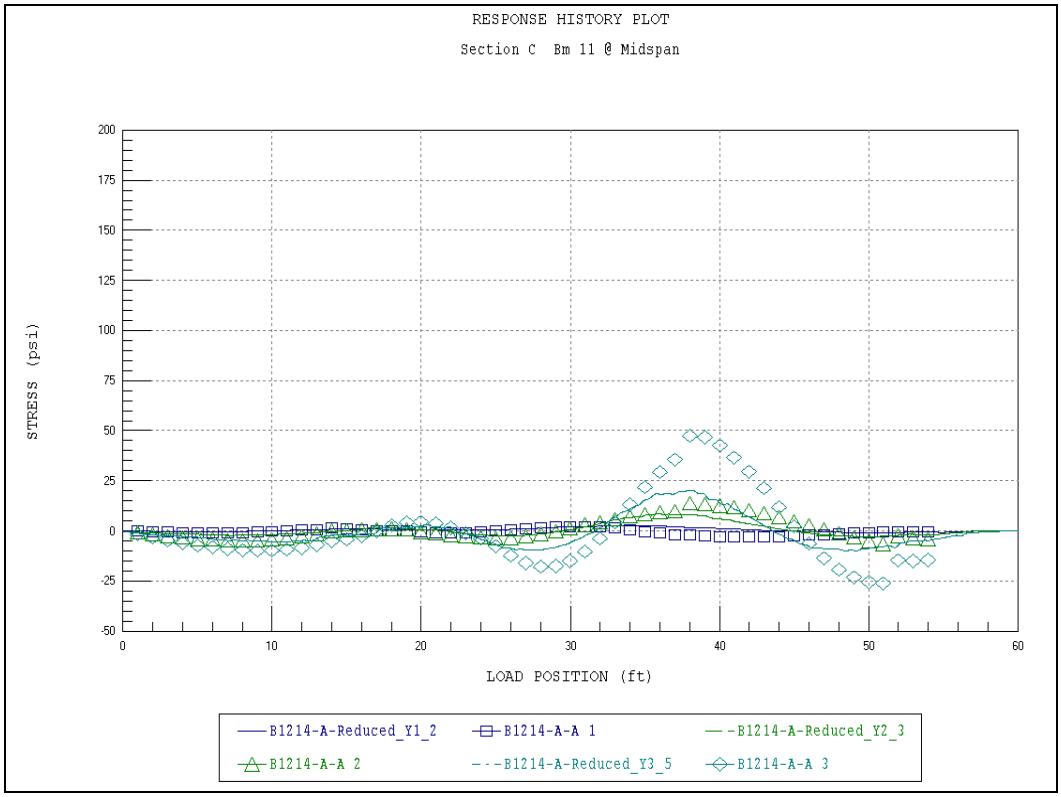

Figure A18. Strain comparison – Sec B – Beam 6.

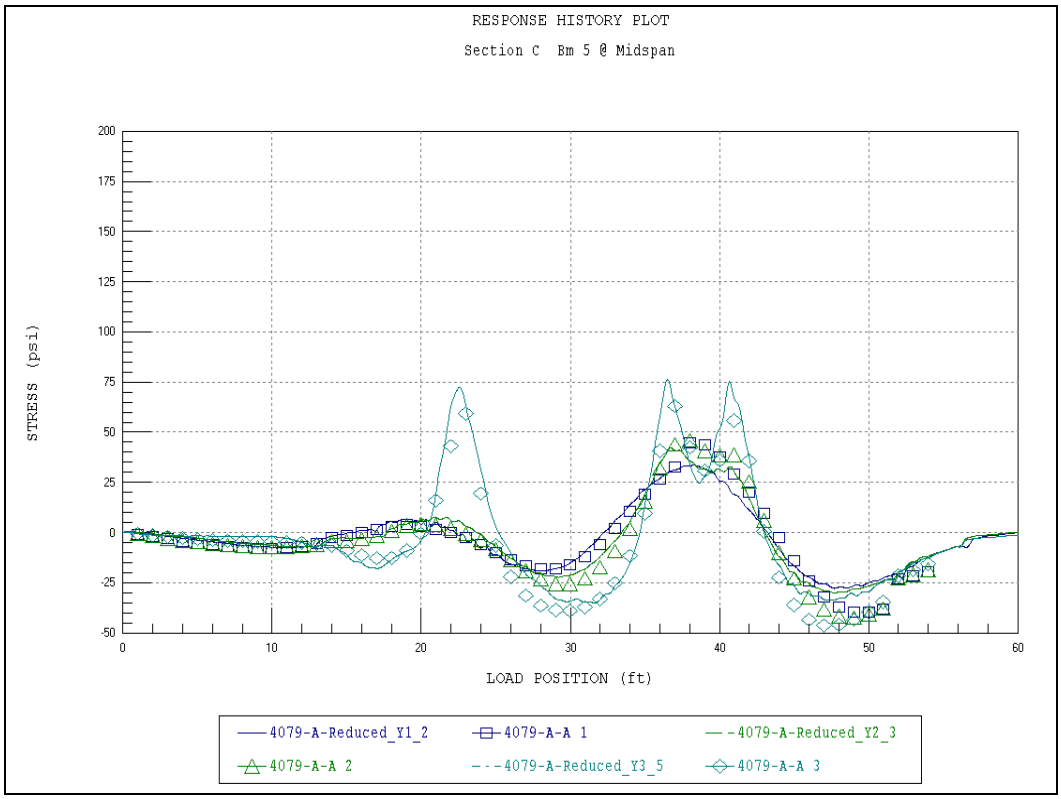

Figure A19. Strain comparison – Sec C – Beam 5.

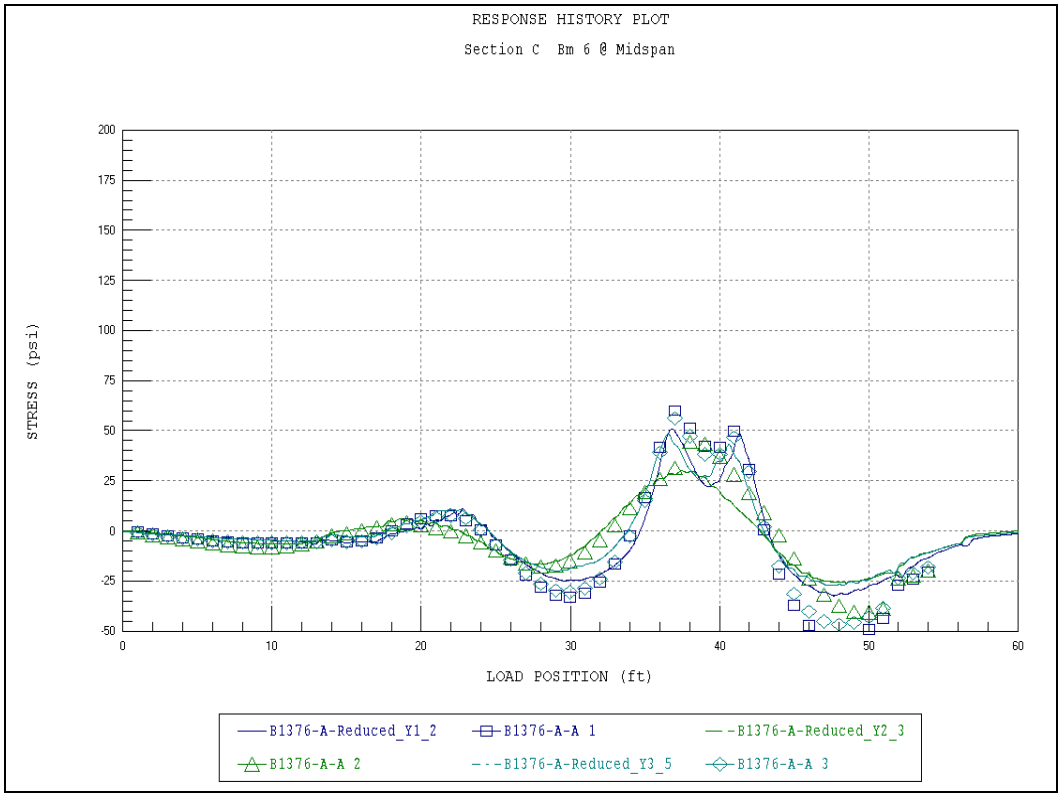

Figure A20. Strain comparison – Sec C – Beam 6.

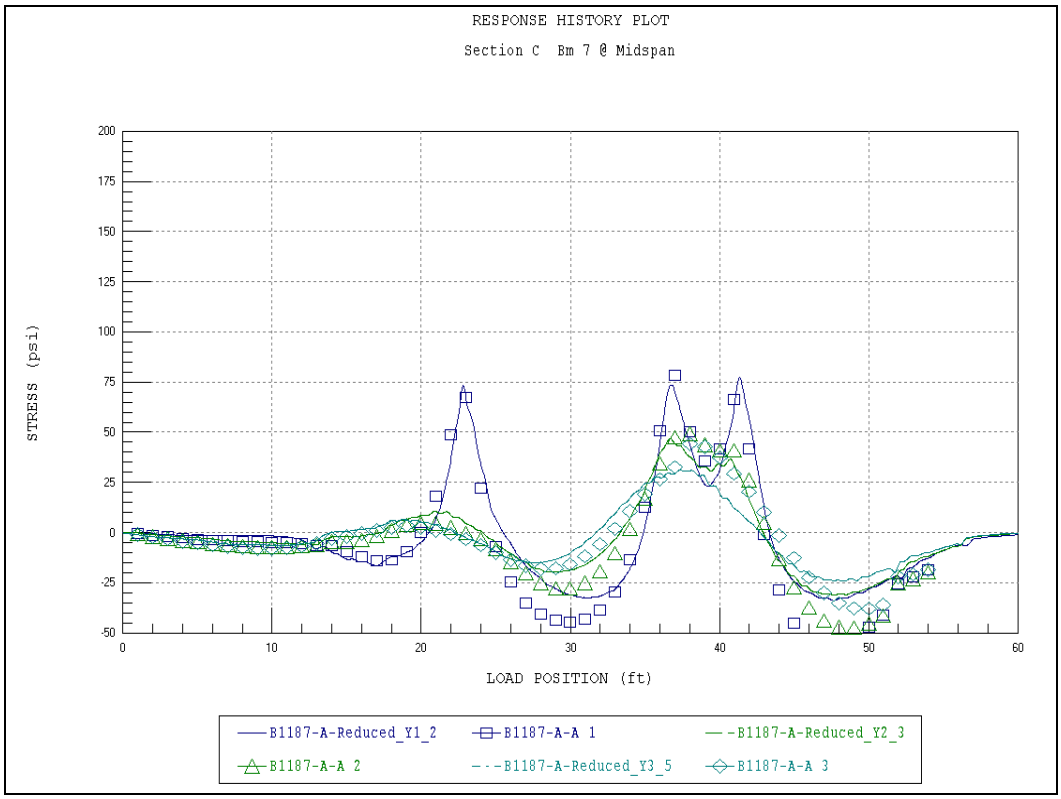

Figure A21. Strain comparison – Sec C – Beam 7.

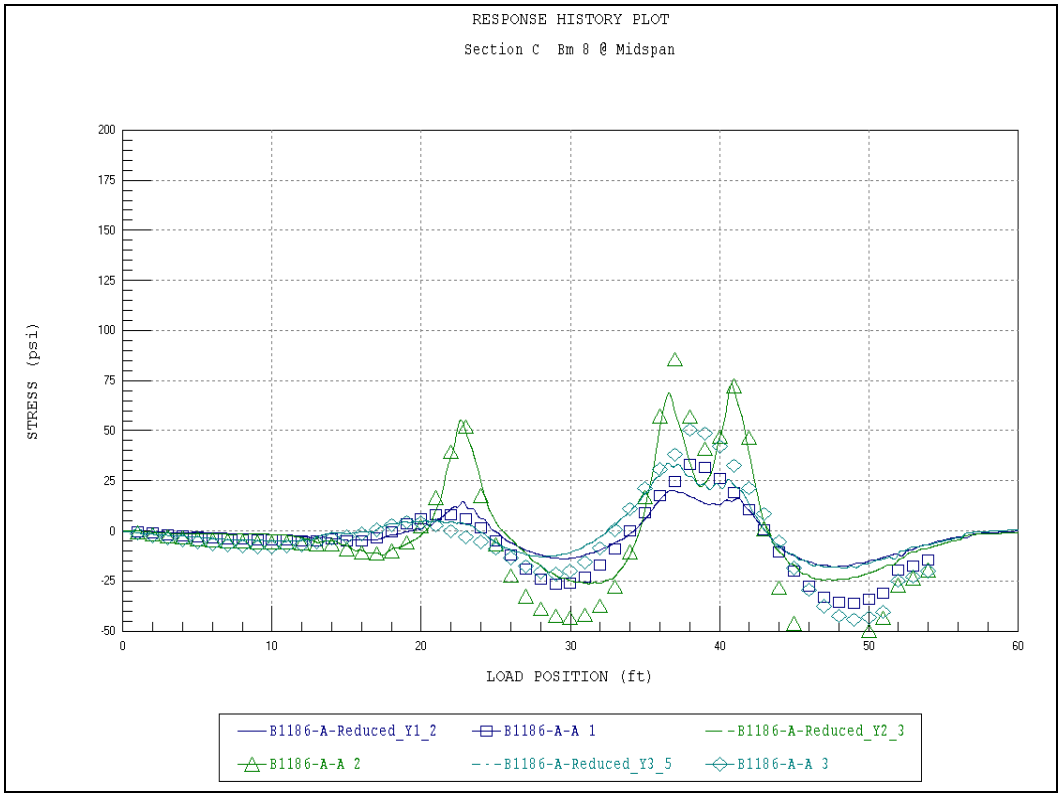

Figure A22. Strain comparison – Sec C – Beam 8.

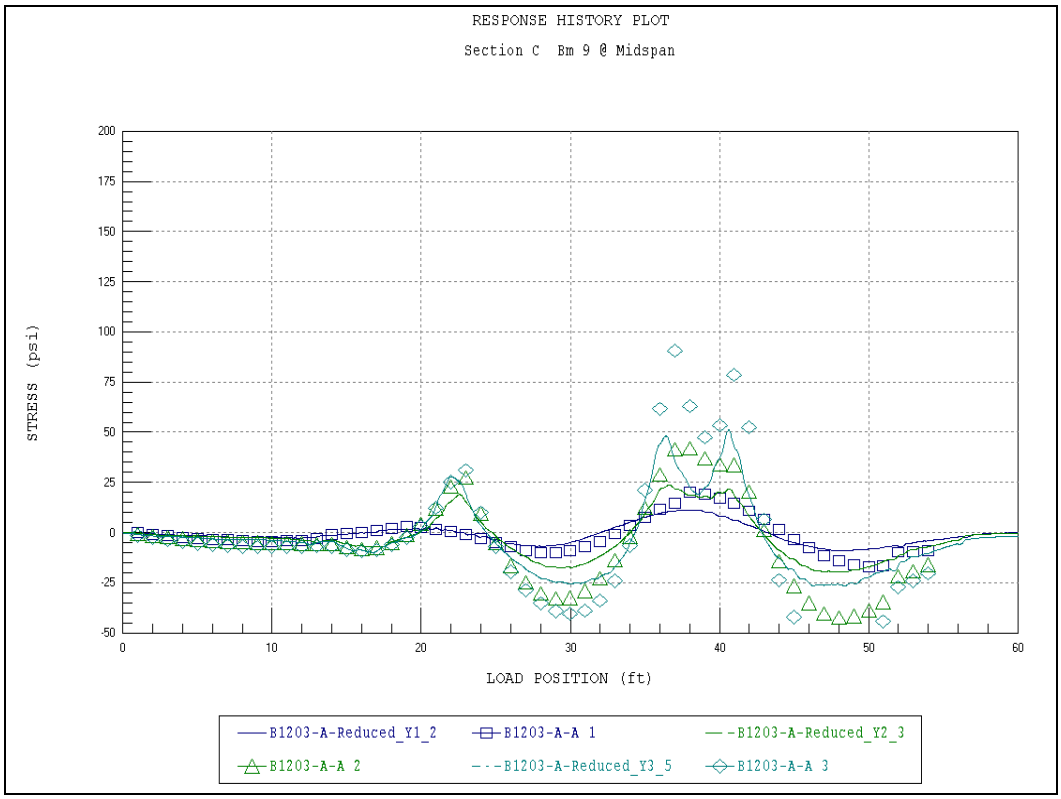

Figure A23. Strain comparison – Sec C – Beam 9.

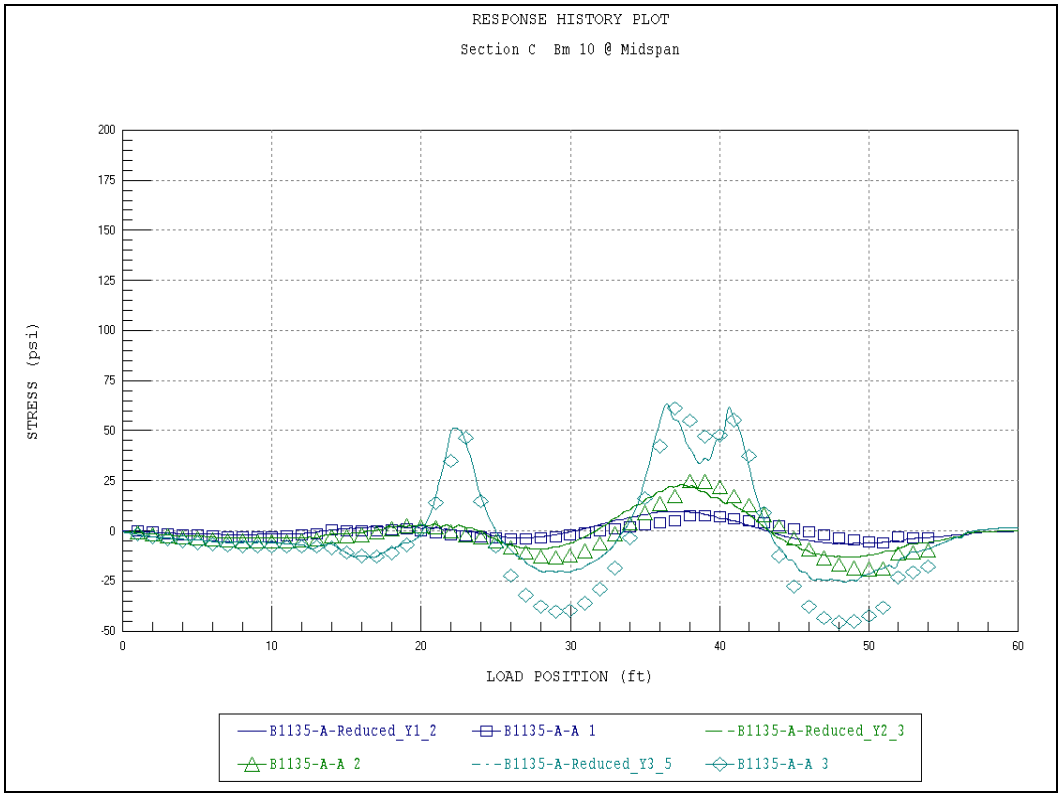

Figure A24. Strain comparison – Sec C – Beam 10.

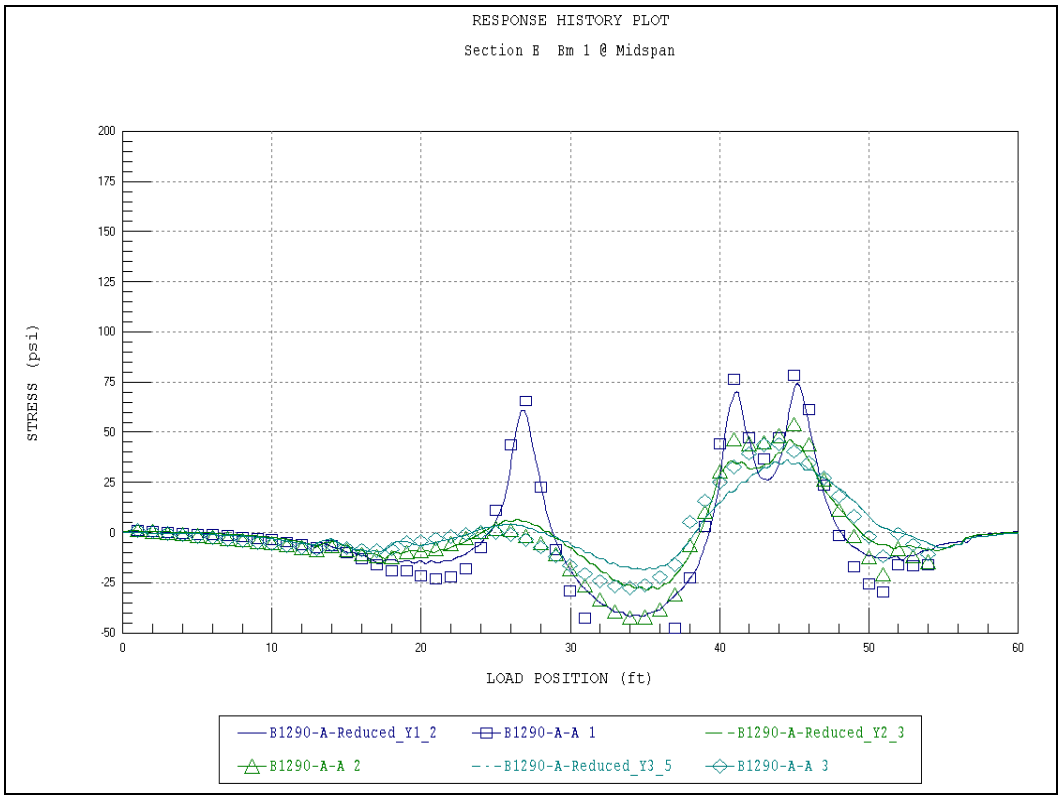

Figure A25. Strain comparison – Sec E – Beam 1.

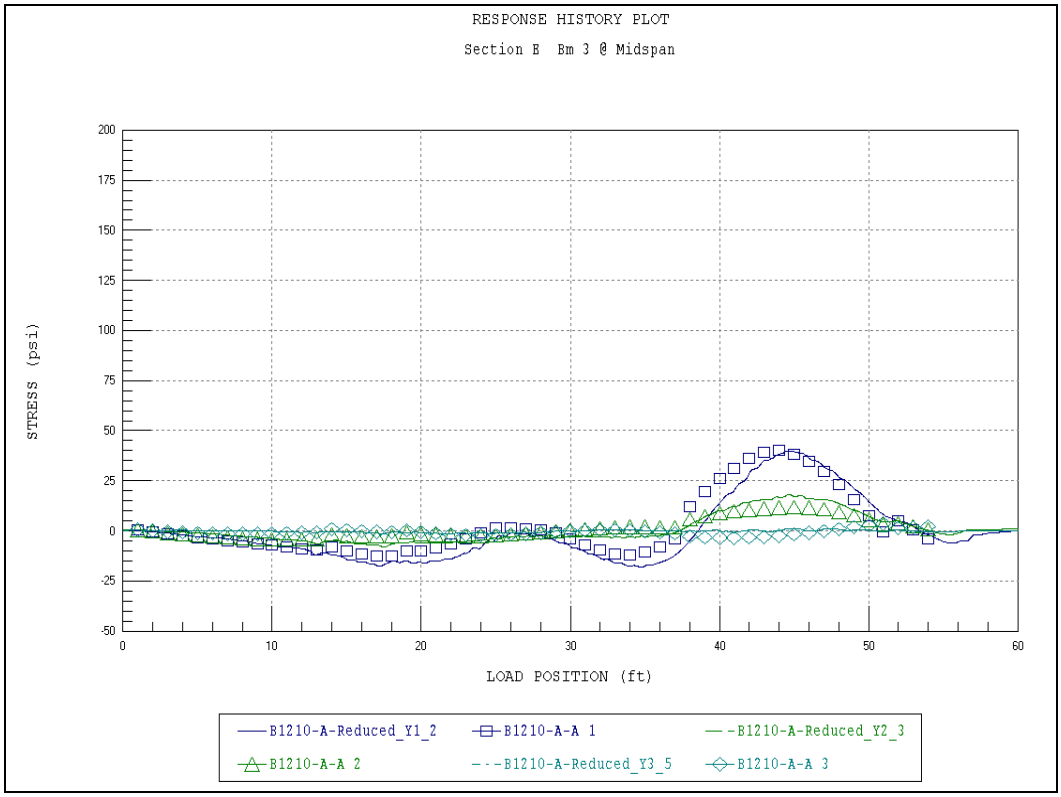

Figure A26. Strain comparison – Sec E – Beam 3.

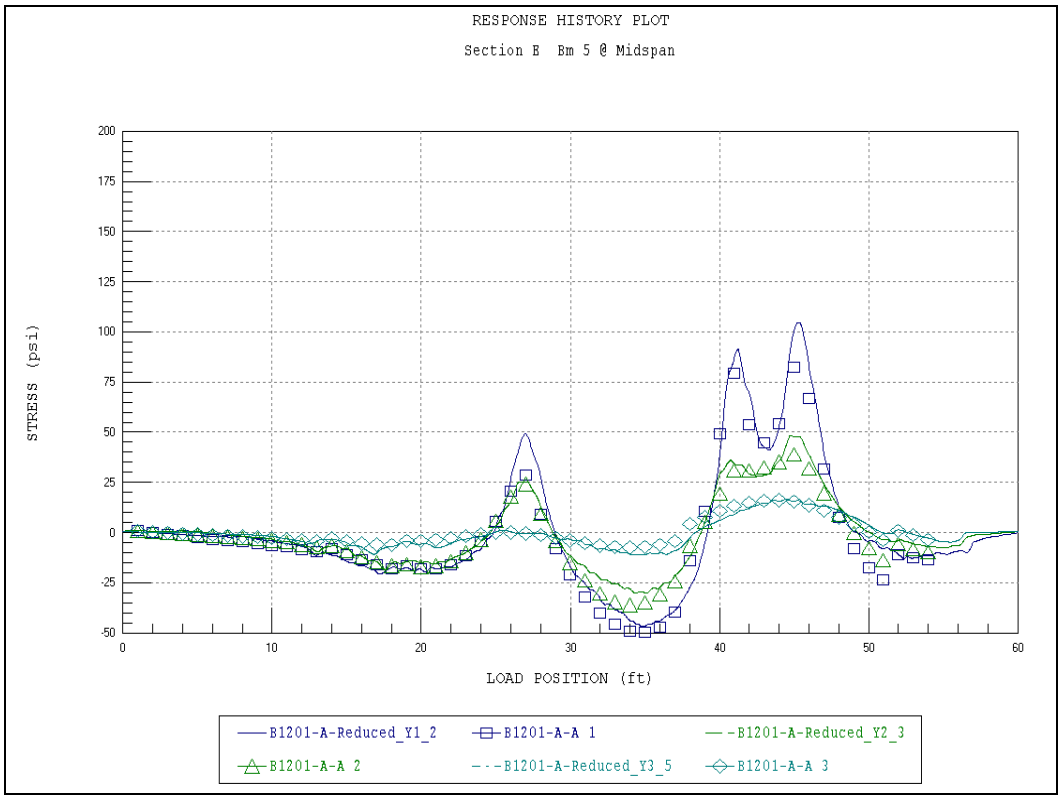

Figure A27. Strain comparison – Sec E – Beam 5.

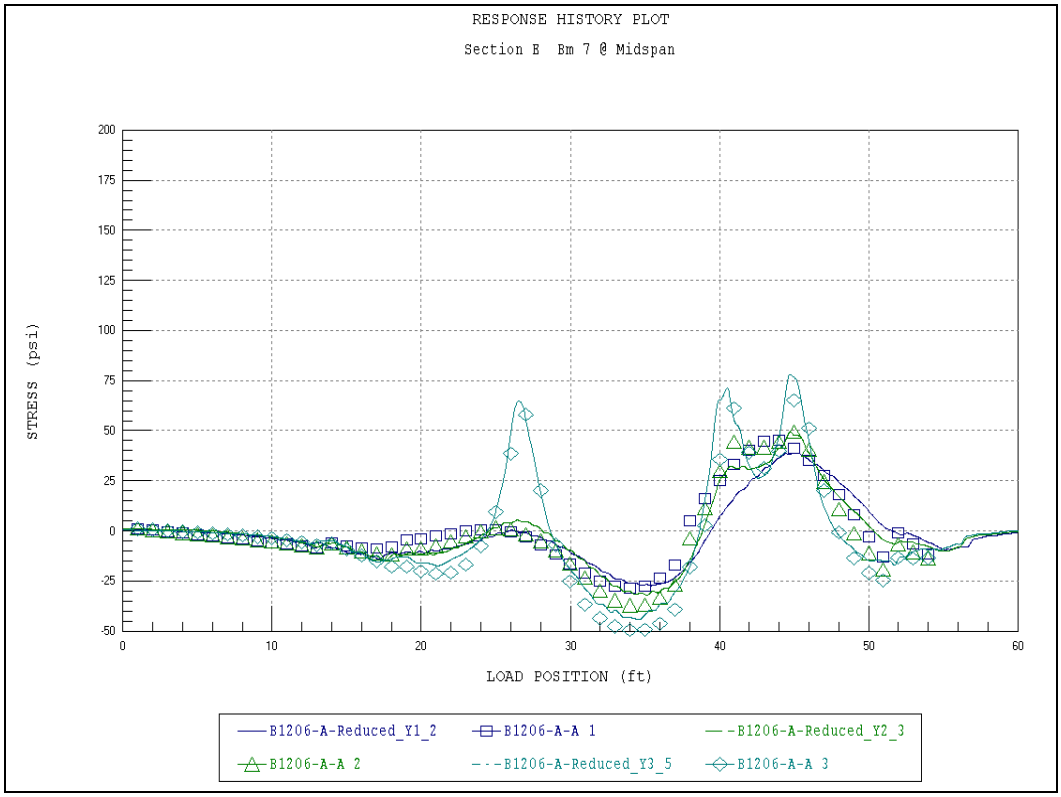

Figure A28. Strain comparison – Sec E – Beam 7.

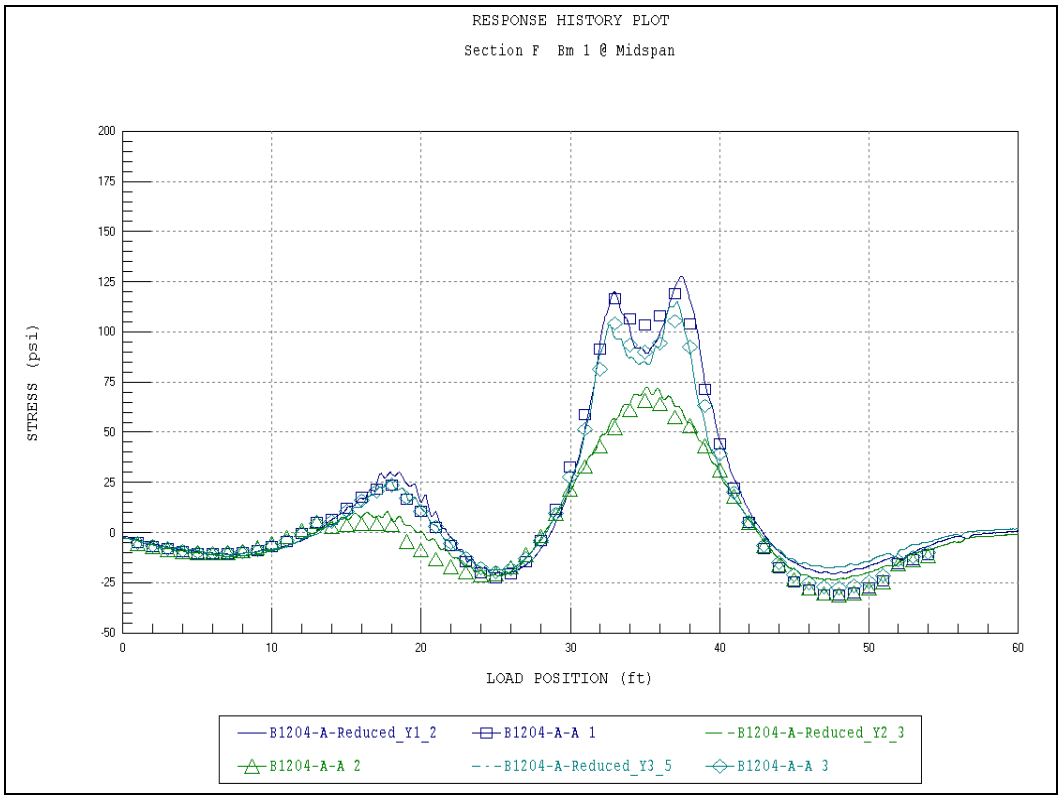

Figure A29. Strain comparison – Sec F – Beam 1.

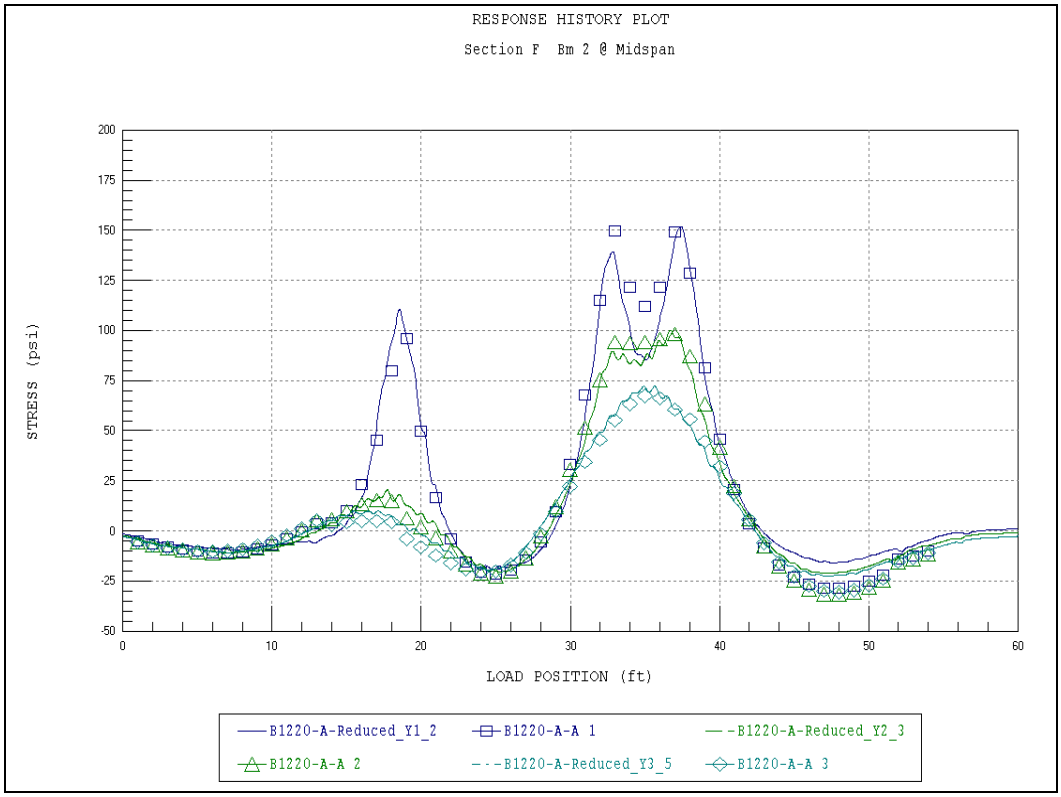

Figure A30. Strain comparison – Sec F – Beam 2.

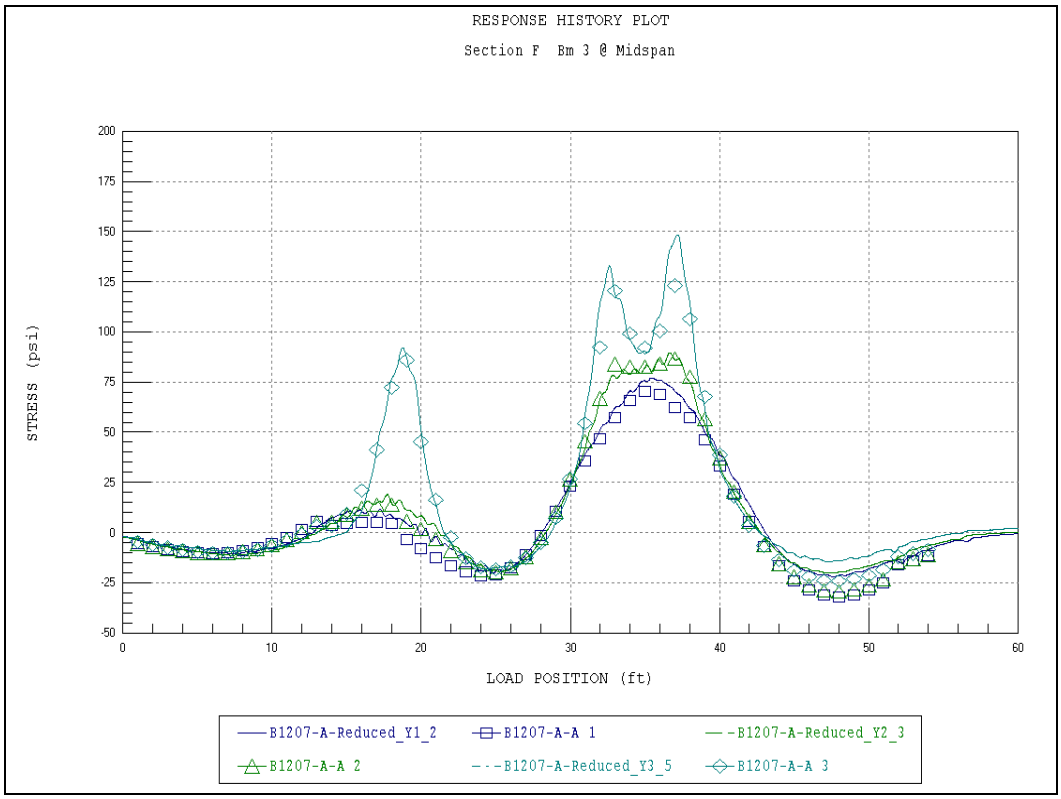

Figure A31. Strain comparison – Sec F – Beam 3.

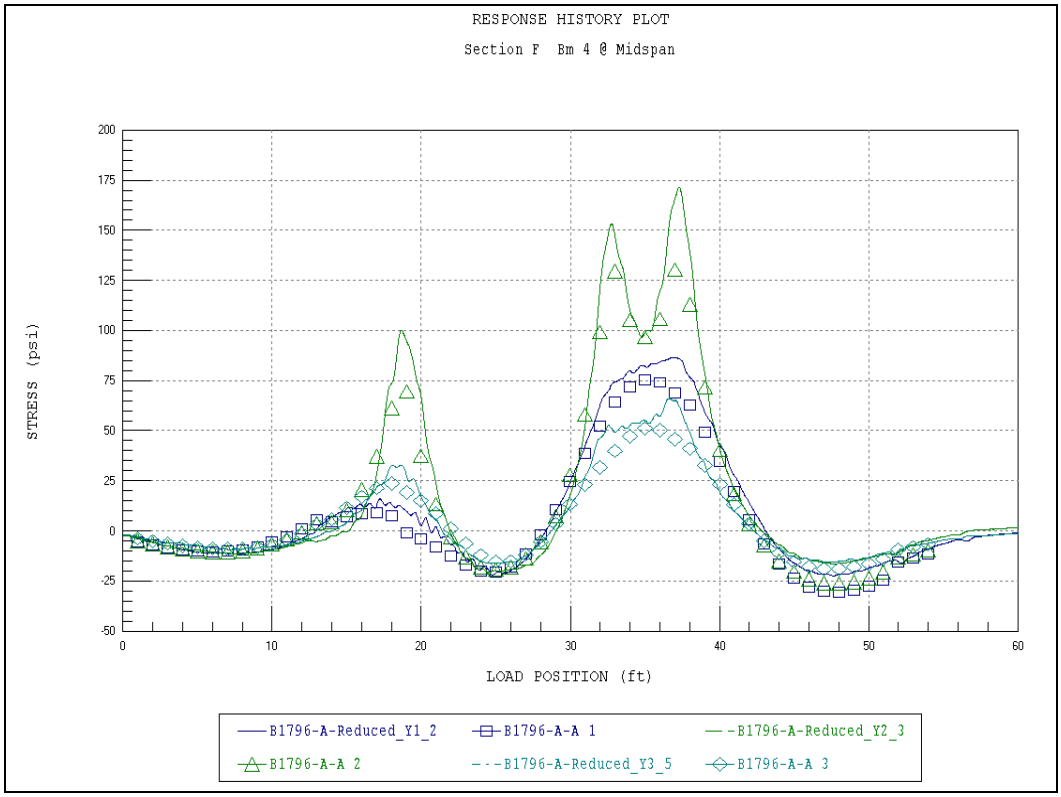

Figure A32. Strain comparison – Sec F – Beam 4.

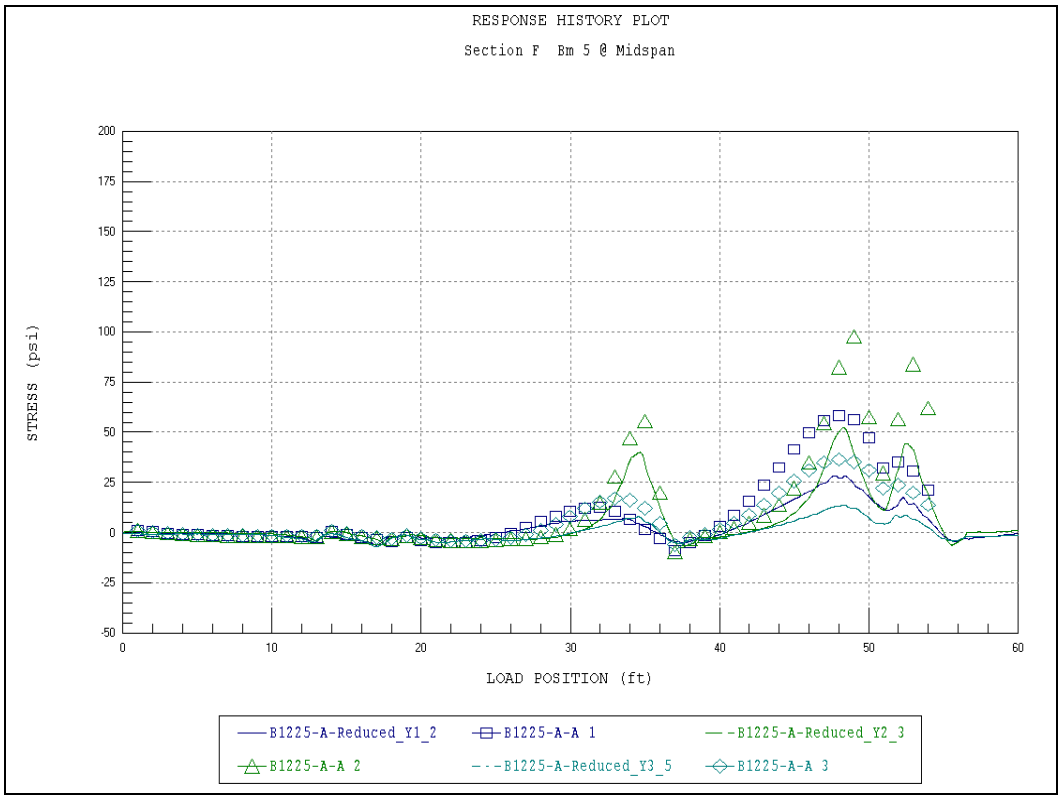

Figure A33. Strain comparison – Sec F – Beam 5.

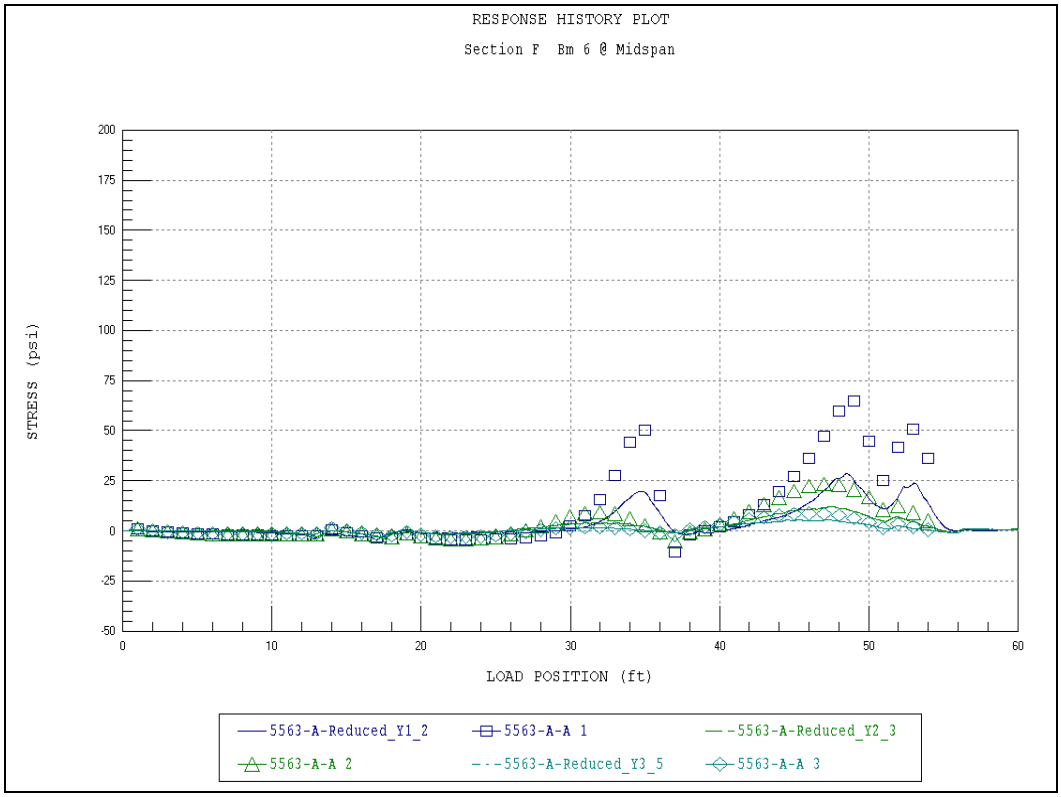

Figure A34. Strain comparison – Sec F – Beam 6.

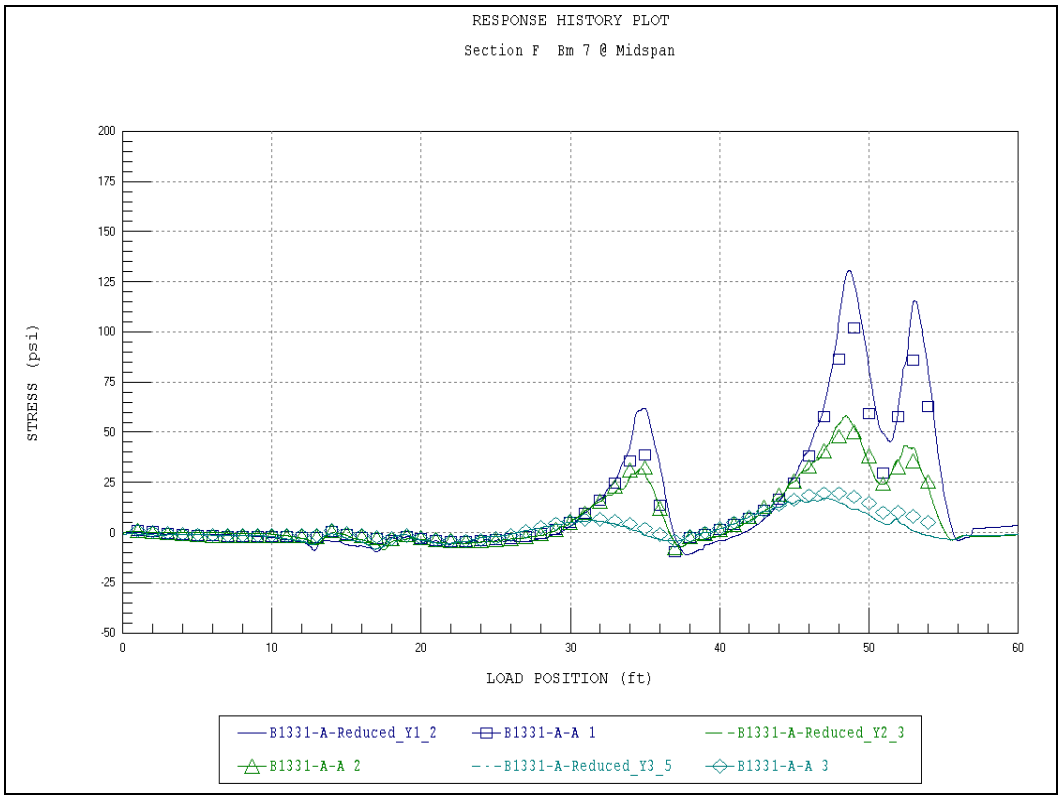

Figure A35. Strain comparison – Sec F – Beam 7.

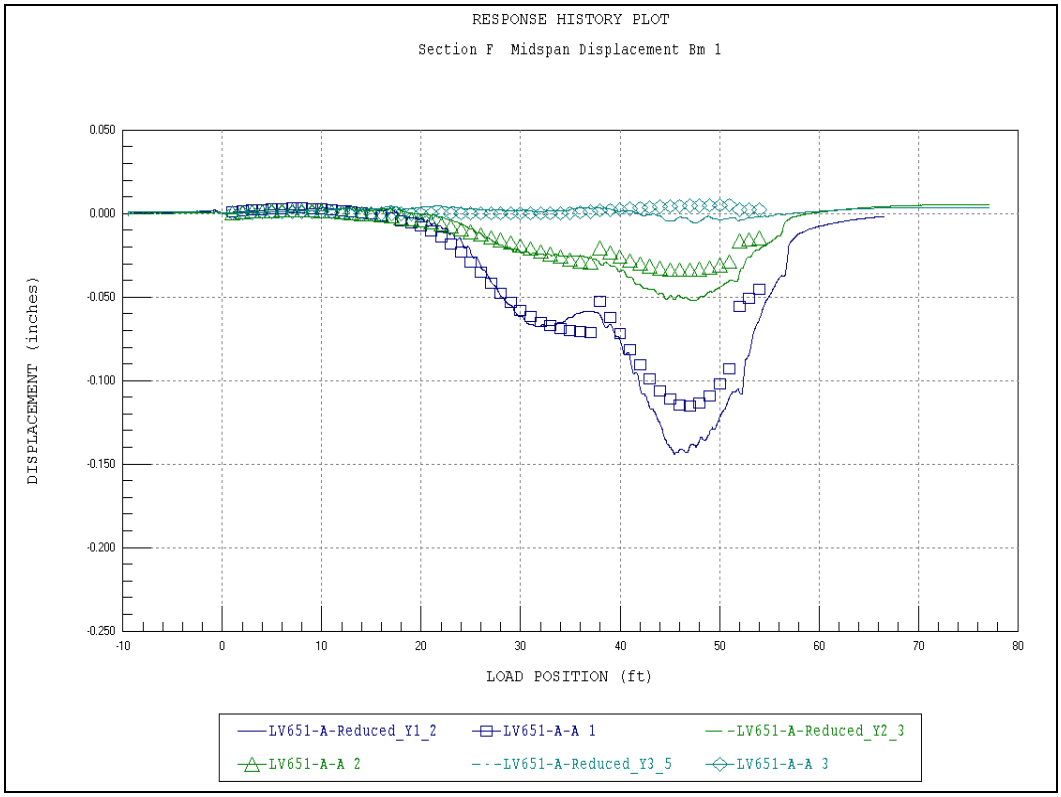

Figure A36. Midspan displacement – Sec F – Beam 1.

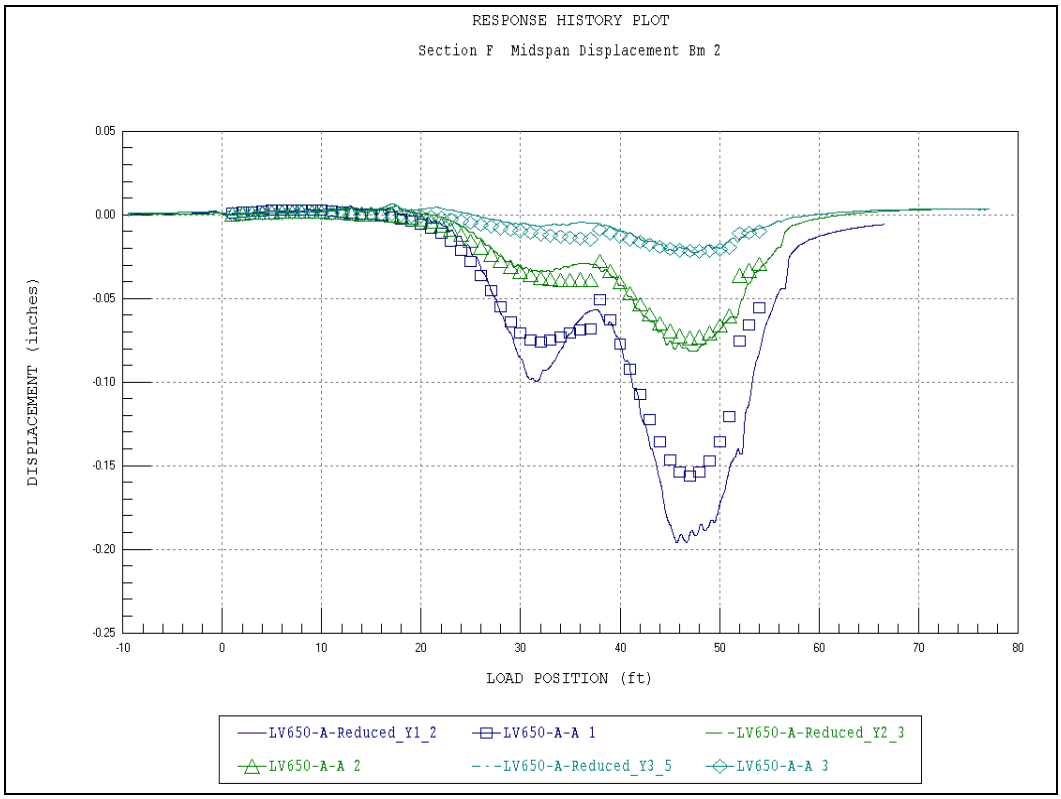

Figure A37. Midspan displacement – Sec F – Beam 2.

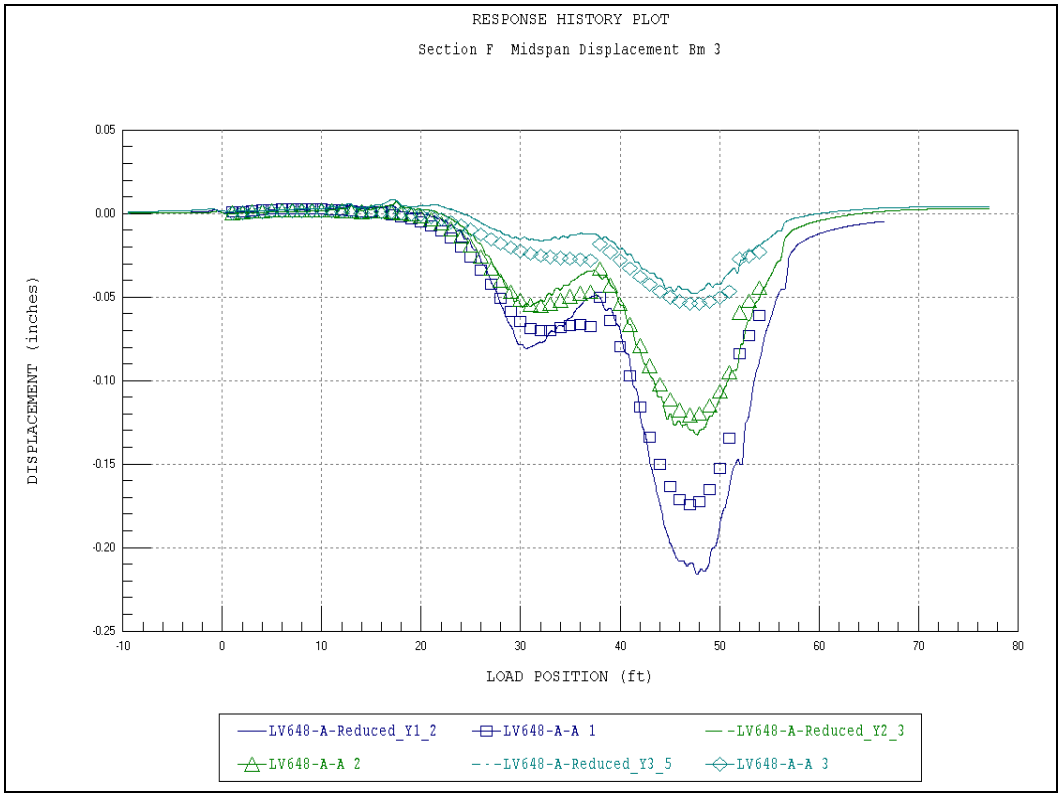

Figure A38. Midspan displacement – Sec F – Beam 3.

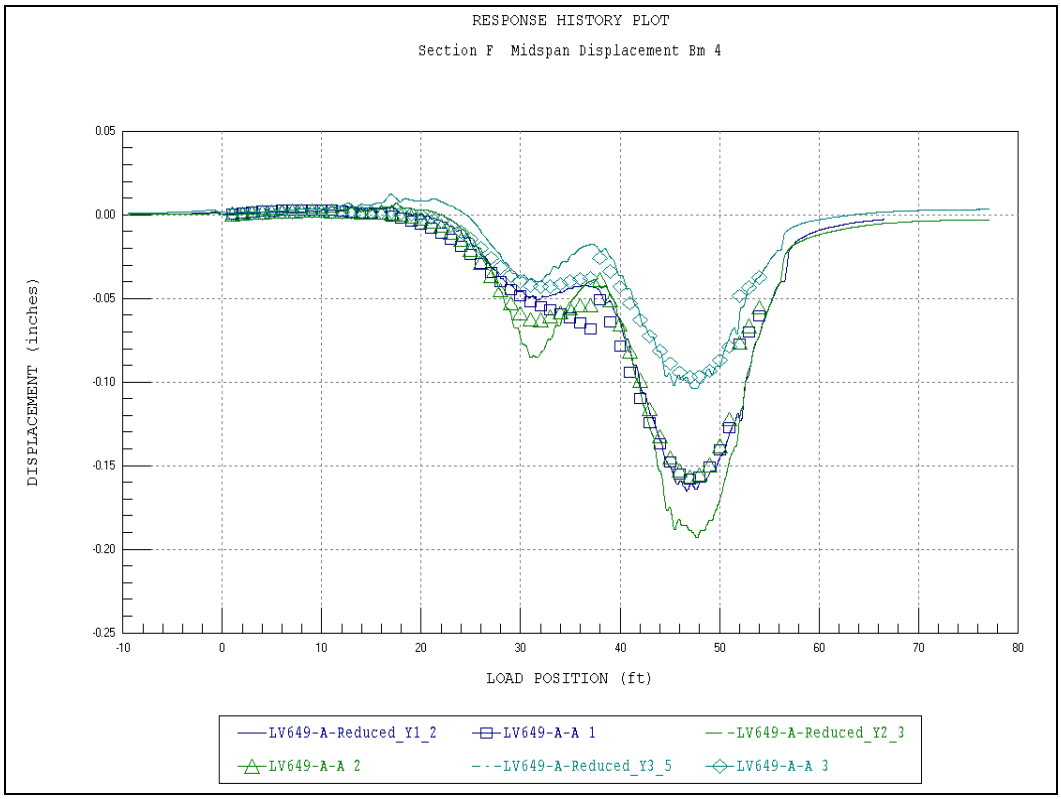

Figure A39. Midspan displacement – Sec F – Beam 4.

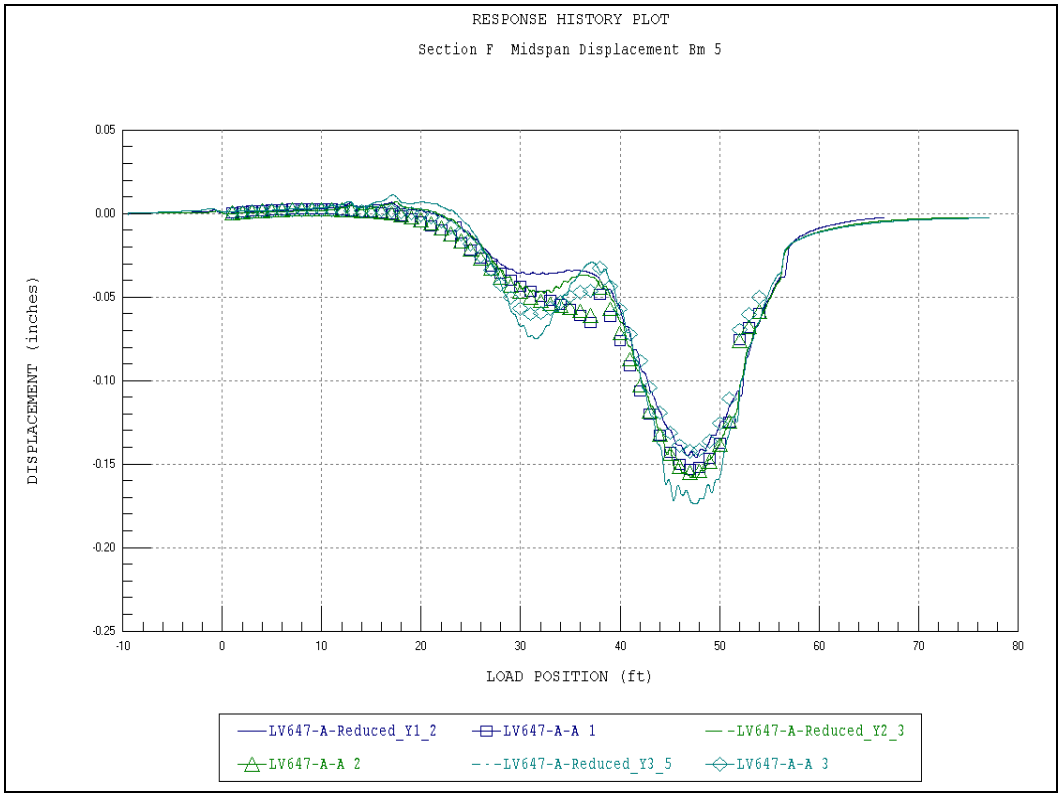

Figure A40. Midspan displacement – Sec F – Beam 5.

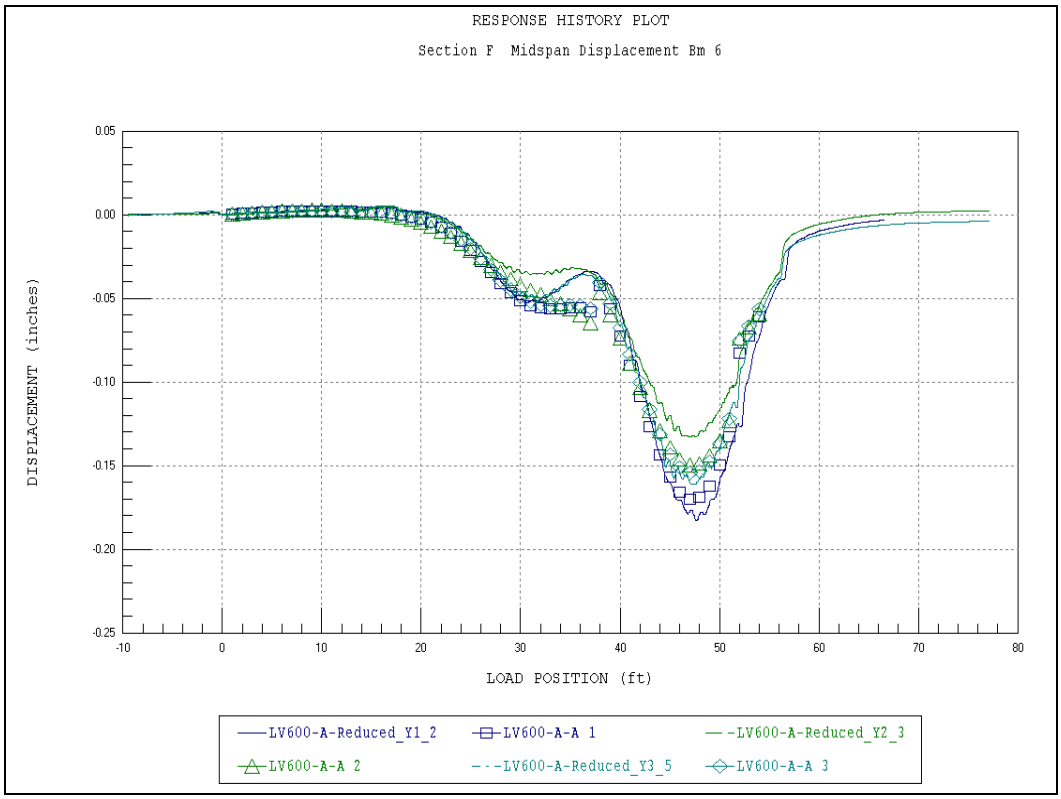

Figure A41. Midspan displacement – Sec F – Beam 6.

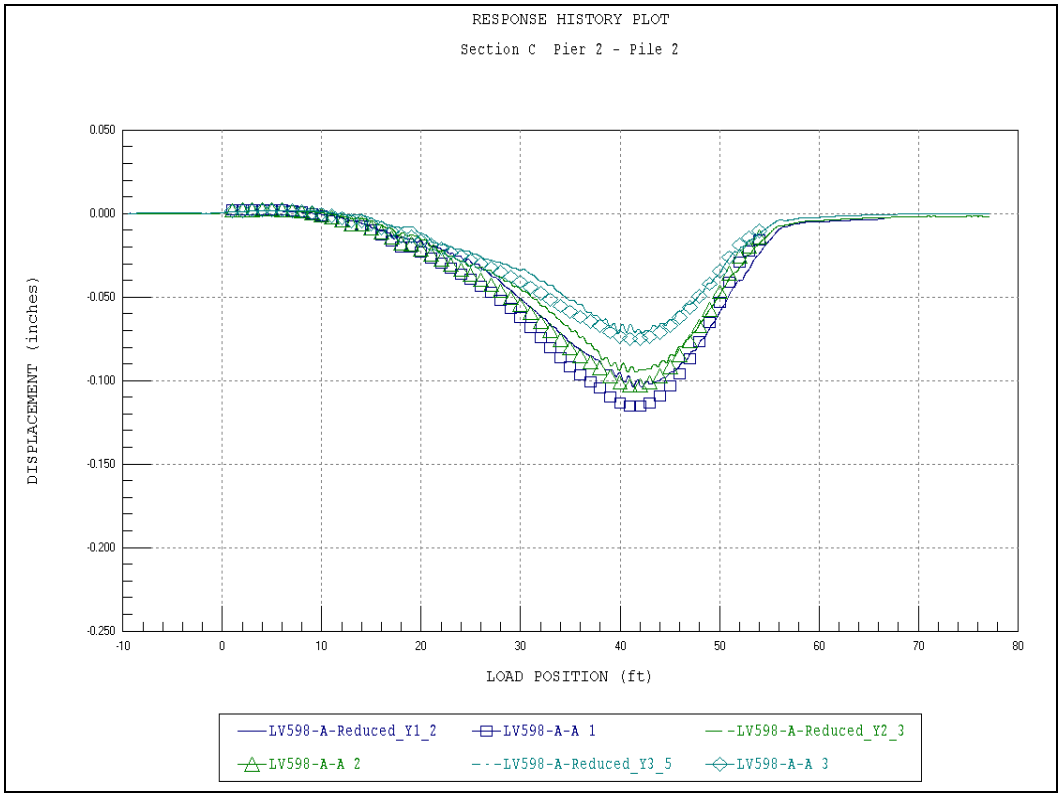

Figure A42. Bent displacement – Sec F – Interior Pile.

Appendix B: Field Notes (Scanned)

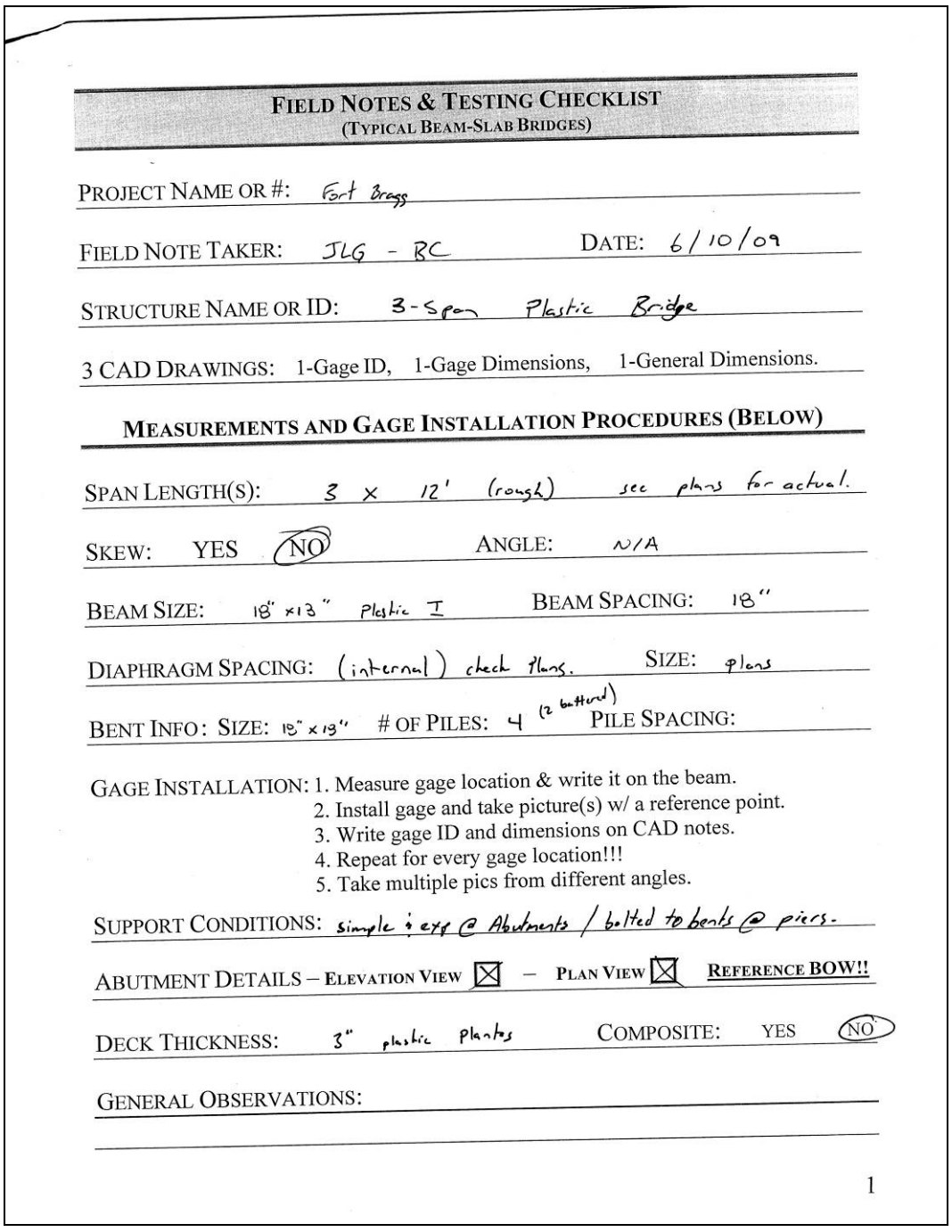

FIELD NOTES & TESTING CHECKLIST
(TYPICAL BEAM-SLAB BRIDGES)

PROJECT NAME OR #: Fort Bragg

FIELD NOTE TAKER: JLG - RC DATE: 6/10/09

STRUCTURE NAME OR ID: 3-Span Plastic Bridge

3 CAD DRAWINGS: 1-Gage ID, 1-Gage Dimensions, 1-General Dimensions.

MEASUREMENTS AND GAGE INSTALLATION PROCEDURES (BELOW)

SPAN LENGTH(S): 3 x 12' (rough) see plans for actual.

SKEW: YES (NO) ANGLE: N/A

BEAM SIZE: 18" x 13" Plastic I BEAM SPACING: 18"

DIAPHRAGM SPACING: (internal) check plans. SIZE: plans

BENT INFO: SIZE: 18" x 13" # OF PILES: 4 (2 battered) PILE SPACING:

GAGE INSTALLATION: 1. Measure gage location & write it on the beam.
2. Install gage and take picture(s) w/ a reference point.
3. Write gage ID and dimensions on CAD notes.
4. Repeat for every gage location!!!
5. Take multiple pics from different angles.

SUPPORT CONDITIONS: simple & exp @ Abutments / bolted to bents @ piers.

ABUTMENT DETAILS – ELEVATION VIEW ☒ – PLAN VIEW ☒ REFERENCE BOW!!

DECK THICKNESS: 3" plastic planks COMPOSITE: YES (NO)

GENERAL OBSERVATIONS:

1

Figure B1. Field testing notes (Sheet 1 of 13).

MEASUREMENTS AND TESTING PROCEDURES (ABOVE)

BEGINNING OF WORLD (BOW) VERIFY NORTH ON PLANS: (YES) NO
(X=0, Y=0, location)
SE corner - Edge of beam ; ℄ of bearing.

BOW PHOTOS: ☐ ROAD MARKINGS PHOTOS: ☐

ROADWAY WIDTH (CURB-TO-CURB): 16'-3½" SYMMETRIC: (YES) NO

STRUCTURE WIDTH (Out-to-Out): 17'-5"

WEARING SURFACE: 3"x 12" plastic Planks. THICKNESS: 3"

STARTING TEST POSITION: -10' DIRECTION: North

VEHICLE ROLL OUT (5 REVS!): 24'-2" (10.8 ft) same as last bridge. A/C LOCATION: Axis / Front

*****MAKE SURE YOU PUT THE A/C ON THE SAME WHEEL AS WAS USED TO MEASURE THE ROLL OUT*****

VEHICLE MEASUREMENTS:

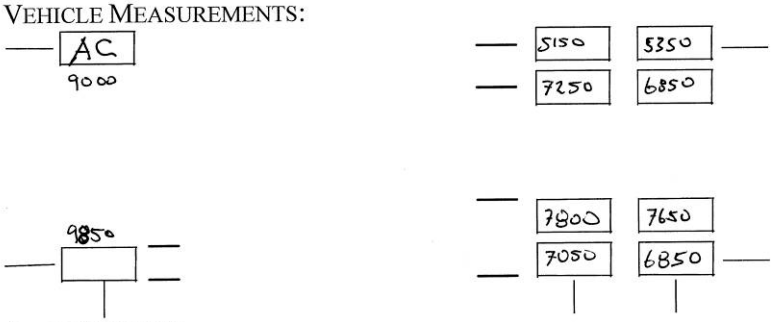

AXLE WEIGHTS:

FRONT: 18.850 REAR: 53.95 K GROSS: 72.8 K

VEHICLE PROVIDED BY: Fort Bragg

TRAFFIC CONTROL PROVIDED BY: N/A

ACCESS PROVIDED BY: N/A

2

Figure B1. (Sheet 2 of 13).

LATERAL TESTING POSITIONS: (REFERENCED FROM BOW)

Y1: 3.0' Y2: 4' - 10½"

Y3: 13' - 7" Y4:

Y5: Y6:

LATERAL POSITIONS CHECKED BY:

TESTING OPERATIONS (WINSTS)

VERIFY GAGE ID & # OF CHANNELS WITH WINSTS: ☐ ✱ missed ERDC-04

RUN WINSTS TO VERIFY RESPONSES: GOOD

WEATHER CONDITIONS & AMBIENT TEMPERATURE: ~ 73 °F overcast Deck Temp: 87°F Bottom Beam Temp: 75°F

RUNNING THE FIELD TESTS

STS OPERATOR: JLG TRUCK OPERATOR: Kevin

CONTROLLED SEMI-STATIC TESTS

SAMPLE RATE: 40 Hz

GAIN: 32

FILE NAME	LATERAL POSITION	COMMENTS
Plastic3S_1.dat	Y1	GOOD — LVDT's not quite back to zero.
Plastic3S_2.dat	Y1	→ drove further off bridge - GOOD
_3.dat	Y2	GOOD
_4.dat	Y2	GOOD
_5.dat	Y3	GOOD
_6.dat	Y3	GOOD
_7.dat	Y2	Stop truck on w/ front axle @ mid-span of Span 3

3

Figure B1. (Sheet 3 of 13).

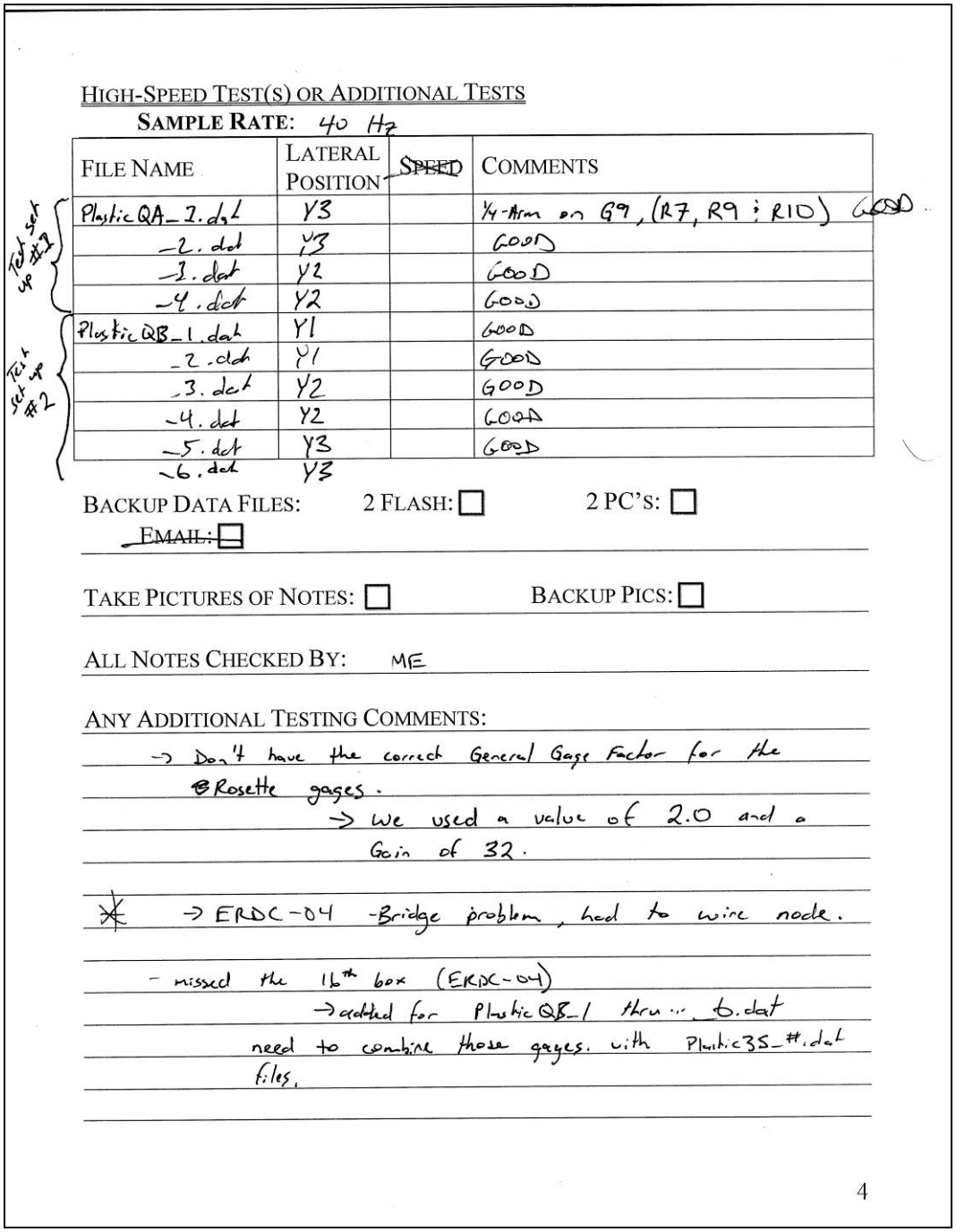

HIGH-SPEED TEST(S) OR ADDITIONAL TESTS

SAMPLE RATE: 40 Hz

	FILE NAME	LATERAL POSITION	~~SPEED~~	COMMENTS
Test set up #1	PlasticQA_1.dat	Y3		¼-Arm on G9, (R7, R9 ; R10) GOOD
	_2.dat	Y3		GOOD
	_3.dat	Y2		GOOD
	_4.dat	Y2		GOOD
Test set up #2	PlasticQB_1.dat	Y1		GOOD
	_2.dat	Y1		GOOD
	_3.dat	Y2		GOOD
	_4.dat	Y2		GOOD
	_5.dat	Y3		GOOD
	_6.dat	Y3		

BACKUP DATA FILES: 2 FLASH: ☐ 2 PC'S: ☐

~~EMAIL:~~ ☐

TAKE PICTURES OF NOTES: ☐ BACKUP PICS: ☐

ALL NOTES CHECKED BY: ME

ANY ADDITIONAL TESTING COMMENTS:

→ Don't have the correct General Gage Factor for the @Rosette gages.
→ We used a value of 2.0 and a Gain of 32.

✳ → ERDC-04 -Bridge problem, had to wire node.

- missed the 16th box (ERDC-04)
→ added for PlasticQB_1 thru ... _6.dat
need to combine those gages. with Plastic35_#.dat files,

4

Figure B1. (Sheet 4 of 13).

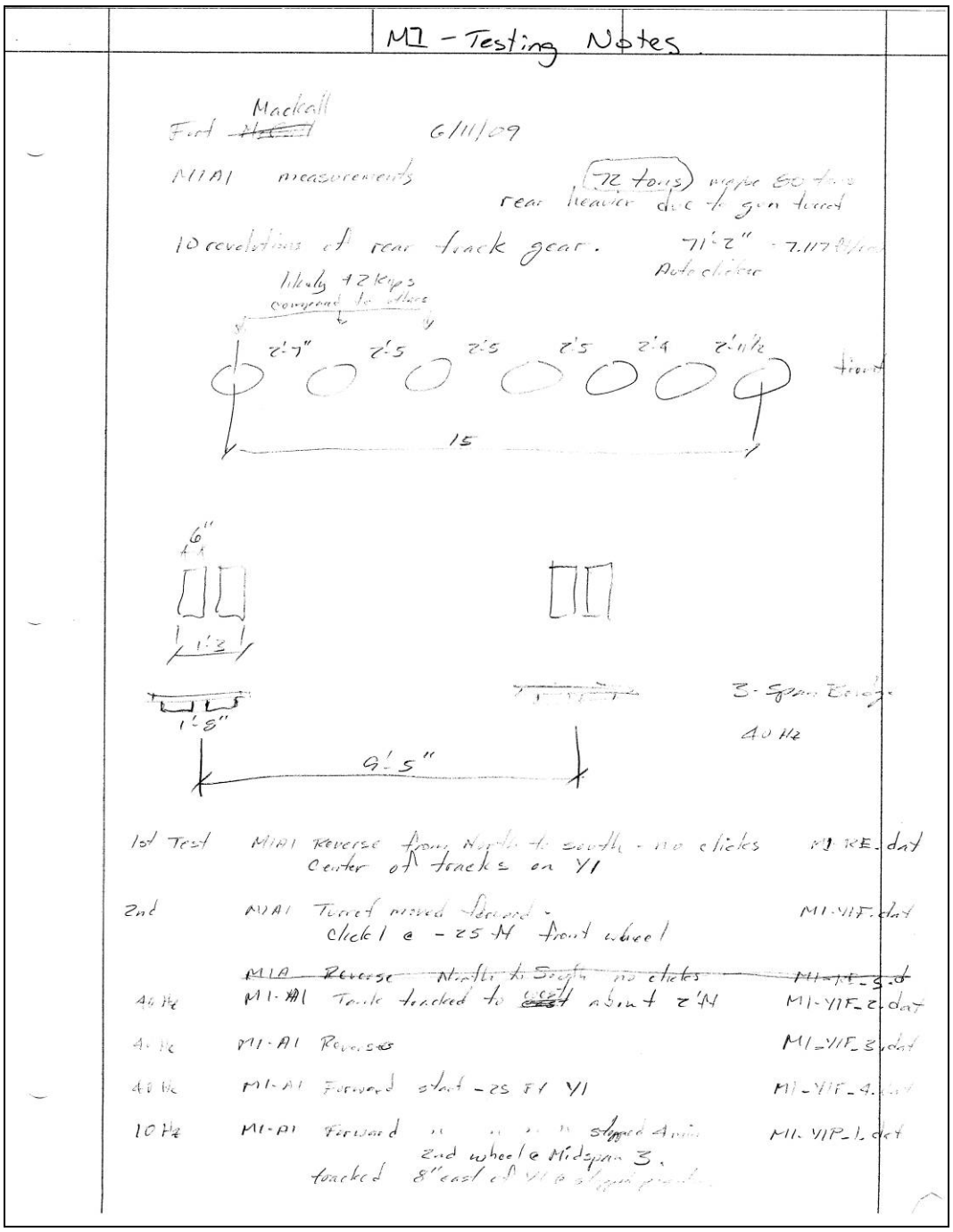

Figure B1. (Sheet 5 of 13).

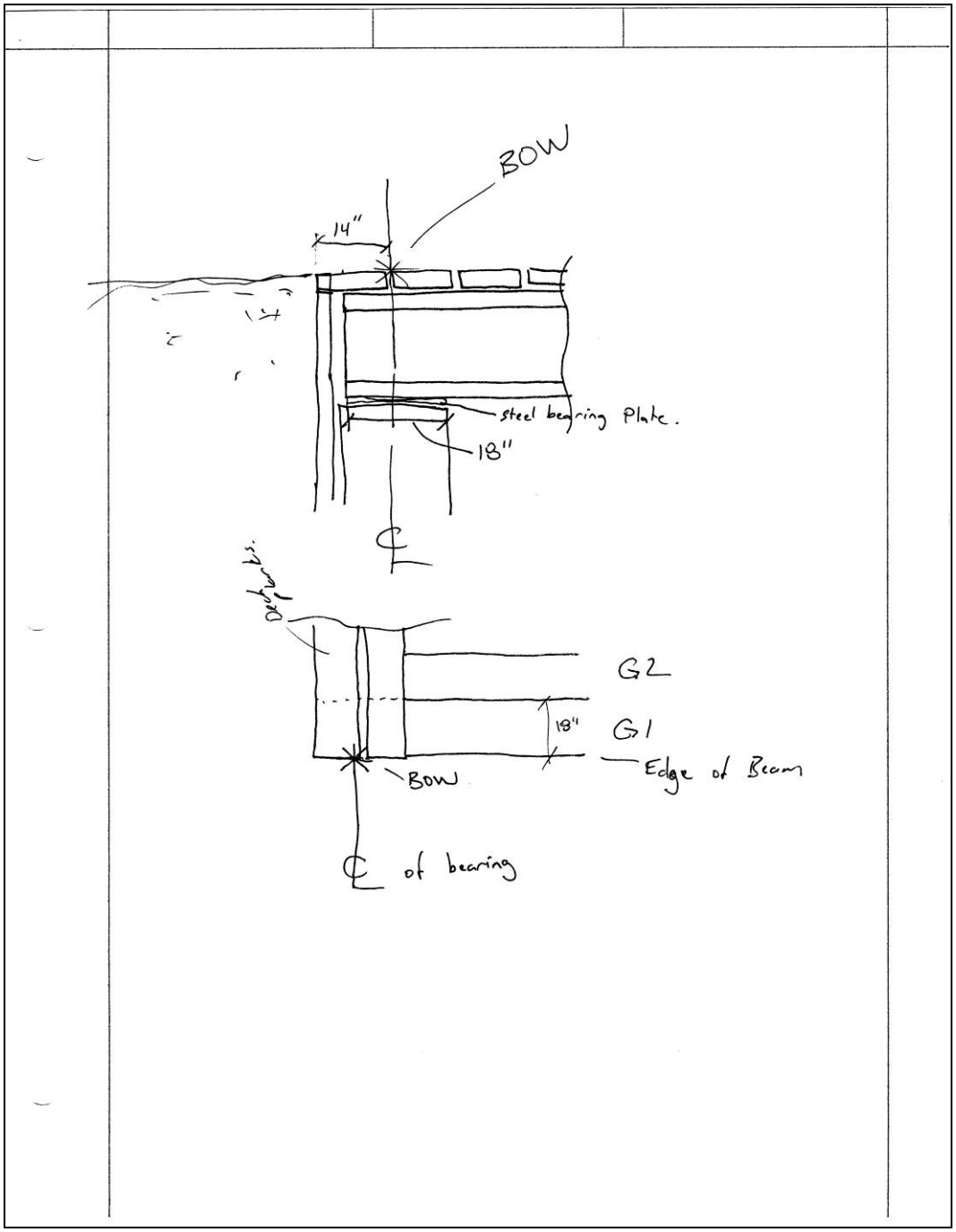

Figure B1. (Sheet 6 of 13).

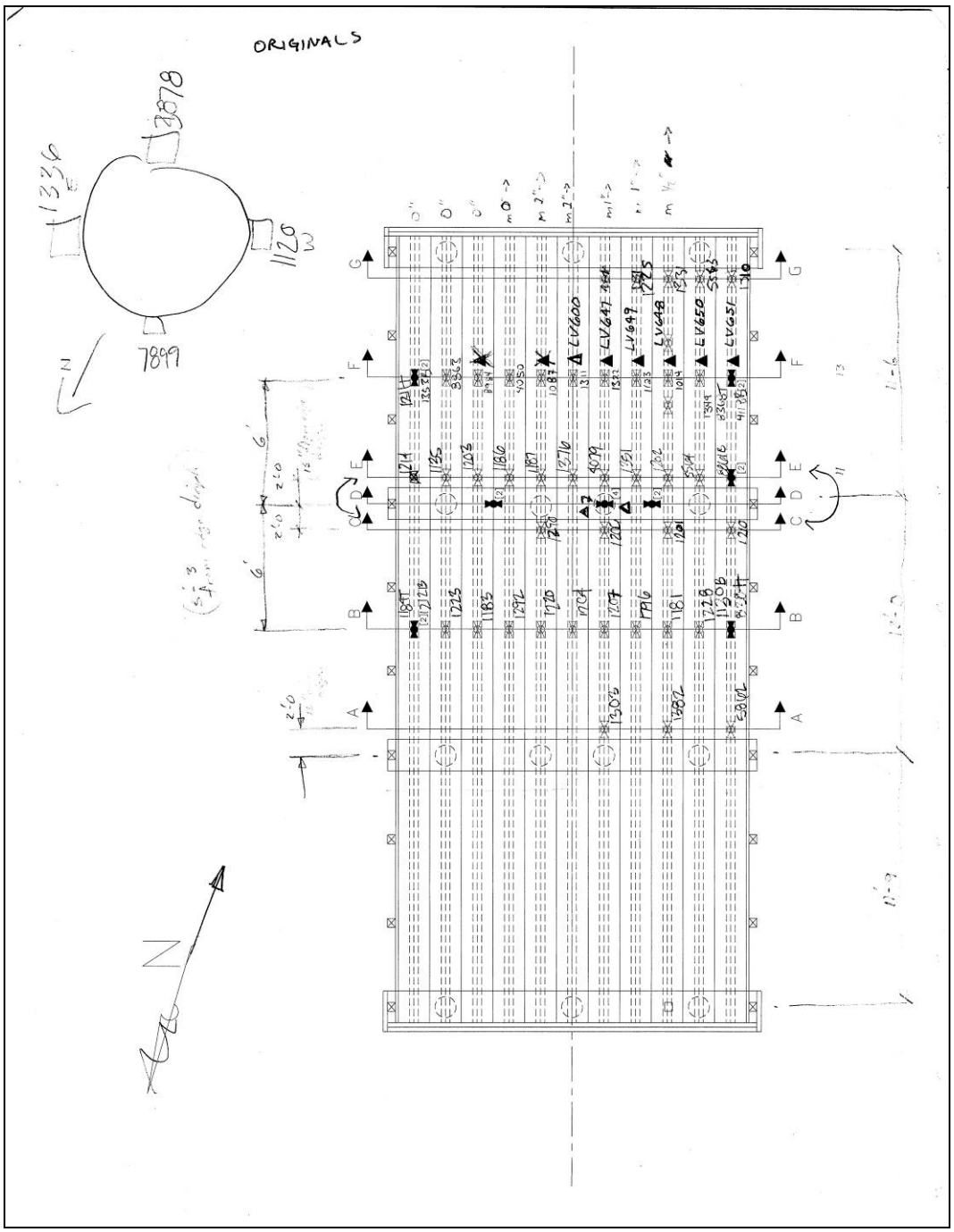

Figure B1. (Sheet 7 of 13).

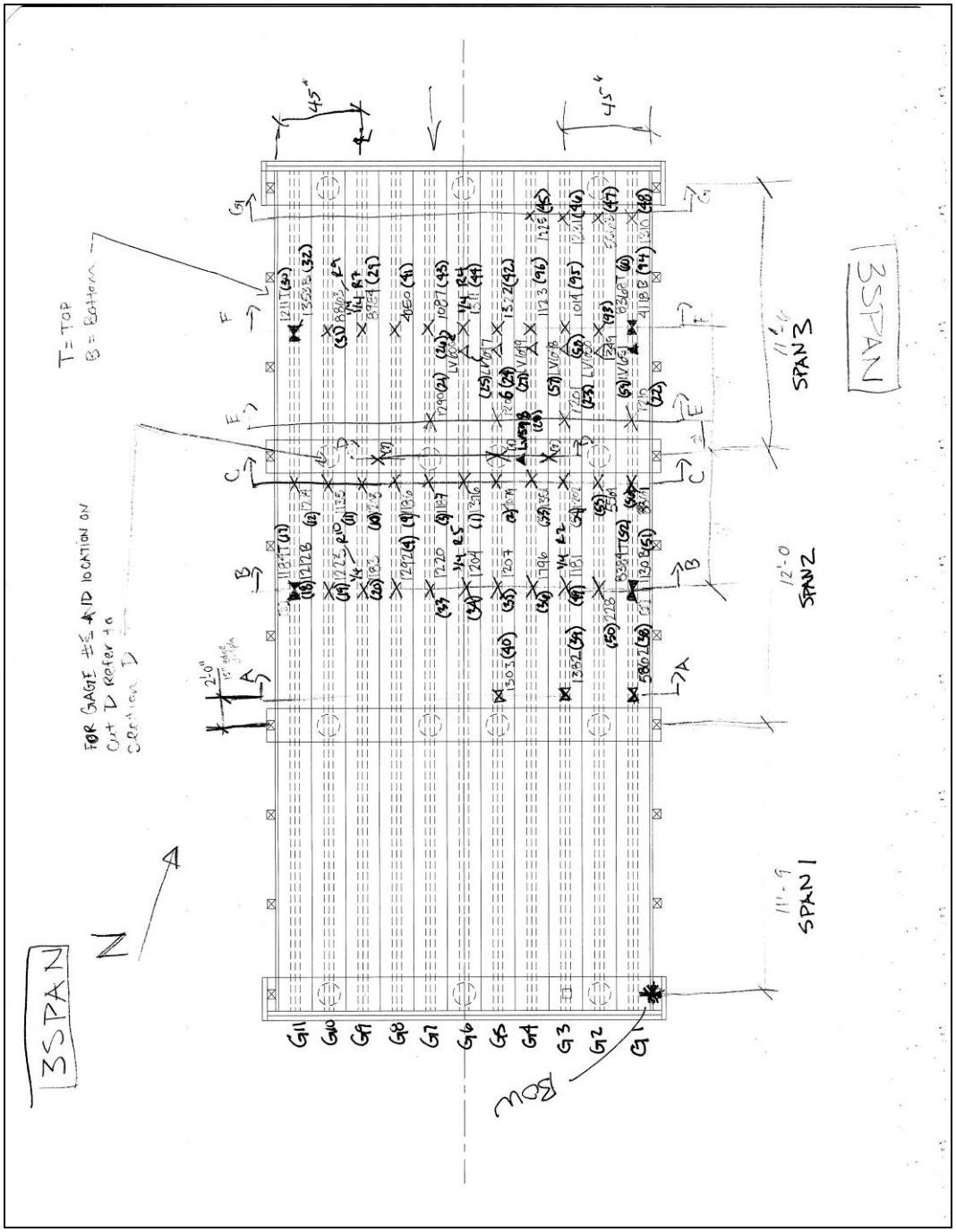

Figure B1. (Sheet 8 of 13).

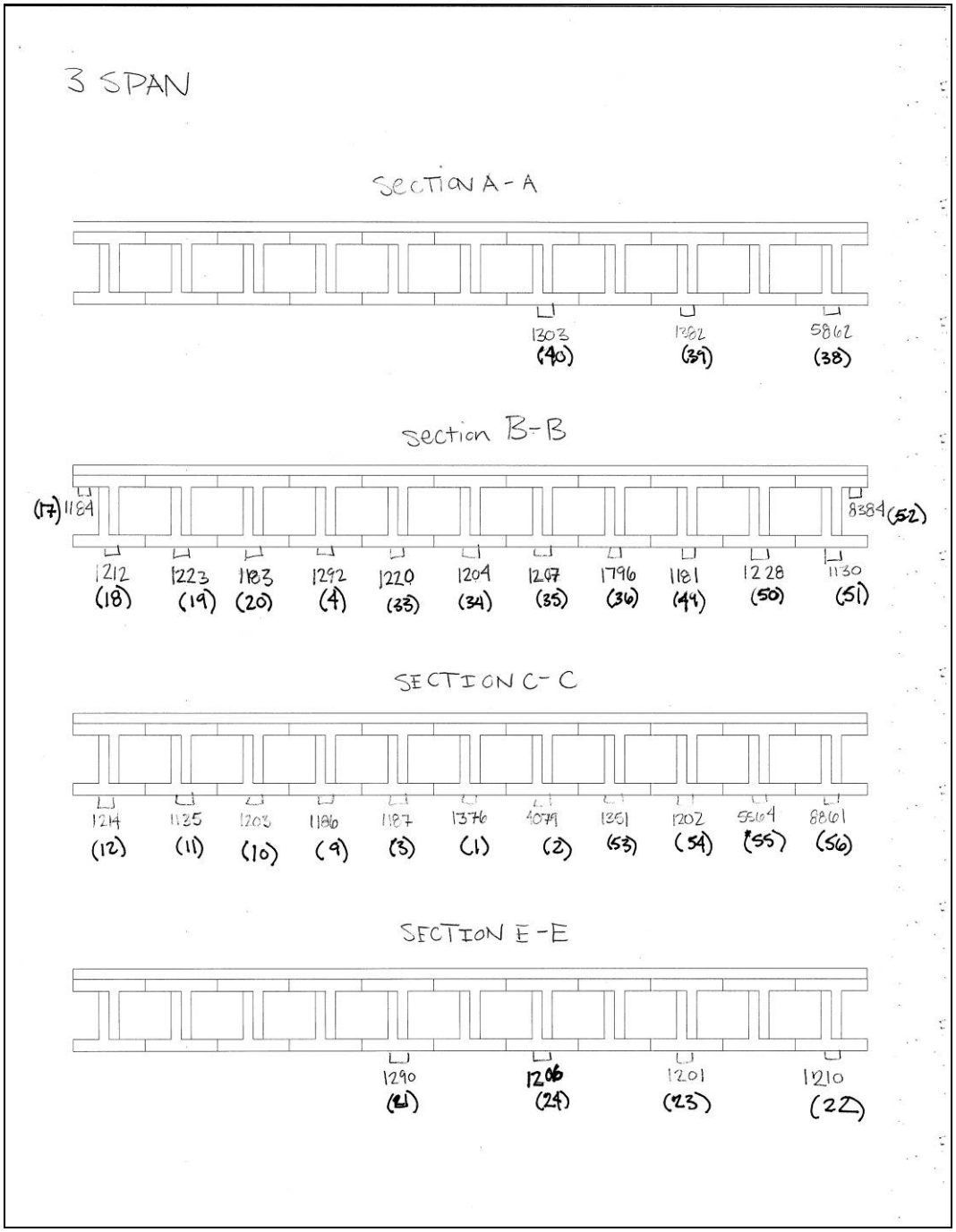

Figure B1. (Sheet 9 of 13).

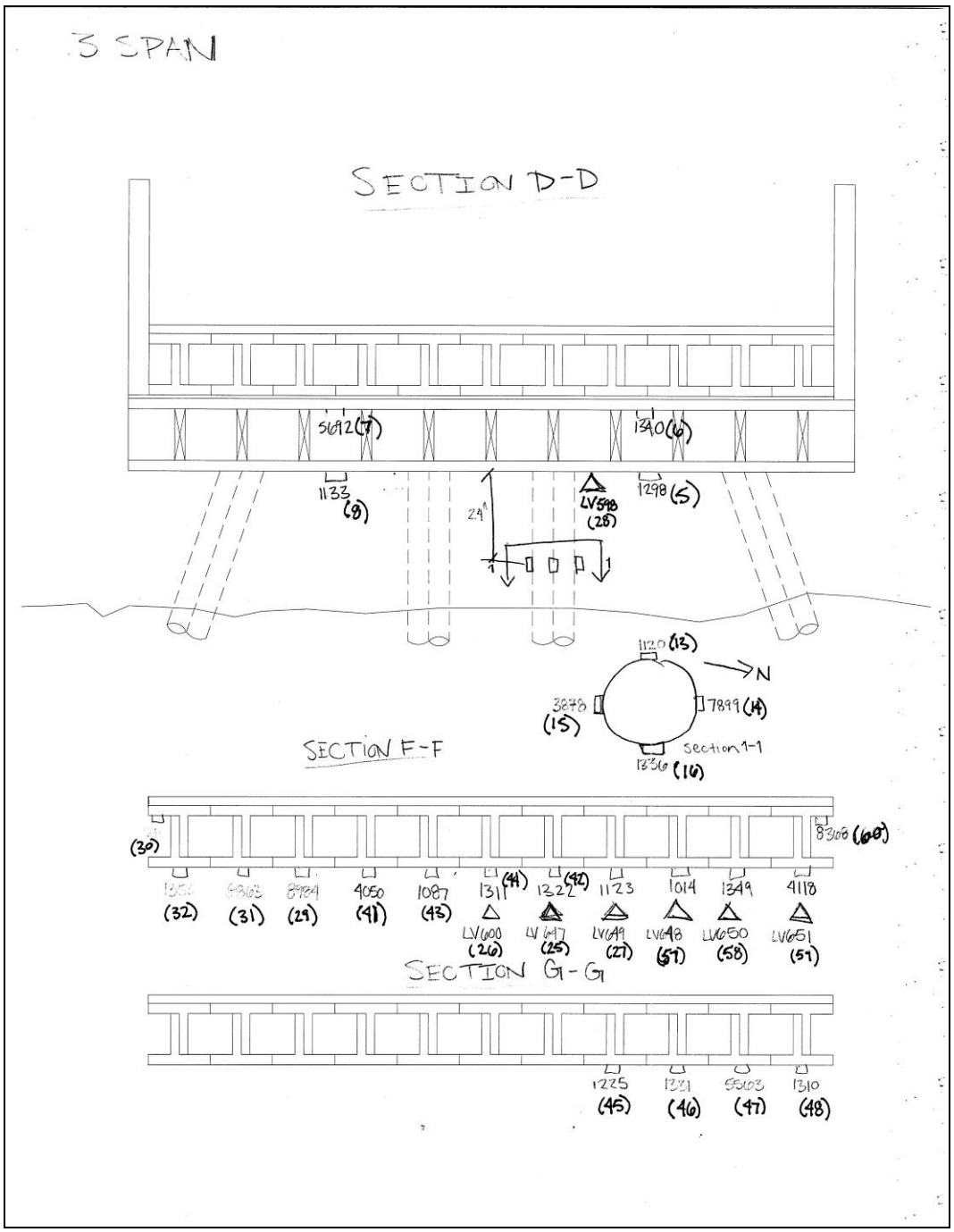

Figure B1. (Sheet 10 of 13).

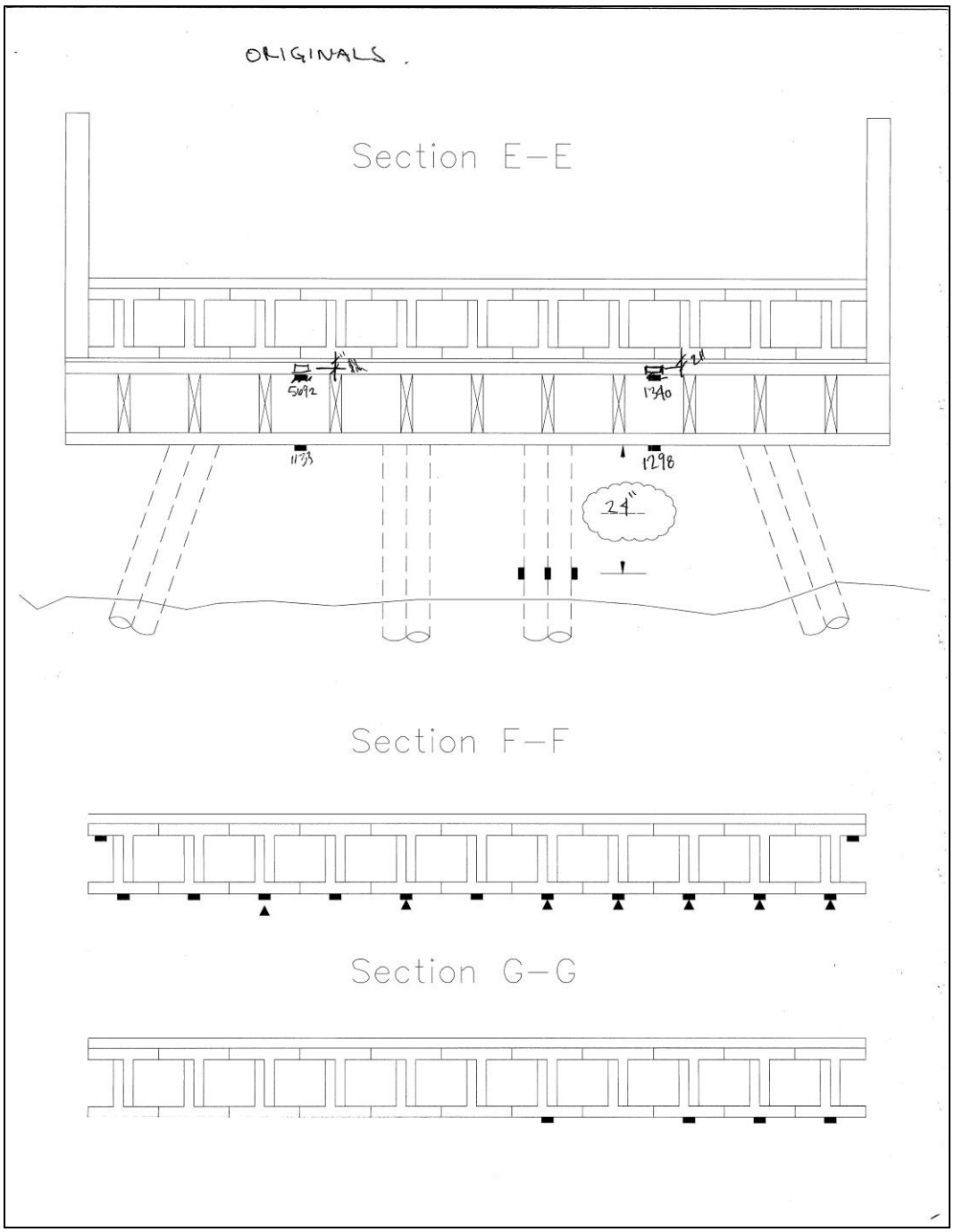

Figure B1. (Sheet 11 of 13).

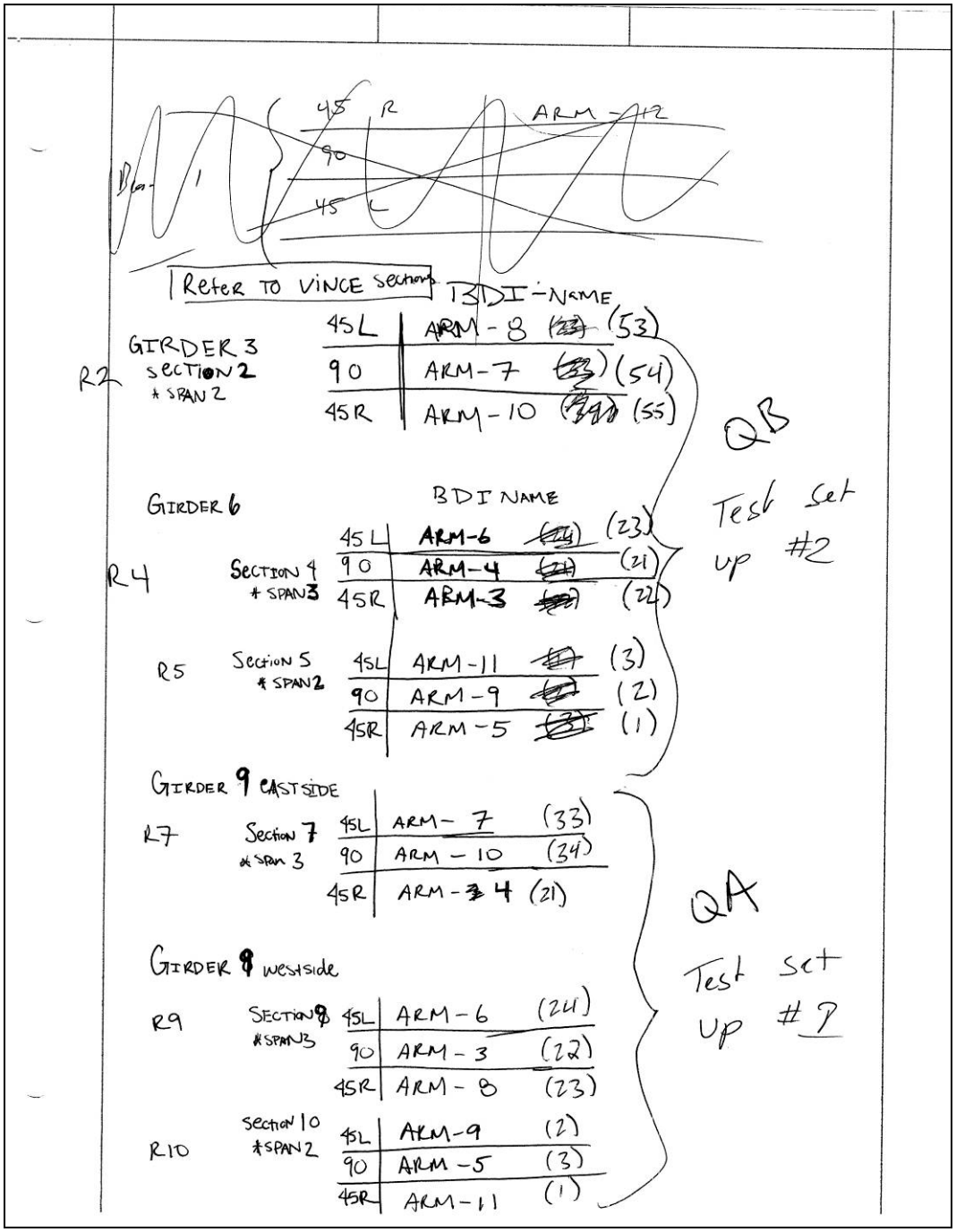

Figure B1. (Sheet 12 of 13).

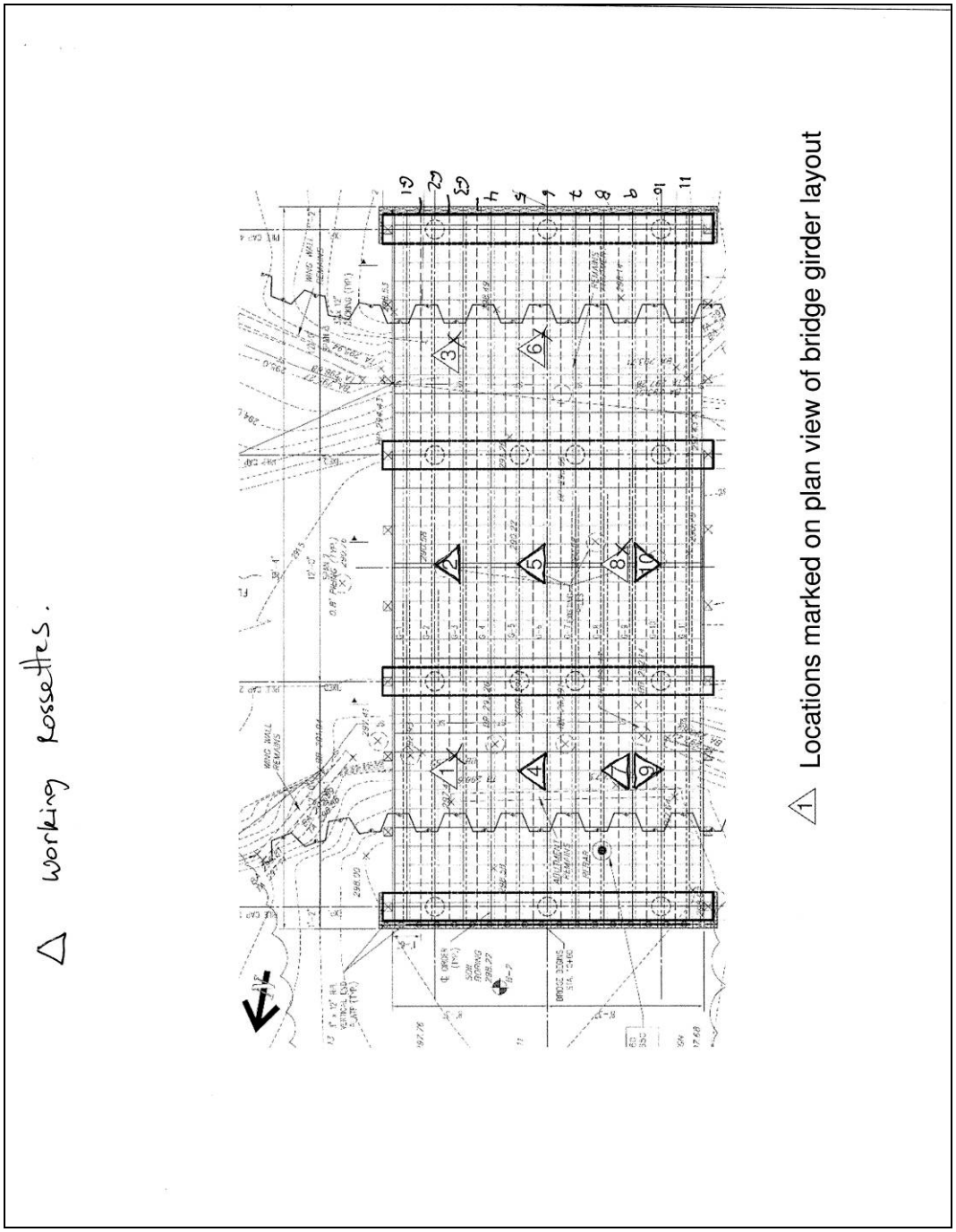

Figure B1. (Sheet 13 of 13).

Appendix C: BDI Field Testing Procedures

Background

The motivation for developing a relatively easy-to-implement field-testing system was to allow short-and medium-span bridges to be tested on a routine basis. Original development of the hardware was started in 1988 at the University of Colorado under a contract with the Pennsylvania Department of Transportation (PennDOT). Subsequent to that project, the Integrated Technique was refined in another study funded by the Federal Highway Administration (FHWA) in which 35 bridges located on the Interstate system throughout the country were tested and evaluated. Further refinement has been implemented over the years through testing and evaluating hundreds of bridges, lock gates, and other structures.

Structural testing hardware

The real key to being able to complete the field testing quickly is the use of strain transducers (rather than standard foil strain gages) that can be attached to the structural members in just a few minutes. These sensors were originally developed for monitoring dynamic strains on foundation piles during the driving process. They have been adapted for use in structural testing through special modifications, have very high accuracy, and are periodically recalibrated to NIST standards. Please refer to Appendix D for specifications on the BDI strain transducers.

In addition to the strain sensors, the data acquisition hardware has been designed specifically for structural live-load testing, which means it is extremely easy to use in the field. Please see Appendix D for specifications on the BDI Structural Testing System. Briefly, some of the features include military-style connections for quick assembly and self-identifying sensors that dramatically reduce bookkeeping efforts. The WinSTS testing software has been written to allow easy hardware configuration and data-recording. Other enhancements include the BDI AutoClicker, which is an automatic load position indicator that is mounted directly on the vehicle. As the test truck crosses the structure along the preset path, a communication radio sends a signal to the STS, which receives it and puts a mark in the data. This allows the field strains to be compared with analytical strains as a function of vehicle position, not only as a function of time.

Refer to Appendix D for the AutoClicker specifications. The end result of using all of the above-described components is a system that can be used by people other than computer experts or electrical engineers. Typical testing times with the STS range from 20 to 60 channel tests being completed in 1 day, depending on access and other field conditions.

The following general directions outline how to run a typical diagnostic load test on a short- to medium-span highway bridge up to about 200 ft in length. With only minor modifications, these directions can be applied to railroad bridges (use a locomotive rather than a truck for the load vehicle), lock gates (monitor the water level in the lock chamber), amusement park rides (track the position of the ride vehicle), and other structures in which the live load can be applied easily. The basic scenario is to first instrument the structure with the required number of sensors; run a series of tests; then, remove all the sensors. These procedures can often be completed within 1 workday, depending on field conditions such as access and traffic.

Instrumentation of structure

This outline is intended to describe the general procedures used for completing a successful field test on a highway bridge using the BDI-STS. For a detailed explanation of the instrumentation and testing procedures, please contact BDI and request a copy of the Structural Testing System (STS) Operation Manual.

Attaching strain transducers

Once a tentative instrumentation plan has been developed for the structure in question, the strain transducers must be attached and the STS prepared for running the test. There are several methods for attaching the strain transducers to the structural members depending on whether they are steel, concrete, timber, fiber-reinforced polymer (FRP), or other. For steel structures, quite often the transducers can be clamped directly to the steel flanges of rolled sections or plate girders. If significant lateral bending is assumed to be present, then one transducer may be clamped to each edge of the flange. In general, the transducers can be clamped directly to painted surfaces. The alternative to clamping is the tab attachment method that involves cleaning the mounting area and then using a fast-setting cyanoacrylate adhesive to temporarily install the transducers. Small steel “tabs” are used with this technique and they are removed when

testing is completed, and touch-up paint can be applied to the exposed steel surfaces.

Installation of transducers on prestressed concrete (PS/C) and FRP members is usually accomplished with the tab technique outlined above, while readily available wood screws and a battery-operated hand drill are used for timber members. Installing transducers on reinforced concrete (R/C) is more complex in that gage extensions are used and must be mounted with concrete studs.

Figures C1–C2 illustrate transducers mounted on steel and on R/C members.

Figure C1. Strain transducers mounted on a steel girder.

Assembly of system

Once the transducers have been mounted, they are connected to the four-channel STS units, which are also located on the bridge. The STS units can be easily clamped to the bridge girders, or if the structure is concrete and no flanges are available on which to set the STS units, transducer tabs glued to the structure and plastic zip-ties or small wire can be used to mount them.

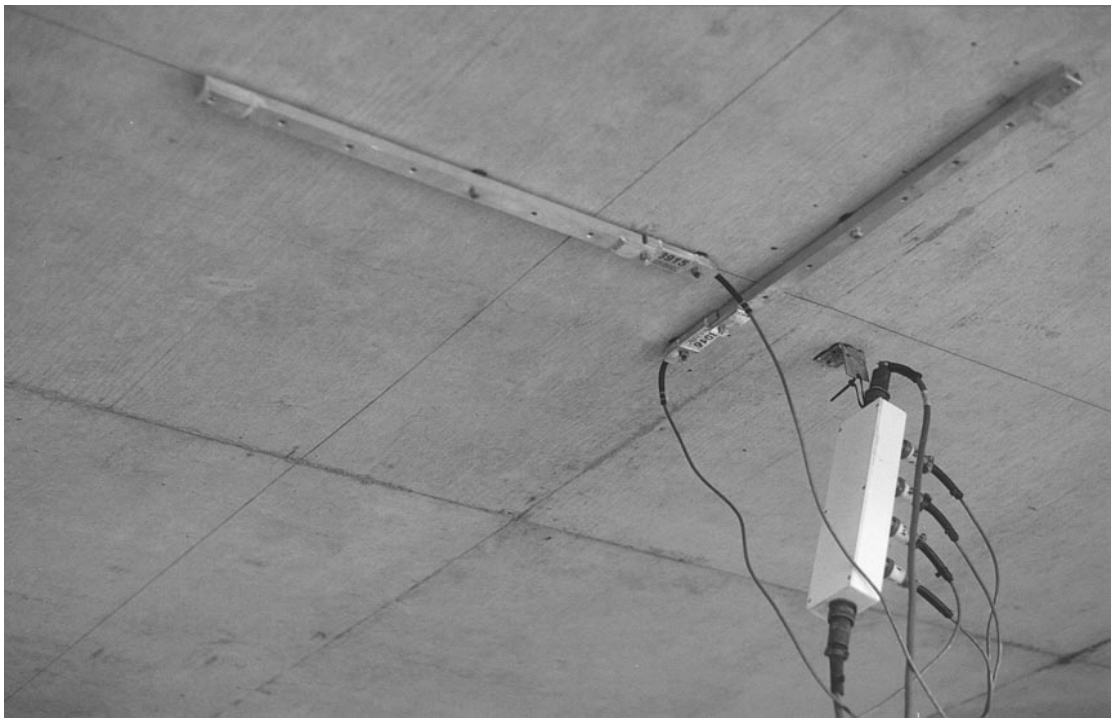

Figure C2. Transducer with gage extensions mounted on R/C slab.

Since the transducers will identify themselves to the system, there is no special order that they must be plugged into the system. The only information that must be recorded is the transducer serial number and its location on the structure. Signal cables are then used to connect STS units, either in series or in a "tree" structure through the use of cable splitters. If several gages are close to each other, the STS units can be plugged directly to each other without the use of a cable.

Once all of the STS units have been connected together, only one cable must be run and connected to the STS Power Supply located near the personal computer. Once power and communication cables are connected, the system is ready to acquire data. One last step entails installing the AutoClicker on the test vehicle, as shown in Figure C3.

Establishing load vehicle positions

Once the structure is instrumented and the loading vehicle prepared, some reference points must be established on the deck to determine where the vehicle will cross. This process is important so that future analysis comparisons can be made with the loading vehicle in the same locations as occurred in the field. Therefore, a "zero" or initial reference point

Figure C3. AutoClicker mounted on test vehicle.

is selected and usually corresponds to the point on the deck directly above the abutment bearing and the centerline of one of the fascia beams. All other measurements on the deck will then be related to this zero reference point. For concrete T-beams, box beams, and slabs, this can correspond to where the edge of the slab or the beam web meets the face of the abutment. If the bridge is skewed, the first point encountered from the direction of travel is used. In any case, it should be a point that is easily located on the drawings for the structure.

Once the zero reference location is known, the lateral load paths for the vehicle are determined. Often, the painted roadway lines are used for the driver to follow, if they are in convenient locations. For example, for a two-lane bridge, a northbound shoulder line will correspond to Y1 (passenger-side wheel), the center dashed line to Y2 (center of truck), and the southbound shoulder line to Y3 (driver's side wheel). Often, the structure

will be symmetrical with respect to its longitudinal centerline. If so, it is good practice to take advantage of this symmetry by selecting three Y locations that are also symmetric. This will allow for a data quality check, since the response should be very similar, say, on the middle beam if the truck is on the left side of the bridge or the right side of the bridge. In general, it is best to have the truck travel in each lane (at least on the lane line) and also as close to each shoulder or sidewalk as possible. When the deck layout is completed, the loading vehicle's axle weights and dimensions are recorded.

Running the load tests

After the structure has been instrumented and the reference system laid out on the bridge deck, the actual testing procedures are completed. The WinSTS software is initialized and configured. When all personnel are ready to commence the test, traffic control is initiated and the Run Test option is selected, which places the system in an activated state. When the truck passes over the first deck mark, the AutoClicker is tripped, and data are being collected at the specified sample rate. An effort is made to get the truck across with no other traffic on the bridge. When the rear axle of the vehicle completely crosses over the structure, the data collection is stopped and several strain histories evaluated for data quality. Usually, at least two passes are made at each "Y" position to ensure data reproducibility, and then if conditions permit, high-speed or dynamic tests are completed.

The use of a moving load as opposed to placing the truck at discrete locations has two major benefits. First, the testing can be completed much quicker, meaning there is less impact on traffic. Second, and more importantly, much more information can be obtained (both quantitative and qualitative). Discontinuities or unusual responses in the strain histories, which are often signs of distress, can be easily detected. Since the load position is monitored, as well, it is easy to determine what loading conditions cause the observed effects. If readings are recorded only at discrete truck locations, the risk of losing information between the points is great. The advantages of continuous readings have been proven many times.

When the testing procedures are complete, the instrumentation is removed and any touch-up work completed.

Appendix D: BDI Equipment Specifications

Specifications: BDI Strain Transducers

Figure D1. BDI strain transducer.

Table D1. Strain transducer specifications.

Effective gage length	3.0 in (76.2 mm). Extensions available for use on R/C structures.
Overall size	4.4 in x 1.2 in x 0.5 in (110 mm x 33 mm x 12 mm).
Cable length	10 ft (3 m) standard, any length available.
Material	Aluminum.
Circuit	Full Wheatstone bridge with four active 350Ω foil gages, 4-wire hookup.
Accuracy	± 2%, individually calibrated to NIST standards.
Strain range	Approximately ±4000 με.
Force req'd for 1000 με	Approximately 9 lb (40 N).
Sensitivity	Approximately 500 με/mV/V.
Weight	Approximately 3 oz (88 g).
Environmental	Built-in protective cover, also water resistant.
Temperature range	-60°F to 250°F (-50°C to 120°C) operation range.
Cable	BDI RC-187: 22 gage, two individually shielded pairs w/drain.
Options	Fully waterproofed, heavy-duty cable, special quick-lock connector.
Attachment methods	C-clamps or threaded mounting tabs, and quick-setting adhesive.

Specifications: BDI Wireless Structural Testing System

Figure D2. BDI structural testing system.

Table D2. Structural testing system specifications.

Channels	4 to 128, Expandable in multiples of 4
Hardware Accuracy	± 0.2% (2% for Strain Transducers)
Sample Rates	0.1 – 500 Hz (Internal over-sampling rate is 19.5-312 kHz)
Max Test Lengths	21 min at 100 Hz 128K samples per channel maximum test lengths
Gain Levels	1, 2, 4, 6, 16, 32, 64, 128
Digital Filter	Fixed by selected sample rate
Analog Filter	200 Hz, -3db, 3rd order Bessel
Max. Input Voltage	10.5 Volts DC
Battery Power	9.6 NiMH rechargeable battery (Programmable low-power sleep mode)
Alternative Power	9 – 48 Volts DC input
Excitation Voltages *Standard* *LVDT/Other*	 5 Volts DC 5.5 Volts DC
A/D Resolution	0.3 uV/bit (24-Bit ADC)
PC Requirements	Windows XP or higher
PC Interface	Wi-Fi Ethernet 802.11b: 10/100 Mbps

Auto Zeroing	Sensors automatically zero before each test
Enclosures	Aluminum splash resistant
Sensor Connections	All aluminum military grade, circular bayonet “snap” lock
Vehicle Tracking	BDI AutoClicker, switch closure detection
Sensors	BDI Intelliducer Strain Transducer Also supports LVDT’s, foil strain gages, accelerometers, Load Cells, and other various DC output sensors Single RS232 serially interfaced sensor
Onboard PC *Processor* *RAM*	 520 MHz Intel XScale PXA270 64 MB
Dimensions *Base Station* *STS 4-Channel Node*	 10” x 6” x 4” 11” x 3.5” x 3.23”

Specifications: BDI Wireless Structural Testing System

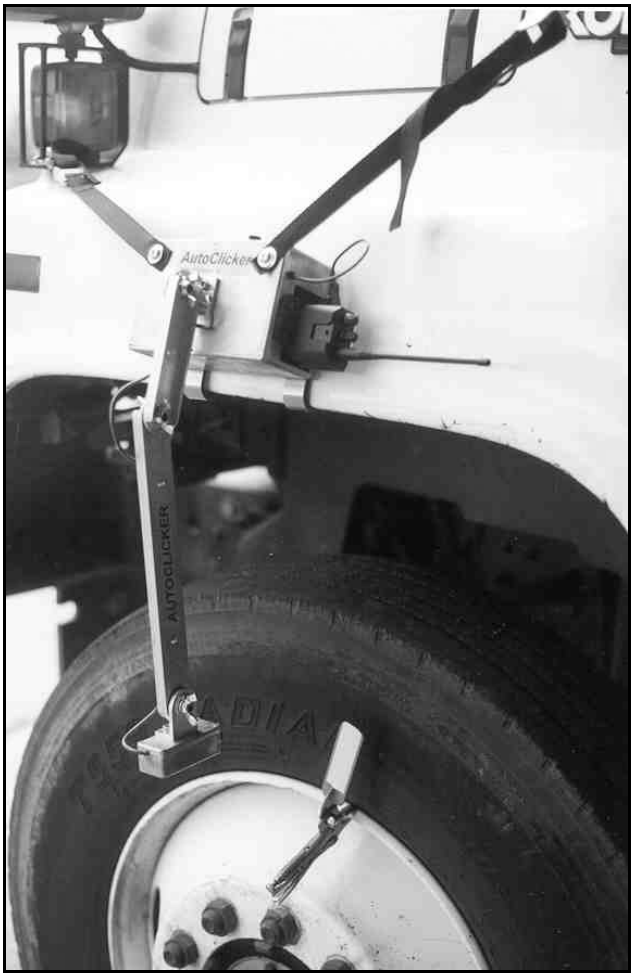

Figure D3. AutoClicker mounted on test truck.

Table D3. AutoClicker specifications.

3 Handheld Radios	Motorola P1225 2-Channel (or equal) modified for both “Rx” and “Tx.”
Power	9V battery
Mounting	Universal front fender mounting system
Target	Retroreflective tape mounted on universal wheel clamp
Bands/Power	VHF/1 Watt or UHF/2 Watt
Frequencies	User-specified
Data Acquisition System Requirements	TTL/CMOS input (pull-up resistor to 5V)
Output	Isolated contact closure (200V 0.5A max switch current)

Appendix E: Modeling and Analysis – The Integrated Approach

Introduction

For load testing to be a practical means of evaluating short- to medium-span bridges, it is apparent that testing procedures must be economical to implement in the field and the test results translatable into a load rating. A well-defined set of procedures must exist for the field applications as well as for the interpretation of results. An evaluation approach based on these requirements was first developed at the University of Colorado during a research project sponsored by the Pennsylvania Department of Transportation (PennDOT). Over several years, the techniques originating from this project have been refined and expanded into a complete bridge rating system.

The ultimate goal of the Integrated Approach is to obtain realistic rating values for highway bridges in a cost-effective manner. This is accomplished by measuring the response behavior of the bridge due to a known load and determining the structural parameters that produce the measured responses. With the availability of field measurements, many structural parameters in the analytical model can be evaluated that are otherwise conservatively estimated or ignored entirely. Items that can be quantified through this procedure include the effects of structural geometry, effective beam stiffness, realistic support conditions, effects of parapets and other nonstructural components, lateral load transfer capabilities of the deck and transverse members, and the effects of damage or deterioration. Often, bridges are rated poorly because of inaccurate representations of the structural geometry or because the material and/or cross-sectional properties of main structural elements are not well defined. A realistic rating can be obtained, however, when all of the relevant structural parameters are defined and implemented in the analysis process.

One of the most important phases of this approach is a qualitative evaluation of the raw field data. Much is learned during this step to aid in the rapid development of a representative model.

Initial data evaluation

The first step in structural evaluation consists of a visual inspection of the data in the form of graphic response histories. Graphic software was developed to display the raw strain data in various forms. Strain histories can be viewed in terms of time or truck position. Since strain transducers are typically placed in pairs, neutral axis measurements, curvature responses, and strain averages can also be viewed. Linearity between the responses and load magnitude can be observed by the continuity in the strain histories. Consistency in the neutral axis measurements from beam to beam and as a function of load position provides great insight into the nature of the bridge condition. The direction and relative magnitudes of flexural responses along a beam line are useful in determining if end restraints play a significant role in the response behavior. In general, the initial data inspection provides the engineer with information concerning modeling requirements and can help locate damaged areas.

Having strain measurements at two depths on each beam cross section, flexural curvature and the location of the neutral axis can be computed directly from the field data. Figure E1 illustrates how curvature and neutral axis values are computed from the strain measurements.

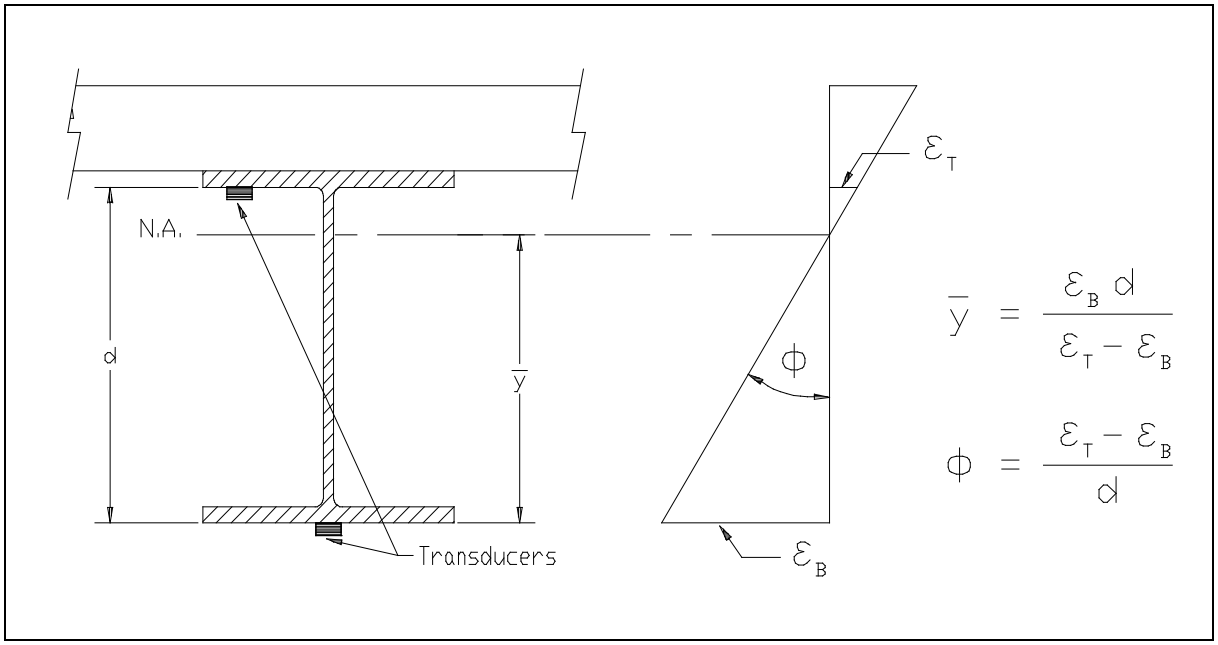

Figure E1. Illustration of neutral axis and curvature calculations.

The consistency in the Neutral Axis (N.A.) values between beams indicates the degree of consistency in beam stiffness. Also, the consistency of the N.A. measurement on a single beam as a function of truck position provides a good quality check for that beam. If a beam's stiffness changes with respect to the applied moment (i.e. loss of composite action or loss of effective flange width due to a deteriorated deck), it will be observed by a shift in the N.A. history.

Since strain values are translated from a function of time into a function of vehicle position on the structure and the data acquisition channel and the truck position tracked, a considerable amount of bookkeeping is required to perform the strain comparisons. In the past, this required manipulation of result files and spreadsheets that was tedious and a major source of error. This process in now performed automatically by the software, and all of the information can be verified visually.

Finite element modeling and analysis

The primary function of the load test data is to aid in the development of an accurate finite element model of the bridge. Finite element analysis is used because it provides the most general tool for evaluating various types of structures. Since a comparison of measured and computed responses is performed, it is necessary that the analysis be able to represent the actual response behavior. This requires that actual geometry and boundary conditions be realistically represented. In maintaining reasonable modeling efforts and computer run times, a certain amount of simplicity is also required. Hence, a planar grid model is generated for most structures, and linear-elastic responses are assumed. A grid of frame elements is assembled in the same geometry as the actual structure. Frame elements represent the longitudinal and transverse members of the bridge. The load transfer characteristics of the deck are provided by attaching plate elements to the grid. When end restraints are determined to be present, elastic spring elements having both translational and rotational stiffness terms are inserted at the support locations.

Loads are applied in a manner similar to the actual load test. A model of the test truck, defined by a two-dimensional group of point loads, is placed on the structure model at discrete locations along the same path that the test truck followed during the load test. Gage locations identical to those in the field are also defined on the structure model so that strains can be computed at the same locations under the same loading conditions.

Evaluation of rotational end restraint

A common requirement in structural identification is the need to determine effective spring stiffness that best represents in situ support conditions. While it is generally simple to evaluate a spring constant in terms of moment per rotation, the value generally has little meaning to the engineer. A more conceptual approach is to evaluate the spring stiffness as a percentage of a fully restrained condition, e.g., 0% being a pinned condition and 100% being fixed. This is best accomplished by examining the ratio of the beam or slab stiffness to the rotational stiffness of the support.

As an illustration, a point load is applied to a simple beam with elastic supports (Figure E2). By examining the moment diagram, it is apparent that the ratio of the end moment to the midspan moment (M_e/M_m) equals 0.0 if the rotational stiffness (K_r) of the springs is equal to 0.0. Conversely, if the value of K_r is set to infinity (rigid), the moment ratio will equal 1.0. If a fixity term is defined as the ratio (M_e/M_m), which ranges from 0 to 100 percent, a more conceptual measure of end restraint can be obtained.

The accuracy of the model is determined numerically by the analyzing using several The next step is to relate the fixity term to the actual spring stiffness (K_r). The degree to which the K_r affects the fixity term depends

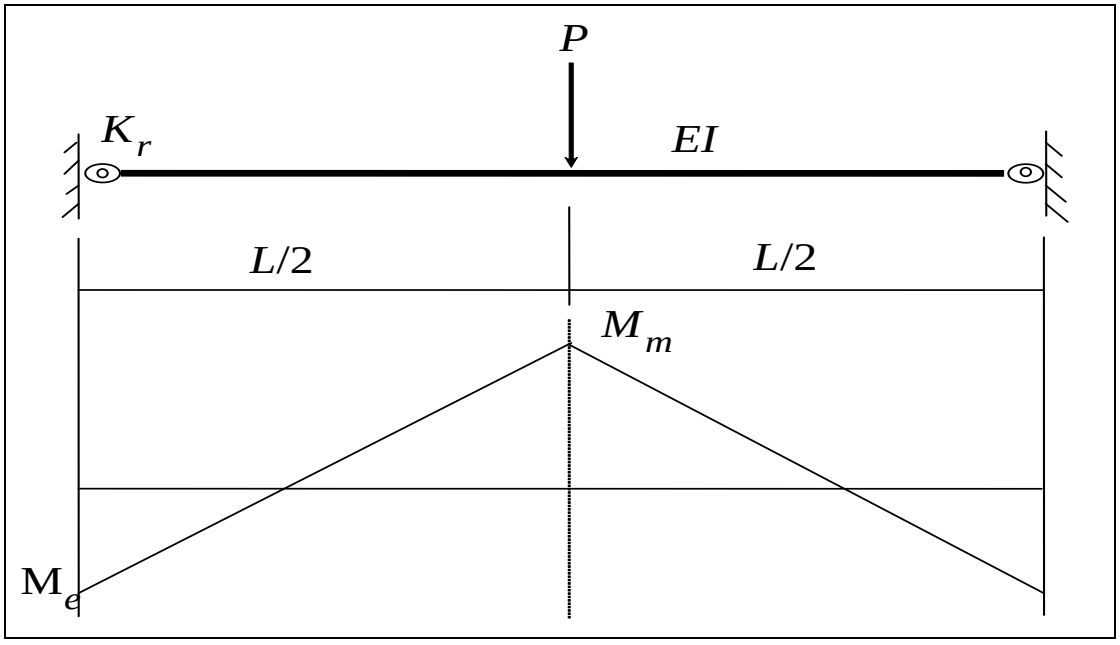

Figure E2. Moment diagram of beam with rotational end restraint.

on the beam or slab stiffness to which the spring is attached. Therefore, the fixity term must be related to the ratio of the beam stiffness to the spring stiffness. Figure E3 contains a graphical representation of the end restraint effect on a simple beam. Using the graph, a conceptual measure of end restraint can be defined after the beam and spring constants are evaluated through structural identification techniques.

Model correlation and parameter modification

The accuracy of the model is determined numerically by the analyzing using several statistical relationships and through visual comparison of the strain histories. The numeric accuracy values are useful in evaluating the effect of any changes to the model, while as the graphical representations provide the engineer with the best perception for why the model is responding differently than the measurements indicate. Member properties that cannot be accurately defined by conventional methods or directly from the field data are evaluated by comparing the computed

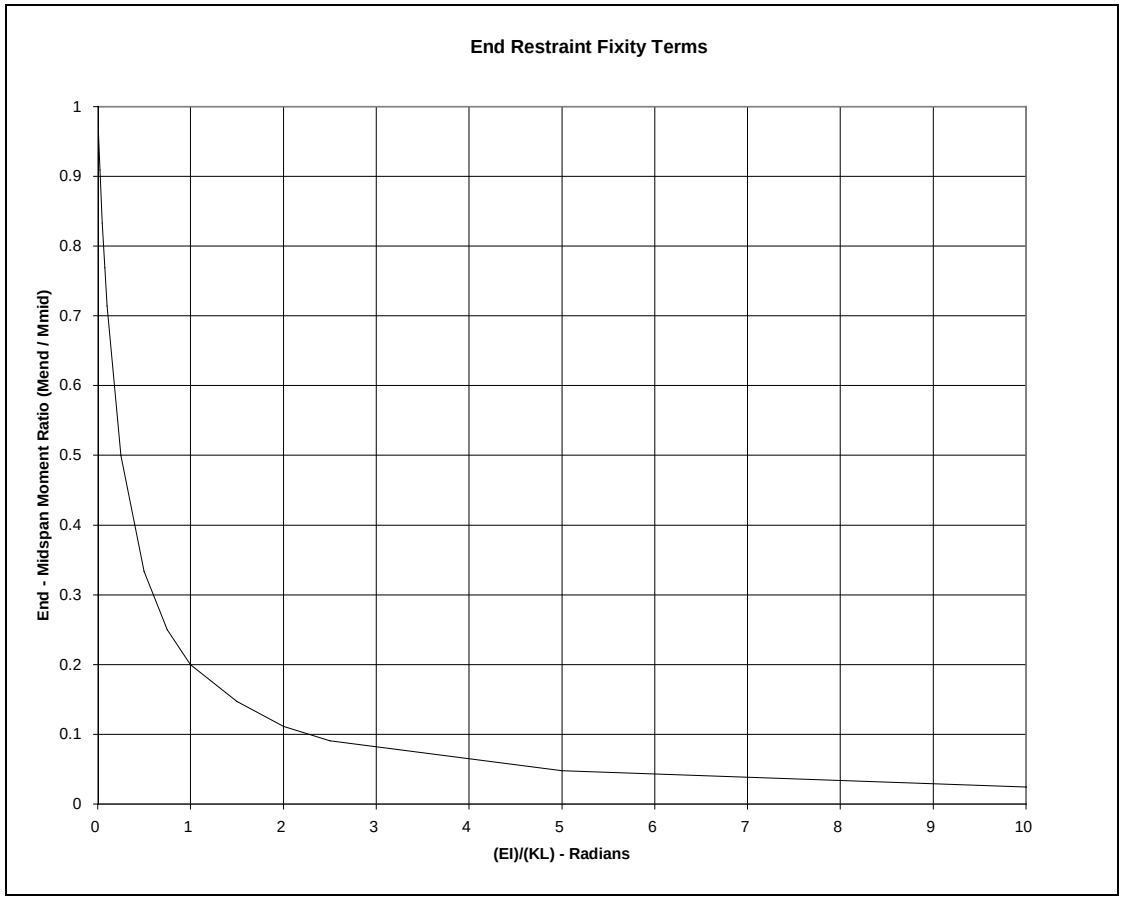

Figure E3. Relationship between spring stiffness and fixity ratio.

strains with the measured strains. These properties are defined as variable and are evaluated such that the best correlation between the two sets of data is obtained. It is the engineer's responsibility to determine which parameters need to be refined and to assign realistic upper and lower limits to each parameter. The evaluation of the member property is accomplished with the aid of a parameter identification process (optimizer) built into the analysis. In short, the process consists of an iterative procedure of analysis, data comparison, and parameter modification. It is important to note that the optimization process is merely a tool to help evaluate various modeling parameters. The process works best when the number of parameters is minimized, and reasonable initial values are used.

During the optimization process, various error values are computed by the analysis program that provides a quantitative measure of model accuracy and improvement. The error is quantified in four different ways, each providing a different perspective of the model's ability to represent the actual structure, i.e., an absolute error, a percent error, a scale error, and a correlation coefficient.

The **absolute error** is computed from the absolute sum of the strain differences. Algebraic differences between the measured and theoretical strains are computed at each gage location for each truck position used in the analysis; therefore, several hundred strain comparisons are generally used in this calculation. This quantity is typically used to determine the relative accuracy from one model to the next and to evaluate the effect of various structural parameters. It is used by the optimization algorithm as the objective function to minimize. Because the absolute error is in terms of micro-strain (mε), the value can vary significantly depending on the magnitude of the strains, the number of gages, and the number of different loading scenarios. For this reason, it has little conceptual value except for determining the relative improvement of a particular model.

A **percent error** is calculated to provide a better qualitative measure of accuracy. It is computed as the sum of the strain differences squared divided by the sum of the measured strains squared. The terms are squared so that error values of different sign will not cancel each other and to put more emphasis on the areas with higher strain magnitudes. A model with acceptable accuracy will usually have a percent error of less than 10%.

The **scale error** is similar to the percent error except that it is based on the maximum error from each gage divided by the maximum strain value from each gage. This number is useful because it is based only on strain measurements recorded when the loading vehicle is in the vicinity of each gage. Depending on the geometry of the structure, the number of truck positions and various other factors, many of the strain readings are essentially negligible. This error function uses only the most relevant measurement from each gage.

Another useful quantity is the **correlation coefficient,** which is a measure of the linearity between the measured and computed data. This value determines how well the shapes of the computed response histories match the measured responses. The correlation coefficient can have a value between 1.0 (indicating a perfect linear relationship) and -1.0 (exact opposite linear relationship). A good model will generally have a correlation coefficient greater than 0.90. A poor correlation coefficient is usually an indication that a major error in the modeling process has occurred. This is generally caused by poor representations of the boundary conditions or the loads were applied incorrectly, e.g., truck traveling in wrong direction.

Table E1 contains the equations used to compute each of the statistical error values.

Table E1. Error functions.

Error Function	Equation
Absolute Error	$\Sigma \lvert \varepsilon_m - \varepsilon_c \rvert$
Percent Error	$\Sigma (\varepsilon_m - \varepsilon_c)^2 / \Sigma (\varepsilon_m)^2$
Scale Error	$\frac{\Sigma \max \lvert \varepsilon_m - \varepsilon_c \rvert_{gage}}{\Sigma \max \lvert \varepsilon_m \rvert_{gage}}$
Correlation Coefficient	$\frac{\Sigma (\varepsilon_m - \overline{\varepsilon_m})(\varepsilon_c - \overline{\varepsilon_c})}{\Sigma \sqrt{(\varepsilon_m - \overline{\varepsilon_m})^2 (\varepsilon_c - \overline{\varepsilon_c})^2}}$

In addition to the numerical comparisons made by the program, periodic visual comparisons of the response histories are made to obtain a conceptual measure of accuracy. Again, engineering judgment is essential in determining which parameters should be adjusted so as to obtain the most accurate model. The selection of adjustable parameters is performed by

determining what properties have a significant effect on the strain comparison and determining which values cannot be accurately estimated through conventional engineering procedures. Experience in examining the data comparisons is helpful; however, two general rules apply concerning model refinement. When the shapes of the computed response histories are similar to the measured strain records but the magnitudes are incorrect, member stiffness probably should be adjusted. When the shapes of the computed and measured response histories are not very similar, the boundary conditions or the structural geometry are not well represented and must be refined.

In some cases, an accurate model cannot be obtained, particularly when the responses are observed to be nonlinear with load position. Even then, a great deal can be learned about the structure, and intelligent evaluation decisions can be made.

Appendix F: Load Rating Procedures

A load rating factor is a numeric value indicating a structure's ability to carry a specific load. Load rating factors were computed by applying standard design loads along with the structure's self-weight. Rating factors are computed for various structural components and are equal to the ratio of the component's live-load capacity and the live load applied to that component, including all appropriate load factors. A load rating factor greater than 1.0 indicates a member's capacity exceeds the applied loads with the desired factors of safety. A rating factor less than 1.0 indicates a member is deficient such that a specific vehicle cannot cross the bridge with the desired factor of safety. A number near 0.0 indicates the structure cannot carry its own dead weight and maintain the desired safety factor. The lowest component rating-factor generally controls the load rating of the entire structure. Additional factors are applied to account for variability in material, load application, and dynamic effects. Two levels of load rating are performed for the bridge. An inventory level rating corresponds to the design stress levels and/or factors of safety and represents the loads that can be applied on a daily basis. The operating rating levels correspond to the maximum load limits above which the structure may experience damage or failure.

For borderline bridges (those that calculations indicate a posting is required), the primary drawback to conventional bridge rating is an over-simplified procedure for estimating the load applied to a given beam, i.e., wheel load distribution factors, and a poor representation of the beam itself. Due to lack of information and the need for conservatism, material and cross-section properties are generally over-estimated, and beam end supports are assumed to be simple when in fact even relatively simple beam bearings have a substantial effect on the midspan moments. Inaccuracies associated with conservative assumptions are compounded with complex framing geometries. From an analysis standpoint, the goal here is to generate a model of the structure that is capable of reproducing the measured strains. Decisions concerning load rating are then based on the performance of the model once it is proven to be accurate.

The main purpose for obtaining an accurate model is to evaluate how the bridge will respond when standard design loads, rating vehicles, or permit

loads are applied to the structure. Since load testing is generally not performed with all of the vehicles of interest, an analysis must be performed to determine load rating factors for each truck type. Load rating is accomplished by applying the desired rating loads to the model and computing the stresses on the primary members. Rating factors are computed using the equation specified in the AASHTO Manual for Condition Evaluation of Bridges.

It is important to understand that diagnostic load testing and the integrated approach are most applicable to obtaining inventory (service load) rating values. This is because it is assumed that all of the measured and computed responses are linear with respect to load. The integrated approach is an excellent method for estimating service-load stress values, but it generally provides little additional information regarding the ultimate strength of specific structural members. Therefore, operating rating values must be computed using conventional assumptions regarding member capacity. This limitation of the integrated approach is not viewed as a serious concern, because load responses should never be permitted to reach the inelastic range.

Operating and/or load factor rating values must also be computed to ensure a factor of safety between the ultimate strength and the maximum allowed service loads. The safety to the public is of vital importance, but as long as load limits are imposed such that the structure is not damaged, then safety is no longer an issue.

The following is an outline describing how field data is used to help in developing a load rating for the superstructure. These procedures will only complement the rating process and must be used with due consideration to the substructure and inspection reports.

1. **Preliminary investigation**: Verification of linear and elastic behavior through continuity of strain histories, locate neutral axis of flexural members, detect moment resistance at beam supports, and qualitatively evaluate behavior.
2. **Develop representative model**: Use graphic preprocessors to represent the actual geometry of the structure, including span lengths, girder spacing, skew, transverse members, and deck. Identify gage locations model identical to those applied in the field.

3. **Simulate load test on computer model**: Generate 2-dimensional model of test vehicle and apply to structure model at discrete positions along same paths defined during field tests. Perform analyses and compute strains at each gage location for each truck position.
4. **Compare measured and initial computed strain values**: Various global and local error values at each gage location are computed, and visual comparisons are made with postprocessor.
5. **Evaluate modeling parameters**: Improve model based on data comparisons. Engineering judgment and experience is required to determine which variables are to be modified. A combination of direct evaluation techniques and parameter optimization are used to obtain a realistic model. General rules have been defined to simplify this operation.
6. **Model evaluation**: In some cases it is not desirable to rely on secondary stiffening effects if it is likely they will not be effective at higher load levels. It is beneficial, though, to quantify their effects on the structural response so that a representative computer model can be obtained. The stiffening effects that are deemed unreliable can be eliminated from the model prior to the computation of rating factors. For instance, if a noncomposite bridge is exhibiting composite behavior, then it can conservatively be ignored for rating purposes. However, if it has been in service for 50 years and it is still behaving compositely, chances are that very heavy loads have crossed over it, and any bond-breaking would have already occurred. Therefore, probably some level of composite behavior can be relied upon. When unintended composite action is allowed in the rating, additional load limits should be computed based on an allowable shear stress between the steel and concrete and an ultimate load of the noncomposite structure.
7. **Perform load rating:** Apply HS-20 and/or other standard design, rating and permit loads to the calibrated model. Rating and posting load configuration recommended by AASHTO are shown in Figure F1.

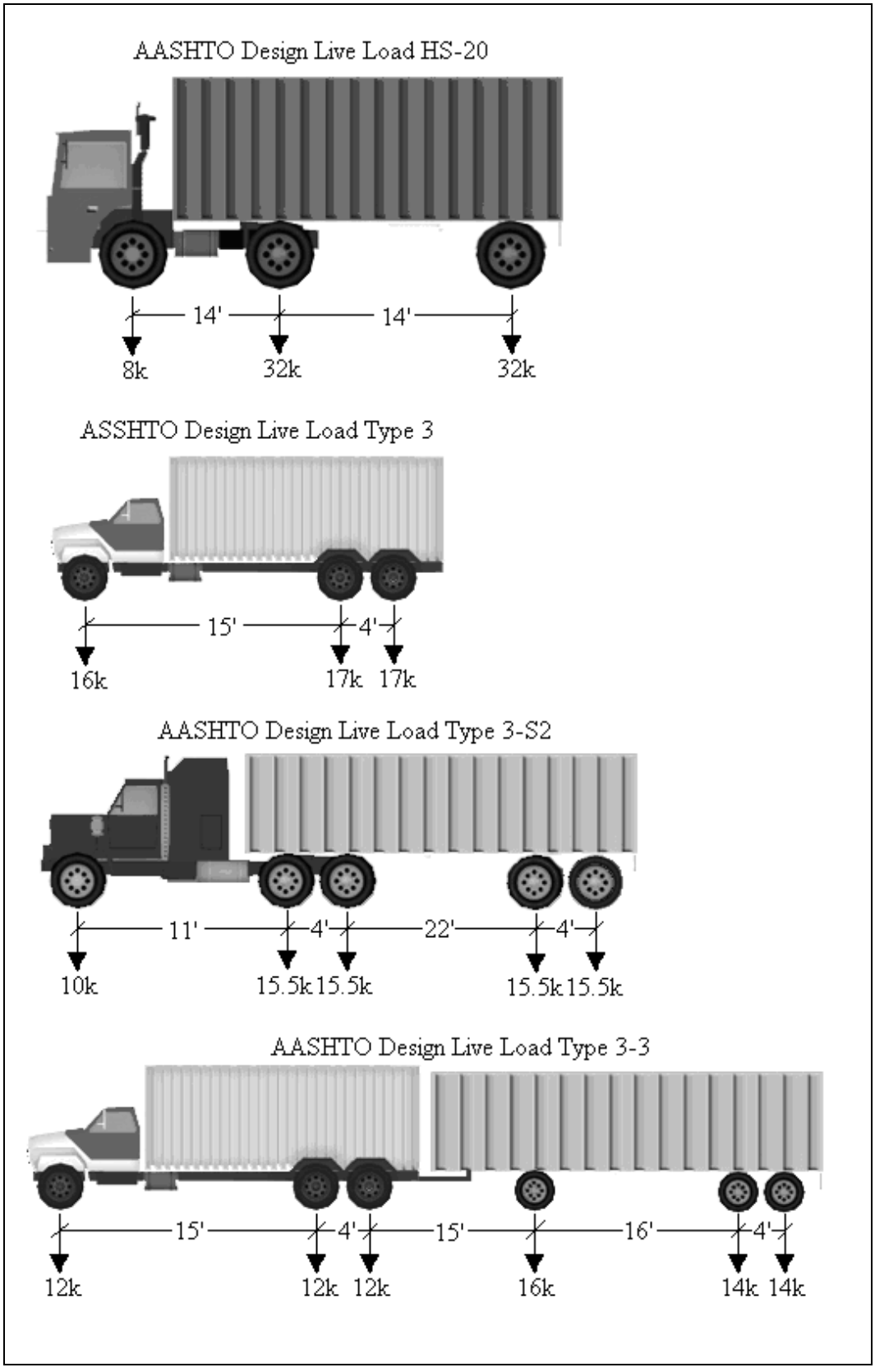

Figure F1. AASHTO rating and posting load configurations.

8. The same rating equation specified by the **AASHTO - Manual for the Condition Evaluation of Bridges** is applied:

$$RF = \frac{C - \gamma_{DC}(DC) - \gamma_{DW}(DW) \pm \gamma_P(P)}{\gamma_{LL}(LL + IM)} \quad \text{(F1)}$$

where:

RF = rating factor for individual member
C = member capacity
γDC = LRFD load factor for structural components and attachments
DC = dead-load effect due to structural components
γDW = LRFD load factor for wearing surfaces and utilities
DW = dead-load effect due to wearing surface and utilities
γP = LRFD load factor for permanent loads other than dead loads = 1.0
P = permanent loads other than dead loads
γ_{LL} = LRFD load factor for live load
LL = live-load effect
IM = impact effect, either AASHTO or measured.

The only difference between this rating technique and standard beam rating programs is that a more realistic model is used to determine the dead-load and live-load effects. Two-dimensional loading techniques are applied because wheel load distribution factors are not applicable to a planar model. Stress envelopes are generated for several truck paths and envelopes for paths separated by normal lane widths are combined to determine multiple lane loading effects.

9. **Consider other factors**: Other factors such as the condition of the deck and/or substructure, traffic volume, and other information in the inspection report should be taken into consideration, and the rating factors adjusted accordingly.

Table F1. LRFR load and resistance factors.

Dead Load	Allowable Stress (serviceability limit state)	1.00
	DC (Dead-load effects due to structural components and attachments)	1.25
	DW (Dead-load effect due to wearing surface and utilities)	1.50
Live Load	Allowable Stress (serviceability limit state)	1.00
	Inventory	1.75
	Operating	1.35
Condition Factor, φ_C	Good or Satisfactory	1.00
	Fair	0.95
	Poor	0.85
System Factor, φ_S	Welded Members in Two-Girder/Truss/Arch Bridges	0.85
	Riveted Members in Two-Girder/Truss/Arch Bridges	0.90
	Multiple Eyebar Members in Truss Bridges	0.90
	Three-Girder Bridges with Girder Spacing ≤6 ft	0.85
	Four-Girder Bridges with Girder Spacing ≤4 ft	0.95
	All other Girder Bridges and Slab Bridges	1.00
	Floorbeams with Spacing >12 ft and Noncontinuous Stringers	0.85
	Redundant Stringers Subsystems Between Floorbeams	1.00

Table F2. LRFD resistance factors.

Capacity	Steel Resistance Factor	R/C Resistance Factor	PS/C Resistance Factor
Flexure, Φ_b	1.00	0.90	1.00
Shear, Φ_v	1.00	0.90	0.90

REPORT DOCUMENTATION PAGE

Form Approved
OMB No. 0704-0188

1. REPORT DATE *(DD-MM-YYYY)*	2. REPORT TYPE	3. DATES COVERED *(From - To)*
June 2010	Final report	

4. TITLE AND SUBTITLE

Field Testing and Load Rating of the World's First Thermoplastic Bridge: Bridge T-8518, Camp Mackall, Fort Bragg, North Carolina

5a. CONTRACT NUMBER

5b. GRANT NUMBER

5c. PROGRAM ELEMENT NUMBER

6. AUTHOR(S)

Brett Commander and Henry Diaz-Alvarez

5d. PROJECT NUMBER

5e. TASK NUMBER

5f. WORK UNIT NUMBER

7. PERFORMING ORGANIZATION NAME(S) AND ADDRESS(ES)

Bridge Diagnostics, Inc.
1965 57th Court North, Suite 106, Boulder, CO 80301;
U.S. Army Engineer Research and Development Center
Geotechnical and Structures Laboratory
3909 Halls Ferry Road, Vicksburg, MS 39180-6199

8. PERFORMING ORGANIZATION REPORT NUMBER

ERDC/GSL TR-10-19

9. SPONSORING / MONITORING AGENCY NAME(S) AND ADDRESS(ES)

U.S. Army Installation Management Command
Arlington, VA 22202

10. SPONSOR/MONITOR'S ACRONYM(S)

11. SPONSOR/MONITOR'S REPORT NUMBER(S)

12. DISTRIBUTION / AVAILABILITY STATEMENT

Approved for public release; distribution is unlimited.

13. SUPPLEMENTARY NOTES

14. ABSTRACT

Live-load tests were conducted on Bridge T-8518 located on Tuckers Road in Camp Mackall near Fort Bragg, North Carolina. This bridge was tested because it was constructed of a new structural material consisting primarily of recycled plastic lumber (RPL). The primary goal of the testing was to obtain the responses of the bridge to the live loads in order to determine its load capacity ratings for both civilian and military vehicles and, specifically, to determine if the RPL structure could safely carry an M1 tank.

A finite element model of the entire superstructure was developed and used to calculate the responses of the RPL bridge. The results from the calculations were reasonably accurate when compared with the measured field data but were very sensitive to small variations in load position due to the spacing of the bridge beams and the flexibility of the plank deck.

Once a realistic yet conservative model of the structure was obtained, load ratings were computed based on an allowable stress approach. Allowable stress limits that were provided by the manufacturer corresponded to stresses that could be applied to the RPL

(Continued)

15. SUBJECT TERMS

BDI	Load test	RPL
Corrosion prevention	Recycled plastic lumber	Thermoplastic bridge

16. SECURITY CLASSIFICATION OF:			17. LIMITATION OF ABSTRACT	18. NUMBER OF PAGES	19a. NAME OF RESPONSIBLE PERSON
a. REPORT	b. ABSTRACT	c. THIS PAGE			19b. TELEPHONE NUMBER *(include area code)*
UNCLASSIFIED	UNCLASSIFIED	UNCLASSIFIED		115	

14. ABSTRACT (Concluded)

material for a long period of time with deformations 100% recoverable once the load was removed. These stress limits were a small fraction of the ultimate stress limits for RPL. However, an ultimate load capacity would be difficult to calculate because it would result in highly nonlinear and time-dependent responses with extremely large deformations.

The load rating results only apply to the bridge superstructure. Deformations of the RPL piles were measured during the load test, but no assessment could be made concerning the pile capacity. The pile capacity should be verified from the design engineer and the piling contractor to ensure that the piles have sufficient bearing strength to withstand the load limits of the superstructure.